

UCSF

UC San Francisco Electronic Theses and Dissertations

Title

Control of Membrane Fusion During Yeast Mating

Permalink

<https://escholarship.org/uc/item/4057t831>

Author

Engel, Alex

Publication Date

2008-01-04

Peer reviewed|Thesis/dissertation

Control of Membrane Fusion During Yeast Mating

by
Alex Engel

DISSERTATION

Submitted in partial satisfaction of the requirements for the degree of

DOCTOR OF PHILOSOPHY

in
Cell Biology

in the
GRADUATE DIVISION

of the

ACKNOWLEDGEMENTS

I would like to acknowledge the many excellent science mentors with whom I have had the privilege to interact: Allan Hargus and Bill Moore in Seattle; Dan O’Leary, Cynthia Selassie, Bruce Telzer, and David Becker in Claremont; Len Seligman, my undergraduate thesis advisor, for his encouragement at the bench; and Raul Andino and Dave Toczyski at UCSF. More intimately, every assemblage of the Walter Lab has provided great fun and support. A few members merit individual praise. Jason Brickner and Tobi Walther were wonderful leaders in the Walter Lab and made it their business to be involved with both experimental details and the direction of the project. Tomás Aragon has also been a great help to the cell fusion group and provided more ideas for experiments than could ever be done. Most importantly, I need to thank the individuals who collaborated with me, agonized over the data, and shared moments of success—Max Heiman, Pablo Aguilar, and Peter Walter. It has been a great pleasure working closely with these intelligent and very engaging people. For providing an outside perspective and input, I thank thesis committee members Dave Toczyski and Randy Schekman. Andrew Krutchinsky and Kati Madzihradzky, patient and dedicated mass spectroscopy experts, taught me much about their craft for which I am appreciative.

Finally, I am grateful to many inspired people for helping me stay productive, focused, and happy—UCSF colleagues Sebastián Bernales, Claudia Rubio, Shannon Behrman, Greg Tully, Muluye Liku, Chris Wilson, Liam Holt, and Niels Bradshaw; close friends Ben Mirus, Jessica Togasaki, and Gabrielle Wong-Parodi; the Badgers; and my family, Esther Neeser, Tom Engel, Juliane Engel, and Irene Neeser.

The text of Chapter 2 is a reprint of the material as it appears in *Molecular Biology of the Cell*. The research was directed and supervised by Peter Walter. Pablo Aguilar and Alex Engel collaborated in designing the experiments, performing the experiments, and writing the manuscript.

The text of Chapter 4 is a reprint of the material as it appears in *The Journal of Cell Biology*. The research was directed and supervised by Peter Walter. Max Heiman carried out the genetic screen, cloning, and electron microscopy work, and wrote the majority of the manuscript. Alex Engel designed and carried out the Kex2 substrate bioinformatics and experimental verification, tested the *fus1/fus2* genetic interaction with *prm1*, performed the cell integrity studies, and contributed to writing the manuscript.

CONTROL OF MEMBRANE FUSION DURING YEAST MATING

ALEX ENGEL

ABSTRACT

To maintain the integrity and identity of membrane-bound compartments, membrane fusion is promoted by fusases in a non-leaky manner. During yeast mating, two partners of a mating pair must fuse their cell membranes. The multipass membrane protein Prm1p promotes this extracytoplasmic fusion event. Less than half of *prm1 x prm1* mating pairs successfully fuse, instead arresting at the step of membrane fusion or undergoing simultaneous cell lysis. *prm1 x prm1* mating pair lysis is enhanced when extracellular Ca^{2+} is removed. As revealed by time-lapse microscopy, mating pair fusion and lysis events initiate with identical kinetics. Furthermore, cytoplasmic continuity is generated concurrent with cell lysis. These results suggest that cell lysis is linked to the mechanism of cell fusion. Prm1p promotes cell fusion and prevents cell lysis as a covalently linked homodimer. Substitution of cys-120 and cys-545 prevents covalent dimerization but does not decrease association of Prm1p monomers. Mutants unable to form the covalent link between dimers are severely compromised for Prm1p activity. *PRM1* mutants show a unique genetic interaction with *KEX2*, a gene encoding a late-Golgi protease. Though *prm1 x wt* and *wt x kex2* (*MATa x MATα*) mating pairs do not have strong mating defects, *prm1 x kex2* mating pairs fuse with less than 50% efficiency. Unfused *wt x kex2* mating pairs exhibit membrane enclosed structures embedded in the cell wall separating

mating partners (“blebs”). When *PRM1* is deleted, some *prm1 x prm1kex2* mating pairs extend protrusions into the space of the partner cell that are apparently devoid of cytoplasmic contents (“enormous barren bubbles”). Another mating-induced membrane protein, Fig1p, is required for efficient cell membrane fusion during yeast mating. *fig1 x fig1* mating pairs have a mild bilateral fusion defect, and 10% of unfused mating pairs arrest at the step of membrane fusion. *PRM1*, *FIG1*, and *KEX2* all act during late steps of yeast mating; however, mutants of both *KEX2* and *FIG1* are pleiotropic and are likely to influence membrane fusion indirectly. In contrast, Prm1p is intimately involved in controlling the fidelity of membrane fusion and may constitute a part of the yeast cell fusion machinery.

TABLE OF CONTENTS

Chapter 1	Introduction	p. 1
Chapter 2	The Plasma Membrane Proteins Prm1 and Fig1 Ascertain Fidelity of Membrane Fusion During Yeast Mating	p. 26
Chapter 3	The Yeast Cell Fusion Protein Prm1p Requires Covalent Dimerization to Promote Membrane Fusion	p. 55
Chapter 4	The Golgi-resident Protease Kex2 Acts in Conjunction With Prm1 to Facilitate Cell Fusion During Yeast Mating	p. 77
Chapter 5	Membrane Lysis During Biological Membrane Fusion: Collateral Damage by Altered Fusion Machines	p. 123
References		p. 137

LIST OF TABLES

2-1	Influence of Ca ²⁺ on Activity and Fidelity Values	p. 52
3-1	Plasmids constructed for Prm1p covalent dimerization study	p. 75
4-1	Strains used in Kex2 study	p. 120
4-S1	Scoring matrix for prediction of novel Kex2 cleavage sites	p. 122

LIST OF FIGURES

1-1	Formation of a fusion pore via stalk formation and hemifusion diaphragm	p. 23
1-2	Steps of yeast mating	p. 24
2-1	<i>PRM1</i> and <i>FIG1</i> promote the membrane fusion step during mating	p. 45
2-2	Extracellular Ca ²⁺ suppresses cell lysis in $\Delta prm1 \times \Delta prm1$ mating reactions	p. 47
2-3	Kinetics of fusion and lysis initiation in mating populations	p. 48
2-4	Lysis occurs simultaneously in each cell of a mating pair and is concomitant with cytoplasmic mixing	p. 50
2-5	<i>TCB3</i> prevents mating pair lysis in the absence of <i>PRM1</i>	p. 51
2-S1	Kinetics of fusion and lysis initiation of $\Delta prm1 \Delta fig1 \times \Delta prm1 \Delta fig1$ mating pairs	p. 53
3-1	Prm1p reduction-sensitive high molecular weight complex	p. 70
3-2	Prm1p homo-oligomerizes <i>in cis</i>	p. 71
3-3	Two cysteines are required for formation of functional covalent Prm1p dimers	p. 72
3-4	Interaction between Prm1p monomers is not affected by cysteine substitution	p. 73
3-5	Influence of charged residues in the second transmembrane domain of Prm1p on dimerization	p. 74
4-1	Replica mating strategy to isolate enhancers of <i>Δprm1</i>	p. 106
4-2	<i>Δkex2</i> enhances the <i>Δprm1</i> cell fusion defect	p. 108
4-3	<i>Δkex1</i> , but not <i>Δste13</i> , enhances the <i>Δprm1</i> cell fusion defect	p. 110
4-4	Deletion of known Kex2 substrates fails to enhance the <i>Δprm1</i> fusion defect in <i>trans</i>	p. 112
4-5	<i>Δkex1</i> and <i>Δkex2</i> mutants exhibit cell wall phenotypes similar to other	p. 113

	mutants but are unique in synergizing with <i>Aprm1</i>	
4-6	<i>Δkex2</i> x WT mating pairs fail to fuse and develop cell wall-embedded blebs	p. 114
4-7	Serial section analysis of a <i>Δkex2</i> x WT mating pair	p. 115
4-8	<i>Aprm1 Δkex2</i> x <i>Aprm1</i> mating pairs fail to fuse and develop a variety of structures	p. 117
4-9	Serial section analysis of a <i>Aprm1 Δkex2</i> x <i>Aprm1</i> mating pair	p. 118
4-10	Possible models for the mechanism of bleb formation	p. 119
5-1	Models for lipid rearrangements leading to the formation of a fusion pore	p. 135
5-2	Models for regulation of fusion integrity by non-fusase factors	p. 136

CHAPTER 1
INTRODUCTION

Membrane fusion is an important and ubiquitous process in biology. Intracellular membrane fusion is vital to the function of eukaryotic cells where it is required to traffic vesicles and other membrane structures through the secretory system and to maintain the identity and competence of membrane-bound organelles. Extracytoplasmic membrane fusion events are essential for sexual reproduction, formation of syncytia during development, and host infection by enveloped viruses.

During yeast mating the cell membranes of the two haploid cells of a mating pair fuse to form a single diploid cell. In the work described in this thesis, we study this fusion event as a model for both developmental cell fusion and membrane fusion in general. To introduce these fields, this introduction will cover the biophysics of membrane fusion and describe the protein complexes known to mediate membrane merger. Instead of covering the entire repertoire of cell fusion events, attention will be focused on promising models for which proteins thought to be directly involved in membrane fusion have been identified. Finally, a survey of all steps of yeast mating will be made, as early events set up the fusion reaction and early acting factors may also have secondary activities that are required for late events.

Lipid bilayer fusion: Lipid bilayer fusion is an energetically costly process and will not spontaneously occur under conditions found in biologically relevant contexts. In order to fuse two membranes, each bilayer must be destabilized to form non-bilayer fusion intermediates. Once bilayers are brought within a few nanometers of each other, the *cis*-leaflets can fuse, forming a hemifusion stalk in which lipid mixing but not content mixing occurs (Figure 1, B). For this to occur, the water separating the two bilayers must be

squeezed out; for this reason polyethylene glycol (PEG) can be employed to crowd out water and increase the likelihood of membrane fusion. Formation of a hemifusion stalk is energetically costly due to its high membrane curvature, the void volume at the top of the stalk, and line tension. Lateral expansion of the hemifusion stalk allows the trans-layers to come into contact forming a hemifusion diaphragm (Figure 1, C). Rupture of the hemifusion diaphragm results in a fusion pore (Figure 1, D; see Chapter 5 for alternative models).

The energetics of bilayer fusion depends on the properties of the lipids that make up the bilayer. Biological membranes contain a great diversity of lipid species. For the majority of these lipids (i.e., phosphatidylcholine (PC), sphingomelin (SM), phosphatidylserine (PS), cardiolipin (CL), phosphatidic acid (PA)) the cross-sectional area of the polar head groups and hydrocarbon region are similar. Therefore these lipids contribute zero curvature to the membranes in which they reside. By contrast, lysophosphatidylcholine (LPC) has a larger head group compared to its hydrophobic region and thus exhibits positive spontaneous curvature. Finally, cone-shaped lipids, with small head groups relative to the apolar domain, possess negative spontaneous curvature. Such cone shaped lipids include unsaturated species of phosphatidylethanolamine (PE), diacylglycerol (DAG), and fatty acid (FA). Because the stalk is negatively curved, stalk formation is promoted by lipids with spontaneous negative curvature and inhibited by lipids with positive spontaneous curvature.

The bilayer structure of the membrane can be disrupted in many ways. Lateral tension and membrane bending (to curvatures other than the spontaneous curvature) destabilize bilayers. Amphipathic molecules can interact with membranes and generate

discontinuities in the bilayer structure. Even Ca^{2+} , present at high concentrations, can promote stalk formation between bilayers containing anionic phospholipids by bridging the bilayers.

SNARE-mediated fusion: A ubiquitous and essential protein family within eukaryotes, the SNAREs (soluble *N*-ethylmaleimide-sensitive factor attachment protein receptor) are required for most intracellular membrane fusion events. They mediate both heterotypic fusion events (i.e., vesicular transport between the compartments of the secretory pathway) and homotypic fusion events (i.e., vacuole fusion).

SNAREs derive their name from the proteins that prime them for fusion, NSF (*N*-ethylmaleimide-sensitive fusion protein) and SNAP (soluble NSF attachment protein SNAP). The genetic elements encoding these factors—as well as many other membrane fusion players—were uncovered in a screen for temperature sensitive yeast mutants defective in secretion (Novick et al., 1980; Novick and Schekman, 1979). Reconstitution of transport *in vitro* allowed the identification of a *N*-ethylmaleimide (NEM) sensitive protein required for vesicular transport (Beckers et al., 1989; Malhotra et al., 1988). Binding of NSF to Golgi membranes was found to require both a soluble factor, SNAP, and an integral membrane receptor, SNARE proteins (Weidman et al., 1989). Affinity purification of these receptors from bovine brain yielded syntaxins A and B, SNAP-25, and VAMP (Sollner et al., 1993). These proteins had previously been localized to synaptic vesicles (Baumert et al., 1989; Oyler et al., 1989; Trimble et al., 1988) and were functionally implicated in both docking and fusion steps (Bennett et al., 1992; Link et al., 1992).

SNAREs appear to constitute the minimal machinery required for membrane fusion. Reconstitution of SNAREs into liposomes resulted in contents mixing accompanied by minimal leakage (Nickel et al., 1999). Specific complexes of SNAREs anchored in one membrane pair with a SNARE integrated in the other. Changing the arrangement of SNAREs between membranes abrogates their ability to form a fusogenic complex (Parlati et al., 2000). Even more striking was the finding that, despite the presence of so many SNARE family members within a single cell (25 in *Saccharomyces cerevisiae*, 36 in humans, and 54 in *Arabidopsis thaliana*), and the many possibilities of yeast SNARE pairing, the active combinations as assayed in liposome fusion assays were almost all physiologically relevant SNARE complexes (McNew et al., 2000a). This suggests that the compartmental specificity of fusion events could be influenced at the level of SNARE pairing, in addition to control by coat proteins and Rab GTPases. These liposome fusion assays have come under intense criticism due to the extremely slow rate of liposome fusion and the high concentration and variability of SNARE reconstitution. Furthermore, the liposome fusion readout may be complicated by membrane lysis (Chen et al., 2006). With regards to the caveat that liposome fusion represents a lesser task than fusing biological membranes, flipped SNARE proteins designed for cell surface expression were generated. These flipped SNAREs were able to mediate cell-cell fusion events, creating multinucleate syncytia in cell culture (Hu et al., 2003).

The defining characteristic of SNARE proteins is the SNARE motif, which consists of 60-70 residues arranged in heptad repeats. C-terminal to the SNARE motif, most SNAREs have a transmembrane domain, although some lack a true transmembrane

domain but retain membrane association via lipid modification. Another common feature is an independently folded domain N-terminal of the SNARE motif.

The oligomerization of SNARE proteins anchored in opposing membranes is thought to supply the energy required to fuse membranes. During *trans*-SNARE complex formation, four unstructured SNARE motifs fold into α -helices intertwined as a parallel bundle. The energy released by the formation of the SNARE complex, 35 $k_B T$ for C-terminally truncated SNAREs, is one of the highest protein-folding energies observed (Li et al., 2007). These interactions are for the most part hydrophobic, however, the central layer of the bundle invariably consists of three glutamines and one arginine. According to a widely accepted model, the SNARE bundle forms by zippering from the N-terminus towards the C-terminal membrane anchor, pulling opposed membranes together (Melia et al., 2002). A stiff linker between the SNARE domain and the membrane anchor would promote membrane bending or destabilize the membrane, a strain that is relieved when the membranes fuse and a *trans*-SNARE complex becomes a *cis*-SNARE complex. Consistent with this mechanical model, replacement of the transmembrane domains of yeast SNAREs Snc2p and Sso2p with a signal for geranylgeranyl isoprenyl group addition yields dominant negative mutants, presumably because of the greater flexibility of the lipid anchor (Grote et al., 2000). Interestingly, the SNARE complexes formed with the lipid modified Snc2p or Sso2p mutants were still able to promote hemifusion as evidenced by the rescue of the exocytosis defect upon addition of lysophosphatidylcholine, which promotes positive membrane curvature and may lower the energy barrier for fusion of distal leaflets in the hemifusion diaphragm. Replacing transmembrane domains with lipid anchors was also investigated *in vitro*. Though short

lipid anchors (≤ 20 carbon chain) were not able to substitute for the transmembrane domain of the v-SNARE VAMP2, much longer lipids (45 and 55 carbon tails) supported liposome fusion (McNew et al., 2000b). Furthermore, insertion of a flexible linker between the SNARE domain and the membrane anchor of syntaxin and VAMP reduces fusion activity in a linker length-dependent manner (McNew et al., 1999). Formation of a single long helix containing both the SNARE and transmembrane domain is not necessary for membrane fusion as insertion of consecutive prolines in place of the flexible linker does not affect VAMP catalyzed fusion and only mildly reduces syntaxin fusion activity.

Though the formation of a single trans-SNARE complex is energetically highly favorable, it is believed that the formation of multiple SNARE complexes is required to drive membrane fusion. The concentration dependence of a soluble fragment of VAMP2 for fusion inhibition suggested that three SNARE complexes cooperate during vesicle fusion (Hua and Scheller, 2001). Even larger estimates—5 to 8 participating syntaxin molecules—were made modeling a SNARE-lined fusion pore (Han et al., 2004). Finally, atomic force microscopy (AFM) revealed ring-like structures of SNARE complexes when SNAREs were reconstituted in liposomes and vesicles and mixed (Cho et al., 2002).

SNAREs may not be the only proteins intimately involved in the final steps of SNARE-dependent membrane fusion. This is most certainly the case in regulated exocytosis of neurotransmitters. Neurotransmitter release is Ca^{2+} -dependent and this signal triggers exocytosis with a mind-boggling response speed—on the order of milliseconds for the fast release component. The proposed Ca^{2+} sensor for fast release is

synaptotagmin I, a membrane protein with a cytoplasmic domain which binds both Ca^{2+} and negatively charged phospholipids. Importantly, phospholipid binding properties of synaptotagmin is conferred by the Ca^{2+} -bound C_2B domain (Fernandez et al., 2001). Synchronous neurotransmitter release is blocked in synaptotagmin knockout mice (Geppert et al., 1994), and the apparent affinity of synaptotagmin for Ca^{2+} in the presence of phospholipids ($K_d = 5\text{-}10\mu\text{M}$) meshes well with the concentrations required for release (Davletov and Sudhof, 1993). Through the highly positive electrostatic potential of the C_2B domain, synaptotagmin may be able to directly accelerate fusion by destabilizing bilayers. Alternatively, synaptotagmin may indirectly influence membrane fusion by regulating SNARE complexes. Synaptotagmin directly interacts with t-SNAREs and the SNARE bundle (Bai and Chapman, 2004), and has been shown to facilitate the assembly of SNARE complexes *in vitro* (Littleton et al., 2001). Another promising model for synaptotagmin action is to displace complexin, a small soluble protein which can bind to a groove of the SNARE bundle and inhibit complete *trans*-SNARE assembly (Tang et al., 2006).

Opening a fusion pore requires significant energy, and, if current models for how fusion proteins surround the initial fusion pore are correct, dissociation or rearrangement of fusion protein complexes. When lysosomes fuse with the plasma membrane, neither their membrane nor luminal contents is completely released (Jaiswal et al., 2004). However, in synaptotagmin VII knock-out MEFs, the restrictions on contents release and membrane mixing are significantly relieved.

Despite the wealth of evidence for SNAREs being the minimal machinery for fusion, contrary observations have been made in two systems: egg corticle vesicle

exocytosis and yeast vacuole fusion. Ca^{2+} -triggered corticle granule exocytosis was shown to be viable even after proteolysis separating the cytoplasmic portion of SNAREs from the transmembrane anchor (Coorsen et al., 2003; Szule et al., 2003). Vacuole fusion can be arrested after the initiation of trans-SNARE pairing, requiring phosphatase P1 activity and the ATPase membrane subunits V0. SNAREs are still required in these systems, only they do not act in the final step of the fusion reaction.

Viral fusion: Many viruses bud from host cells, packaging their genomes and accessory proteins in a lipid bilayer containing viral transmembrane glycoproteins. These glycoproteins allow released enveloped viruses to bind new host cells and fuse the viral membrane with the cell plasma membrane or endosome membrane.

Viral fusases have a transmembrane domain, which anchors them in the viral envelope, and an amphipathic fusion peptide. The fusion peptide can be located at a proteolytically formed terminus, as in hemagglutinin (HA), or within internal loops, as seen in vesicular stomatitis virus glycoprotein G (VSV-G). Upon receptor binding, fusion peptides are exposed and projected away from the viral membrane to interact with the target membrane. Subsequently, fusase refolding results in large structural changes which bend the fusase molecule into a hairpin structure with both the transmembrane anchor and the fusion peptide located at one end. Further refolding occurs to form the post-fusion structure in which both the membrane anchor and the fusion peptide are present in the same membrane.

Class I viral fusion proteins achieve this refolding by forming a central α -helical coiled-coil structure. This structure closely resembles that of the SNARE-bundle. Class II

fusion proteins form hairpins composed of beta structures, and class III fusion proteins combine elements of both the first two classes. Free energy released through refolding of the class I and class II fusion proteins, which initially reside in a metastable state, may be used to overcome the energetic barrier of membrane fusion. Refolding of a single env trimer creates sufficient energy to fuse membranes, and peptide inhibitors of HIV fusion prevent the coiled-coil structure from completely forming and inhibit viral fusion (Lawless et al., 1996; Peisajovich et al., 2003). VSV-G exists in a pH-dependent equilibrium between pre- and post-fusion states and much less energy is released during the transition to the post-fusion state. In this case, the collaboration of multiple VSV-G oligomers is necessary to catalyze merger. Despite the energetic scorecard, many trimers are thought to be involved in forming a fusion pore, even for class I fusases.

The refolding of viral fusases into a hairpin structure is reminiscent of the SNARE bundle, but instead of having at least one full transmembrane domain anchored in each membrane to be fused, the fusase molecule can use only one transmembrane anchor. This anchor is absolutely essential, as substituting the transmembrane domain of HA with a GPI lipid anchor yields hemifusion instead of complete fusion (Kemble et al., 1994). The fusion peptide provides the link to the other membrane, but its properties are much different than a transmembrane domain. Due to its amphipathic character, fusion peptides may promote stalk formation by destabilizing the host membrane. Fusion peptides have strict sequence requirements—mutation of the N-terminal glycine of the HA fusion peptide to serine results a fusase capable of only hemifusion (Qiao et al., 1999). Alternative models for HA-mediated fusion envisage insertion of the fusion peptide into the viral envelope. Because of oligomerization of HA trimers, the insertion

of many fusion peptides in the viral membrane would cause it to dimple, creating bending stresses that could promote the transition to hemifusion (Kozlov and Chernomordik, 1998). Or, if the fusion peptide were first inserted in the viral membrane and then pulled out during refolding, membrane defects would be created (Bentz, 2000a). Lipids from the trans membrane could resolve the defect, their exit from the host bilayer aided by the removed fusion peptides, leading to stalk formation. Diffusion of lipids from the viral envelope to fill the voids is prevented by a corral-like structure formed by multiple viral fusase trimers.

Fusion of enveloped viruses provides one of the simplest paradigms for membrane fusion. Specificity and targeting are mediated by receptor binding which triggers insertion of the fusion peptide into either the viral or host membrane. Refolding places the membrane anchor and fusion peptide at the same end of the trimer hairpin. By simultaneously destabilizing bilayers and bringing them in close proximity, membrane fusion is achieved.

A new development in the viral field is the emergence of a new, wildly different class of fusion proteins—the FAST proteins. These small (14kD) integral membrane proteins are encoded in reovirus genomes and expand viral infection of by fusing infected cells with neighboring cells (Salsman et al., 2005). Using both liposome-cell and liposome-liposome fusion assays, it was shown that the FAST protein p14 was sufficient for membrane fusion (Top et al., 2005). The FAST proteins are lipid modified and their fusogenic activity requires host factors, such as cadherins, to tether membranes for their fusogenic activity to function. Thus, the role FAST proteins play in membrane fusion is simpler than the viral envelope fusases described above. The fine control of FAST

protein localization, coupling to tethering molecules, and FAST protein oligomerization are important questions regarding how this novel class of proteins fuses membranes.

Mitochondrial fusion: Within eukaryotic cells, mitochondria have a dynamic tubular structure. The constant processes of mitochondrial fusion and fission maintain this structure, and condition specific regulation of the balance between fusion and fission occurs during differentiation and apoptosis (Cervený et al., 2007). To merge, mitochondria must fuse both outer and inner membranes.

Though the mechanism is not yet clear, mitochondrial fusion is achieved through the activities of two outer membrane proteins Fzo1p and Ugo1p, and a protein localized to the intermembrane space, Mgm1p. About half of Mgm1p molecules are anchored in the inner membrane, the rest are proteolytically processed but remain membrane associated. Mammalian homologs mitofusins 1 and 2 and OPA1 have similar activities and processing events. Fzo1p and Mgm1p are dynamin related GTPases. Dynamin self-assembles into rings and spirals and can tubulate lipid bilayers. Upon GTP binding dynamin can constrict and fragment these tubules. Yet it remains controversial whether dynamin acts as a mechanoenzyme or a classical GTPase, by recruiting and activating effectors (Danino and Hinshaw, 2001).

In an *in vitro* mitochondrial fusion assay, the events of outer membrane fusion and inner membrane fusion can be separated (Meeusen et al., 2006). Fzo1p is required for outer membrane fusion. After outer membrane fusion, Mgm1p tethers opposing inner membranes by self-association across membranes. Using temperature sensitive alleles of *MGMI* that were not compromised in tethering, Nunnari and coworkers showed that

Mgm1p is also required downstream of membrane apposition for inner membrane fusion. A few models of how Mgm1p works to promote inner membrane fusion have been proposed: Because Mgm1p self-associates in trans via coiled-coil domains, a SNARE-like mechanism of pulling membranes together is possible. Alternatively, Mgm1p may create inner membrane tubules, yielding fusogenic tips with high curvature (Meeusen et al., 2006).

Worm development: Cell fusion events are common during nematode development, occurring during the formation of varied cell structures in the adult body such as the pharynx, the epidermis, and the uterus. Amazingly, 300 of the 959 adult *C. elegans* hermaphrodite nuclei reside in syncytial cells. The purpose of forming these syncytia is not clear, but mutants unable to perform the normal cell fusions are morphologically abnormal and sometimes form second copies of a structure (Mohler et al., 2002).

Epithelial cell membrane fusion during *C. elegans* development requires a single-pass membrane protein, EFF-1 (Mohler et al., 2002). Expression from the *eff-1* promoter is regulated temporally and spatially, being turned on in both epithelial and non-epithelial cells destined to fuse. Ectopic expression of EFF-1 resulted in cell fusion events between cells that do not normally fuse (Shemer et al., 2004). Further evidence that EFF-1 is a bona fide fusion protein, expression in Sf9 insect cells drives fusion resulting in multinucleate syncytia (Podbilewicz et al., 2006). To catalyze cell fusion, EFF-1 must be expressed by both cells. EFF-1 localizes to membrane interfaces of fusion-fated cells (del Campo et al., 2005). This localization depends on EFF-1 in the partner cell and a stretch of hydrophobic residues in the ectodomain. Also located in the EFF-1 ectodomain is a

putative phospholipase domain; however, mutagenesis of active site residues demonstrated that lipase activity is not required for EFF-1-regulated cell fusion (del Campo et al., 2005).

Most developmental cell fusion events in *C. elegans* require EFF-1, the exceptions being anchor cell fusion, formation of the vulval tube, and sperm-egg fusion. A recent study has shown that anchor cell fusion and formation of the vulval tube are mediated by AFF-1, a protein closely related to EFF-1 (26% identity) (Sapir et al., 2007). Like EFF-1, AFF-1 expression is limited to the cells it fuses and ectopic and heterologous expression are sufficient to catalyze cell fusion.

Mechanistically, it is not understood how EFF-1 and AFF-1 fuse membranes. EFF-1 oligomerizes in *cis* (Podbilewicz et al., 2006), and given that EFF-1 localization depends on expression in partner cells, it is likely that EFF-1 can interact across membranes as well. Solving the structure of the EFF-1 ectodomain oligomers may yield important mechanistic clues.

Yeast mating: The best studied cell-cell fusion event is yeast mating, in which two haploid mating types fuse to form a diploid. This system has been an important model for cell-cell communication, signal transduction, and polarized growth. Less appreciated is the problem of cell wall rearrangement in mating pairs, a complex process where remodeling enzymes must make two cell walls continuous then locally remove material to allow for membrane contact. Finally, diploid formation involves two distinct membrane fusion events—cell membrane fusion and nuclear fusion (“karyogamy”).

Yeast cells can exist in both haploid and diploid states (in addition to many arrangements of higher chromosome number). Both haploid and diploid cells reproduce asexually by budding. When diploid cells are subject to environmental stresses, approximated in the laboratory by sugar and nitrogen starvation, they undergo a meiotic sporulation. The resulting ascospore will contain two spores of each mating type: **a** and α . Sexual reproduction is achieved via the mating of cells of opposite mating types.

The differences between **a** and α cells are created by the transcriptional regulation of a few key mating pathway genes by the mating-type locus (*MAT*). The *Mata*1p and *Mata*2p proteins are encoded by *MAT* α locus. *Mata*1p, in conjunction with *Mcm*1p, drives transcription of α -specific genes, and a *Mata*2p-*Mcm*1p complex blocks transcription of **a**-specific genes, which are transcriptionally active by default. The *Mata*1p protein encoded by the *MAT***a** locus does not have a function in haploid cells, but turns off haploid specific genes in *MAT* α /*MAT***a** diploids by changing the specificity of *Mata*2p. α -specific genes encode α -factor precursors and **a**-factor receptor. **a**-specific genes similarly encode the **a**-factor precursors and the α -factor receptor in addition to *Ste*6p, the exporter for **a**-factor, and *Bar*1, a protease which degrades α -factor. Agglutinins, cell wall proteins that mediate cell adhesion, are also mating type specific. Pheromone and receptor are the key differences between mating types as expression a particular pheromone and receptor pairs in haploids with no mating type specific expression can dictate mating specificity (Bender and Sprague, 1989). Furthermore, these cells are able to fuse and form a diploid with a partner of opposite mating type identity.

Haploid cells choose a mating partner by navigating pheromone gradients to choose a partner with high pheromone expression (Jackson and Hartwell, 1990). The

pathways for biosynthesis and export of α -factor and **a**-factor are very different. α -factor is produced from two precursors which contain multiple repeats of the α -factor sequence. These signal sequence containing precursors are delivered to the ER where the signal sequence is cleaved and the *pro*-domain is glycosylated. *pro*- α -factor then is delivered to the Golgi where the endoproteinase Kex2p cleaves C-terminal to dibasic residues. Finally, these products are trimmed by Kex1p and Ste13p, which remove the new C-terminal dibasic residues and new N-terminal -x-A- spacer dipeptides, respectively, to yield a mature α -factor peptide of 13-residues (see Chapter 4 for a Kex2p activity unrelated to pheromone processing). **a**-factor is made from two short (36 and 38 residues) precursors. The precursor is lipid modified by the addition of a farnesyl group to a C-terminal cysteine by Ram1p and Ram2p. Subsequently, three C-terminal residues are removed and the new C-terminus is methyl-esterified. After N-terminal processing, mature **a**-factor is exported by the multipass transmembrane protein Ste6p, an ABC transporter. Following secretion or export, the mating pheromones diffuse away from the cell in which they were synthesized, creating a gradient that indicates the cell's identity and location. **a** cells secrete a protease, barrier (Bar1), which degrades α -factor. This lowering of the α -factor signal results in increased gradient detection accuracy (Barkai et al., 1998).

Pheromone gradients are sensed by the serpentine G-protein-coupled receptors Ste2p (α -factor receptor) and Ste3p (**a**-factor receptor). α -factor binds its receptor with a K_d of 7 nM (Yu et al., 1989). The C-terminal portion of the peptide is required for receptor binding, whereas the N-terminus is dispensable for binding but required for activation. The active ligand-receptor complex is thought to be a bent peptide; the center

of the peptide is bound in a pocket formed by two extracellular loops, while the aromatic residues at both ends interact with multiple transmembrane domains (Naider and Becker, 2004). Rotation of the transmembrane domains (TMs) or piston-like movements of receptor TMs transmit the information of pheromone binding.

The pheromone response promotes mating pair formation and fusion through multiple branches including transcriptional induction, posttranslational activation, and cell polarization. Pheromone binding by the receptors induces dissociation of the heterotrimeric G-protein ($G\alpha$, GPA1; $G\beta$, STE4; $G\gamma$, STE18), allowing $G\beta\gamma$ to bind the PAK kinase Ste20 and Ste5, initiating a signaling cascade. Ste20 phosphorylates Ste11p, a MAPKKK, which in turn phosphorylates the MAKK Ste7, which phosphorylates the MAPK Fus3. Ste5 serves as a scaffold for the three MAPKs. Activated Fus3 prepares the cell for cell fusion in multiple ways. One important substrate of Fus3 is Far1. Upon Far1 phosphorylation by Fus3, cells arrest in G1, ensuring a single, fully replicated haploid genome prior to karyogamy. A second set of important substrates is Dig1 and Dig2, negative regulators of the transcription factor Ste12. Their phosphorylation relieves Ste12 inhibition and allows transcription of genes containing pheromone response elements (PRE) in their promoters. In addition to Ste12 activation and cell cycle arrest, cell wall integrity and high osmolarity pathway signaling is activated, evoking a complex and large transcriptional response to pheromone treatment. Gene expression profiling utilizing a comprehensive set of conditions and multiple pathway mutants found 383 α -factor regulated genes (Roberts et al., 2000). Of these, about 130 genes were induced by pheromone in a polarization stress-independent manner. Many gene products in this set

have been described to act in pheromone production and sensing, agglutination, cell wall remodeling, membrane fusion, and karyogamy.

Pheromone gradient detection reorients cell polarity towards a partner. To achieve this, two pathways converge that both contain general polarity factors as well as mating specific species. In addition to Ste20p and Ste5p, G β also interacts with Cdc24p and Far1p (Nern and Arkowitz, 1999). Simultaneously, activated Fus3p kinase, possibly recruited by Gpa1p, phosphorylates the formin Bni1p (Matheos et al., 2004). Assembling these components at the cell cortex results in actin cable nucleation. The polarisome core components, Spa2p, Pea2p, and Bud6p, relocalize from the bud rings and direct vesicle traffic towards the mating partner. This directed vesicle traffic results in polarized growth and a morphological change to a pear-shaped cell termed a “shmoo.” Ultrastructural analysis of shmooing cells revealed hundreds of electron dense vesicles 60-70nm concentrated in the shmoo (Baba et al., 1989). These vesicles likely contain hydrolytic enzymes for cell wall removal, as well as newly synthesized fusion-regulating proteins. The plasma membrane of the shmoo has different properties than the membrane surrounding the rest of the cell and is preferentially stained by lipid dyes filipin and laurdan, consistent with the shmoo membrane being a large raft domain (Bagnat and Simons, 2002; Proszynski et al., 2006). Furthermore, the shmoo tip protein Fus1p is resistant to detergent extraction and mislocalizes in mutants unable to produce ergosterol and sphingolipids.

Building a shmoo requires cell wall remodeling to allow polarized growth and maintain cell integrity. *PKC1* mutants unable to sense cell wall stress, lyse at a high rate upon α -factor treatment in hypotonic conditions (Jin et al., 2004). Polarized growth also

triggers an influx of Ca^{2+} (Ohsumi and Anraku, 1985). Two Ca^{2+} influx systems function in non-overlapping contexts: a high-affinity Cch1p-Mid1p Ca^{2+} channel, and a low-affinity Fig1p-dependent pathway (Muller et al., 2001; Muller et al., 2003). Polarization induced Ca^{2+} influx likely plays a role in stress response—Fig1, Cch1, and Mid2 all influence the extent of cell death after extended pheromone treatment (Iida et al., 1990; Zhang et al., 2006).

When shmooing cells finally meet, agglutinins bind them together tightly. The cell walls of each mating partner are stitched together such that wall material at the center of cell-cell contact, the septum, can be safely removed (Gammie et al., 1998; Osumi et al., 1974). The process of septum removal is regulated by many proteins, including Fus1p and Fus2p. Fus1p is a single pass transmembrane protein expressed during mating conditions (McCaffrey et al., 1987). Upon pheromone induction, Fus1p localizes to the shmoo tip; this localization is dependent on Chs5p-mediated polarized transport (Santos and Snyder, 2003). In the absence of Fus1p, mating pairs arrest at the cell wall removal step. Electron micrographs of *fus1 x fus1* mating pairs revealed that most fail to localize and align vesicles adjacent to the septum (Gammie et al., 1998). This polarization phenotype may reflect functional interactions between Fus1p and morphogenesis players Bni1p and GTP-bound Cdc42p suggested by two-hybrid interactions (Nelson et al., 2004). Fus1p also binds and inhibits the osmosensor Sho1p, presumably to allow mating specific cell wall remodeling events. Fusion pore opening is limited and expansion retarded in *fus1 x fus1* mating pairs consistent with its role in removing cell wall material; however, a separate and direct role for Fus1p in pore opening and expansion is formally possible (Nolan et al., 2006).

Another important regulator of cell wall events during yeast mating is Fus2p. Like *FUS1*, *FUS2* is only transcribed in response to pheromone. *FUS2* encodes a large cytoplasmic protein which localizes to the cell volume inside the shmoo (Elion et al., 1995). Fus2p pellets in high speed spins, indicative of association with the cytoskeleton or membranes. Like *fus1 x fus1* mating pairs, *fus2 x fus2* mating pairs also fail to accumulate as many vesicles at the fusion zone as wild-type, but these vesicles were correctly polarized (Gammie et al., 1998). Fus2p interacts with Rvs161p, an amphiphysin homolog with separable fusion and endocytosis activities, and Fus2p is unstable in strains bearing mating defective alleles of *RVS161* (Brizzio et al., 1998). Both *fus2 x fus2* and *rvs161 x rvs161* mating pairs exhibit electron dense plaques at the plasma membrane-septum interface of unfused mating pairs (Gammie et al., 1998). *FUS1* and *FUS2* have distinct functions, as the double mutant has a much more severe cell fusion phenotype than either of the single mutants (Trueheart et al., 1987).

When sufficient cell wall remodeling has occurred such that the plasma membranes of each partner can come into contact, fusion rapidly ensues. Measurements of the initial permeance estimate a pore radius of 25 nm (Nolan et al., 2006). Efficient membrane fusion requires the multipass membrane protein Prm1p (Heiman and Walter, 2000). *PRM1* expression is mating specific, and Prm1p localizes to the shmoo tip in α -factor treated *MATa* cells and the fusion zone in mating pairs. As long as one partner of a mating pair expresses Prm1p, fusion proceeds at nearly wild-type levels. But when both partners lack Prm1p, only 40% of mating pairs successfully fuse plasma membranes. Of the remaining mating pairs, most arrest at the step of membrane fusion with bilayers in tight apposition along an extensive region of contact. A third outcome of *prm1 x prm1*

mating pairs is simultaneous cell lysis (Jin et al., 2004). This lysis is dependent on membrane contact, cannot be suppressed with osmotic support, and is sensitive to the presence of calcium (Aguilar et al., 2007; Jin et al., 2004). Prm1p exists as a covalently linked homodimer and may play a structural role in organizing the fusion machinery (see Chapters 3 and 5).

The final step of yeast mating is karyogamy. After plasma membranes fuse pore expansion and further removal of the septum continue such that nuclei can migrate to the center of the mating pair and fuse. Congression of nuclei require microtubules and the kinesin Kar3p. Recently a model for congression has been proposed in which Kar3p, Bik1p, and Kar9p promote MT plus end interactions of opposed networks and nuclei are pulled together by MT depolymerization (Molk et al., 2006). Once nuclei meet they must undergo two fusion reactions—a cytoplasmic fusion event of the outer nuclear membranes and an ER luminal fusion event to merge inner membranes. Nuclear fusion initiates at the spindle pole body. A pheromone induced transmembrane protein Kar5p localizes near the spindle pole and *KAR5* mutants are strongly deficient in karyogamy despite normal nuclear congression (Beh et al., 1997). Kar5p likely interacts with another integral ER membrane protein Sec71p, as Kar5p is unstable in *sec71* strains and *KAR5* and *SEC71* mutant alleles show fascinating genetic interactions (Brizzio et al., 1999; Kurihara et al., 1994). Sec71p is part of a post-translocational translocation complex with Sec63p and Sec72p, which are also karyogamy players (Ng and Walter, 1996). Sec63p contains a DnaJ domain, which may interact with the Hsp70 DnaK family chaperone Kar2p. Another DnaJ protein, Jem1, is a luminal membrane associated protein also required for karyogamy. The mechanism by which Kar5p and the translocation proteins

promote membrane fusion may involve pulling outer membranes together by translocating an integrated protein from one membrane through a translocation pore in the other membrane. Alternatively, association of translocation pores between opposed membranes and coordinated pore opening could also achieve merging of ER membranes (Peters et al., 2001).

Big questions in membrane fusion: Enormous progress has been made in the last 20 years in identifying membrane fusion proteins and understanding their mechanism of action. For SNARE fusion and enveloped virus fusion detailed questions about stoichiometry and organization can now be asked. For developmental cell fusion events the machinery responsible for fusion remains elusive. All classes of fusases must influence a diverse ensemble of lipids to form non-bilayer structures, progress to fusion pores, and expand the fusion pores. Much remains to be answered regarding the structures of these intermediates and the mechanism by which fusases facilitate their formation.

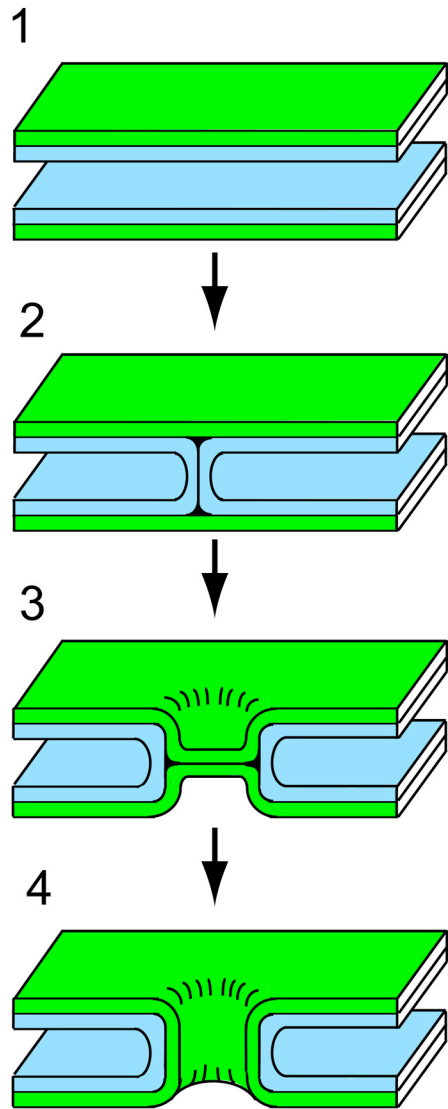


Figure 1. Formation of a fusion pore via stalk formation and hemifusion diaphragm. *Cis*-leaflets are colored blue; *trans*-leaflets are colored green.

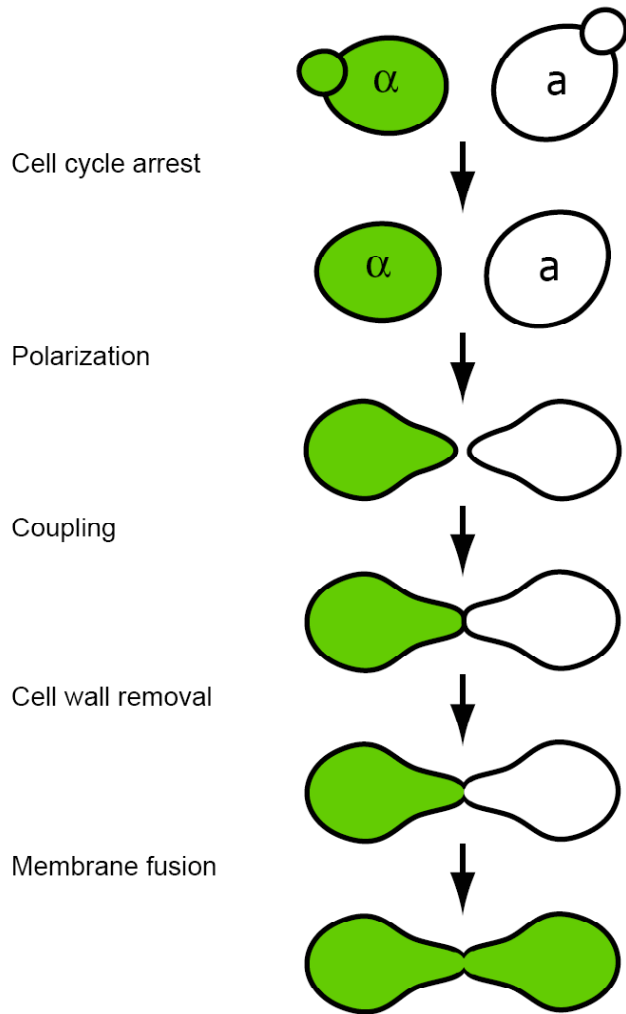


Figure 2. Steps of yeast mating. Cytoplasmic continuity is indicated by the spread of $MAT\alpha$ cytoplasm (green) into the $MATa$ partner.

The material in Chapter 2 was originally published online December 6, 2006 and appeared in print February 1, 2007 (*Mol Biol Cell*. 18:547-56), Copyright © 2007 by The American Society for Cell Biology. The article is available online at:

<http://www.molbiolcell.org/cgi/content/abstract/E06-09-0776v1>

CHAPTER 2

THE PLASMA MEMBRANE PROTEINS PRM1 AND FIG1 ASCERTAIN FIDELITY OF MEMBRANE FUSION DURING YEAST MATING

The Plasma Membrane Proteins Prm1 and Fig1 Ascertain Fidelity of Membrane Fusion During Yeast Mating

Pablo S. Aguilar*#, Alex Engel*, and Peter Walter

Howard Hughes Medical Institute, and

Department of Biochemistry and Biophysics

University of California at San Francisco

San Francisco, CA 94158

* these authors contributed equally to this work

corresponding author:

pablo.aguilar@ucsf.edu

415 476 5676

ABSTRACT

As for most cell-cell fusion events, the molecular details of membrane fusion during yeast mating are poorly understood. The multipass membrane protein Prm1 is the only known component that acts at the step of bilayer fusion. In its absence, mutant mating pairs lyse or arrest in the mating reaction with tightly apposed plasma membranes. We show that deletion of *FIG1*, which controls pheromone-induced Ca^{2+} influx, yields similar cell fusion defects. While extracellular Ca^{2+} is not required for efficient cell fusion of wild type cells, cell fusion in *prm1* mutant mating pairs is dramatically reduced when Ca^{2+} is removed. This enhanced fusion defect is due to lysis. Time-lapse microscopy reveals that fusion and lysis events initiate with identical kinetics, suggesting that both outcomes result from engagement of the fusion machinery. The yeast synaptotagmin ortholog and Ca^{2+} binding protein Tcb3 has a role in reducing lysis of *prm1* mutants, which opens the possibility that the observed role of Ca^{2+} is to engage a wound-repair mechanism. Thus, our results suggest that Prm1 and Fig1 have a role in enhancing membrane fusion and maintaining its fidelity. Their absence results in inefficient fusion and frequent mating pair lysis, which is counteracted by Ca^{2+} -dependent membrane repair.

INTRODUCTION

Membrane fusion is an essential process, affording the dynamic communication between membrane-bounded organelles in all eukaryotic cells. Membrane vesicles constantly pinch off one membrane and fuse with another providing transport shuttles between

distinct compartments. For each fusion event, lipid bilayers have to be brought into tight contact so that lipids can flow between two apposing bilayers, leading to their union. These events are catalyzed by specific fusases, the best characterized ones being the family of SNARE proteins that mediate intracellular transport vesicle delivery, and viral fusion proteins that mediate entry of enveloped viruses into cells by fusion with the plasma membrane or endocytic membranes (Weber *et al.*, 1998; Jahn *et al.*, 2003; Kielian and Rey, 2006).

Biological membranes do not fuse spontaneously because of a large energy barrier that must be overcome by dehydration and destabilization of the apposed membranes. Both viral fusases and SNAREs are thought to overcome this barrier by forming tight coiled-coil interactions that bring membrane anchors from each membrane in close proximity, thereby squeezing out water and distorting the packing of membrane lipids to allow fusion (Sollner, 2004). For other membrane fusion events, such as cell-cell fusion, the players and the mechanism have remained largely elusive.

Cell-cell fusion events occur during sperm-egg fusion in fertilization, syncytia formation during development such as myoblast fusion to form myotubes, tumorigenesis (Chen and Olson, 2005) and the mating of haploid yeast cells to form diploid cells. A common mechanism for cell-cell fusion has not been elucidated, but all characterized fusion mechanisms are thought to involve integral plasma membrane proteins, which bring bilayers into tight apposition and distort them sufficiently to promote lipid flow between them (Jahn *et al.*, 2003). Current models suggest that first a lipid stalk forms between the apposing leaflets of the two bilayers, leading to a state called “hemifusion” in which the outer monolayers are continuous yet the inner monolayers remain distinct.

The hemifusion state is then resolved by establishing a fusion pore through the center of the stalk (Jahn *et al.*, 2003).

A few integral membrane proteins have been described to promote cell-cell fusion, yet it is not clear what relative contributions they provide to the membrane fusion step. EFF-1, for example, is necessary for epidermal cell fusion, which serves in *Caenorhabditis elegans* to form a continuous syncytium (Mohler *et al.*, 2002). EFF-1 is a type-I plasma membrane protein and localizes to fusion zones. Importantly, expression of EFF-1 in cells that would not normally fuse is sufficient to cause cell-cell fusion (Shemer *et al.*, 2004; del Campo *et al.*, 2005), strongly implicating EFF-1 as a core part of the fusion machinery. In myoblast fusion, numerous integral membrane proteins are important for cell migration and adhesion; yet cytoplasmic proteins (such as Ants and Rols) also play important roles and interact with fusion-relevant membrane proteins (Taylor, 2002). The tetraspanin CD9 is required in mouse eggs for fertilization, suggesting that specialized membrane domains may be assembled for fusion by tetraspanins (Kaji *et al.*, 2000; Hemler, 2001).

The fusion of haploid yeast cells of opposite mating types provides a genetically tractable model system to study cell-cell fusion. Despite this experimental advantage, characterization of the yeast plasma membrane fusion machinery has been slow. Diploid formation is a multistep process requiring pheromone secretion and sensing, cell cycle arrest, cell polarization toward the mating partner, cell-cell agglutination, cell wall remodeling so that the two plasma membranes can touch, plasma membrane fusion to form a fused mating pair, and finally karyogamy (White and Rose, 2001).

The first gene, *PRM1*, participating the plasma membrane fusion step *per se* was

initially identified using a bioinformatics approach (Heiman and Walter, 2000). Prm1 is a multipass membrane protein only expressed in the mating context and is required for efficient membrane fusion. Prm1 localizes to the cell surface at the fusion zone in mating pairs. In its absence, 40% remain arrested as unfused mating pairs (prezygotes), with plasma membranes closely apposed but unfused (Heiman and Walter, 2000; Jin *et al.*, 2004). Unfused mating pairs exhibit cytoplasmic bubbles, in which the two apposed plasma membrane are pushed at the zone of contact into one or the other cell of the unfused mating pair (Heiman and Walter, 2000). A second outcome of mating in the absence of *PRM1* is cell lysis. An additional 20% of *prm1Δ* x *prm1Δ* mating pairs lyse. Lysis depends on membrane contact, as further removing *FUS1*, an upstream gene that promotes cell wall removal, suppresses mating pair lysis (Jin *et al.*, 2004). This observation suggests that lysis occurs as a consequence of the engagement of a defective membrane fusion machine. Fusion pores in *prm1Δ* x *prm1Δ* mating pairs have decreased initial permeance, further suggesting that Prm1 is a regulator of the fusion machinery (Nolan *et al.*, 2006).

Ca²⁺ has been implicated as a player in a variety of membrane fusion events. In most of the cases, Ca²⁺ is thought to act as the second messenger signal. During neuronal exocytosis, for example, neurotransmitter release is regulated through the Ca²⁺ binding protein synaptotagmin-I (Koh and Bellen, 2003). Upon Ca²⁺ binding, synaptotagmin-I interacts with phospholipids and syntaxin, a component of the SNARE protein complex that promotes bilayer fusion (Bhalla *et al.*, 2006). Repair of plasma membrane disruption in mammalian cells similarly involves Ca²⁺ dependent exocytosis, in the case of lysosomes or lysosome-derived vesicles, possibly using synaptotagmin VII as the sensor (Reddy *et al.*, 2001). Like the synaptotagmins, myoferlin also possesses multiple C2 Ca²⁺-binding domains. It is upregulated upon muscle injury and is required for efficient

myoblast fusion (Doherty *et al.*, 2005). During vacuole fusion trans-SNARE interactions result in Ca^{2+} release from the vacuole lumen (Merz and Wickner, 2004).

In yeast, mating pairs of cells lacking *FIG1* have subtle fusion defects, which can be enhanced by removing calcium and suppressed using higher calcium concentration (Erdman *et al.*, 1998). *FIG1* encodes a four-spanning membrane protein, is required for a peak of calcium influx seen after pheromone treatment of cells, and promotes rapid death in a fraction of cells exposed to high pheromone (Erdman *et al.*, 1998; Muller *et al.*, 2003a; Zhang *et al.*, 2006). The significance of pheromone-induced Ca^{2+} influx for yeast cell mating is not known.

Here we show that Fig1 is required for efficient membrane fusion during yeast mating and that Ca^{2+} -depletion increases lysis of *fig1* Δ x *fig1* Δ and *prm1* Δ x *prm1* Δ mating pairs. Lysis occurs with identical kinetics as cell-cell fusion initiation, strengthening the hypothesis that mating pair lysis is an off-pathway outcome caused by engagement of defective cell-cell fusion machinery. We identify the yeast synaptotagmin homolog Tcb3 as a mediator of Ca^{2+} -dependent lysis prevention.

RESULTS

***FIG1* has a role in the membrane fusion step of yeast mating**

To identify additional mutants that are defective at the step of membrane fusion, we asked if mating of mutants bearing deletion of non-essential genes results in unfused mating pairs (prezygotes) that display cytoplasmic bubbles as observed in *prm1* Δ x *prm1* Δ matings. Bubble formation is indicative of successful cell wall degradation without plasma membrane fusion. To this end, we screened genes that were identified by a bioinformatics approach as pheromone-induced membrane proteins (Heiman and Walter, 2000). Indeed, mating cells bearing deletions of the most highly pheromone induced candidate gene *FIG1* yielded an accumulation of unfused mating pairs and approximately one-tenth of those showed the bubble phenotype (Figure 1A). This

observation suggests that Fig1 —like Prm1— has a role in promoting membrane fusion during yeast mating. *FIG1* was originally identified as a pheromone induced gene that encodes a membrane protein with four potential transmembrane domains (Erdman *et al.*, 1998).

The cytoplasmic bubbles in unfused mating pairs resulting from *fig1Δ* x *fig1Δ* crosses were indistinguishable in appearance by fluorescent microscopy from the bubbles seen in *prm1Δ* x *prm1Δ* mating pairs (Figure 1A). Examination of thin-sections of *fig1Δ* x *fig1Δ* unfused mating pair bubbles by transmission electron microscopy confirmed that the cell wall between the mating partners was removed over extended areas with membranes protruding into one mating partner (Figure 1B). In these regions, the plasma membranes of both cells were in close, evenly spaced apposition (~10 nm), as previously reported for *prm1Δ* x *prm1Δ* unfused mating pairs (Heiman and Walter, 2000).

We quantified cell fusion efficiency using a microscopy assay, imaging mating pairs with one partner expressing soluble cytosolic GFP. Fused mating pairs are easily distinguished from unfused ones because GFP diffuses throughout the entire mating pair. In addition, we stained cells in each mating reaction with a vital dye, which allowed us to score mating-induced cell lysis (Jin *et al.*, 2004). Unilateral matings in which *FIG1* was deleted in one of either mating type led to only minor, insignificant mating defects (Figure 1C; wt x *fig1Δ*). By contrast, cell fusion was reduced by ~25% in a bilateral cross where both mating partners lacked *FIG1* (Figure 1C; *fig1Δ* x *fig1Δ*; ~20% unfused and ~6% lysed). The fusion defect of *fig1Δ* x *fig1Δ* mating reactions was weaker than the 60% effect typically observed in *prm1Δ* x *prm1Δ* mating reactions (Figure 1C; *prm1Δ* x *prm1Δ*; 35% unfused and 25% lysed). Note that a significant fraction of the increased mating failure in *prm1Δ* x *prm1Δ* mating reactions is due to cell lysis.

The mild cell fusion phenotype of *fig1Δ* x *fig1Δ* mating reactions suggests that *PRM1* is still functional in these strains. This notion is corroborated by the strong synthetic phenotype observed for *prm1Δ fig1Δ* double mutants. Compared with the

prm1Δ x *prm1Δ* mating reaction (~40 % fused mating pairs), the *prm1Δ fig1Δ* x *prm1Δ fig1Δ* double mutant mating reaction suffers a marked reduction (~10% fused mating pairs; Figure 1C). This 4-fold decrease in fusion efficiency is the result of the accumulation of more unfused mating pairs and not of increased lysis.

Unfused mating pairs in *prm1Δ fig1Δ* x *prm1Δ fig1Δ* mating reactions exhibited bubbles, indistinguishable from those seen in the single mutants both in abundance and in morphology as assessed by fluorescence and electron microscopy (Figures 1A and 1B). These results indicate that *FIG1* plays a role at the step of membrane fusion.

The residual fusion activity in *prm1Δ* x *prm1Δ* mating reactions requires extracellular Ca²⁺

Fig1 was recently described as regulator of pheromone-induced Ca²⁺ influx (Muller *et al.*, 2003a). This observation prompted us to explore the possibility that the membrane fusion reaction in cell-cell fusion might require Ca²⁺. As shown in Figure 2A, fusion of wildtype cells was completely insensitive to the Ca²⁺ chelator EGTA. By contrast, we discovered to our surprise that the residual fusion observed in *prm1Δ* x *prm1Δ*, and *prm1Δ fig1Δ* x *prm1Δ fig1Δ* mating reactions was significantly inhibited when Ca²⁺ was removed from the media by addition of EGTA. In the presence of EGTA, the production of fused mating pairs was reduced 10-fold in the *prm1Δ* x *prm1Δ* and *prm1Δ fig1Δ* x *prm1Δ fig1Δ* fusion reactions, and reduced to a lesser degree (1.4-fold) in the *fig1Δ* x *fig1Δ* fusion reaction (Figure 2A). Fusion efficiency of a *fus1Δ* x *fus1Δ* mating reaction where cell fusion is blocked at the cell wall remodeling step (McCaffrey *et al.*, 1987; Trueheart *et al.*, 1987; Gammie *et al.*, 1998) was not sensitive to Ca²⁺ chelation, suggesting that extracellular Ca²⁺ removal affects one or more steps after cell wall remodeling.

Interestingly, the reduction in cell fusion efficiency of the *prm1Δ* x *prm1Δ*, and *prm1Δ fig1Δ* x *prm1Δ fig1Δ* fusion reactions in the absence of Ca²⁺ was due almost

exclusively to an increase in cell lysis (Figure 2A). For the *fig1Δ* x *fig1Δ* fusion reaction, the reduction in fusion efficiency in the absence of Ca²⁺ was due to increases in both cell lysis and accumulation unfused mating pairs.

To confirm that the sensitivity of the mating reaction to EGTA was indeed due to Ca₂₊ removal rather than chelation of some other divalent cation, we developed a quantitative mating assay using liquid growth media (see *Methods*). The cell fusion efficiency of *prm1Δ* x *prm1Δ* mating pairs was the same in synthetic media using the liquid assay as in our standard mating assay on YPD plates. We then removed Ca²⁺ from the synthetic media by incubation with a BAPTA-resin. Cell fusion dropped to levels comparable to those observed in 20 mM EGTA-YPD (Figure 2B), and an equivalent increase in mating pair lysis was measured. Upon readdition of different divalent cations such as Ca²⁺, Mn²⁺, Zn²⁺, Mg²⁺ and Cu²⁺, only Ca²⁺ suppressed the *prm1Δ* x *prm1Δ* fusion defect (Figure 2B). Surprisingly, higher levels of extracellular Ca²⁺ (2 – 10 mM) alleviate the *prm1Δ* x *prm1Δ* fusion defect even further (Figure 2C). These assays performed with a wide range of Ca²⁺ concentrations show a direct relationship between the extracellular concentration of Ca²⁺, cell fusion, and reduction of lysis. We therefore conclude that Ca²⁺ helps prevent cell lysis and promotes fusion, and that it is required in *prm1Δ* x *prm1Δ* mating pairs after cell wall removal.

Fusion and EGTA-induced lysis occur with similar kinetics

The analyses described so far suggest that mating-induced cell lysis and cell fusion are linked events. According to this notion, lysis would result from the initiation of a fusion event that fails to go to completion. One prediction of this scenario is that fusion and lysis events should occur with similar time courses. To test this prediction, we collected kinetic data using time lapse microscopy to determine when fusion and lysis events occur in the lifetime of a mating pair. We followed cell fusion by imaging mating mixtures on agar slips at 2.5 minute intervals for three hours. Because mating pairs form

asynchronously in a mating mixture, we established a reference time point to make comparison between different mating pairs possible. To this end, we defined for each mating pair a time-zero point marking the “onset-of-coupling” as the moment at which cell-cell contact was initiated in a polarized manner and the cell walls of each partner began to merge (Figure 3A). We scored *fusion* as the mixing of cytoplasmic GFP, and *lysis* as both loss of turgor pressure in the mating pair and loss of cytoplasmic GFP (Jin *et al.*, 2004).

After wild-type cells form a mating pair, fusion rapidly ensued. Every observed mating pair fused (n=231) and 97% of these fusion events occurred within the first 20 minutes after onset-of-coupling ($T_{1/2} = 9.5$ min; Figure 3B). When fusion events were binned and plotted over time (Figure 3D, top), the distribution fitted to a Gaussian curve ($r = 0.99$), and the distribution of the same reaction carried out in EGTA was superimposable, indicating that Ca^{2+} removal affected neither kinetics nor extent of wild-type cell fusion. Moreover, we observed virtually no mating-induced lysis under either condition for wild type cells; only ~0.3% of wild-type mating pairs lysed in the presence of EGTA (Figure 3D, bottom).

Although only 40% of *prm1Δ* x *prm1Δ* mating pairs fused, those that did so followed nearly identical kinetics as wild-type cells: 85% of fusion-destined mating pairs fused within the first 20 minutes after onset-of-coupling ($T_{1/2} = 10$ min; Figure 3B). Unlike wild-type cells, a few *prm1Δ* x *prm1Δ* mating pairs fused significantly later than 20 minutes after onset-of-coupling (Figure 3E, top). Over half of such late-fusing mating pairs extended a bubble early in the life of the mating pair, suggesting that these events resulted from an impaired membrane fusion step rather than delayed cell wall removal. In agreement with the results shown in Figure 2, *prm1Δ* x *prm1Δ* fusion was antagonized by EGTA. However the rate at which fusion-destined mating pairs fused was not delayed by Ca^{2+} removal, as 84% of *prm1Δ* x *prm1Δ* fusion events on EGTA occurred within the first 20 minutes after onset-of-coupling ($T_{1/2} = 9.5$ min, Figure 3B).

Under normal conditions, i.e., in the presence of Ca^{2+} , *prm1Δ* x *prm1Δ* mating pairs lysed at a steady, slow rate over the two-hour time frame of the experiment (Figure 3C, black triangles, and Figure 3E, bottom panel, black bars). By contrast, we observed a dramatically changed kinetic profile when lysis was enhanced by Ca^{2+} removal with EGTA. Under these conditions, lysis followed bi-phasic kinetics. Interestingly, all of the additional lysis due to Ca^{2+} removal could be accounted for in an initial rapid burst phase. The $T_{1/2}$ for the burst phase (8.5 min) closely matched that for fusion of wt x wt and *prm1Δ* x *prm1Δ* cells observed in the presence or absence of Ca^{2+} . Lysis continued at later time points with slow kinetics indistinguishable from those seen in the presence of Ca^{2+} (Figure 3C, grey triangles). Thus, *prm1Δ* x *prm1Δ* mating pairs have a tendency to lyse with low frequency in the presence of Ca^{2+} , but lyse frequently during the time window in which fusion takes place in the absence of Ca^{2+} .

Although the fusion defect measured at a late time point after onset-of-coupling in *fig1Δ* x *fig1Δ* fusion reactions was not as strong as that observed for *prm1Δ* x *prm1Δ* fusion reactions, *fig1Δ* x *fig1Δ* mating pairs fused with significantly delayed kinetics ($T_{1/2}$ = 21 min) compared to the $T_{1/2}$ of both wt x wt and *prm1Δ* x *prm1Δ* mating pairs (Figure 3B, circles, and Figure 3F, top panel). Only 45% of fusion events occurred within the first 20 minutes after onset-of-coupling, and the presence or absence of Ca^{2+} did not affect the kinetics of the reaction. Similar to *prm1Δ* x *prm1Δ* mating reactions, *fig1Δ* x *fig1Δ* mating pair lysis occurred at a slow rate both in the presence and absence of Ca^{2+} , and a rapid burst phase of increased lysis paralleling the window of *fig1Δ* x *fig1Δ* fusion was superimposed on the slow phase in the absence of Ca^{2+} (Figure 3C and 3F). The *prm1Δ fig1Δ* x *prm1Δ fig1Δ* double mutant fusion reaction exhibited identical delays in fusion and lysis as *fig1Δ* x *fig1Δ* mating kinetics (Supplementary Figure S1).

As a basis for comparison, we also characterized the behavior of mutants that have cell wall remodeling defects. When bilateral crosses of *fus1Δ* x *fus1Δ* and *fus2Δ* x *fus2Δ* were performed, we observed an even more apparent delay in the initiation of

fusion ($T_{1/2} = 45$ min and 35 min, respectively; Figure 3G and data not shown), indicating that cell wall remodeling mutants cause a large delay in fusion, unlike the *prm1Δ* and *fig1Δ* mutants analyzed above.

Cell lysis and cytoplasmic mixing occur synchronously

In a few of the lysed mating pairs in the time course experiments shown in Figure 3, we observed transient spreading of GFP from the *MATα* cell in which it was expressed into the *MATa* mating partner, indicating that fusion and cytoplasmic mixing preceded or was simultaneous with lysis (Jin *et al.*, 2004). We therefore recorded high time resolution movies to resolve content mixing and fusion. The results in five out of five movies recorded were identical. Selected time frames of a representative movie imaging *prm1Δ* x *prm1Δ* mating pairs in the presence of EGTA at 5-second intervals are shown in Figure 4. Content mixing was first evident in the 5-second frame as monitored by GFP spreading (Figure 4A and 4B, arrows; Supplementary Movie 1). In all cases we observed that lysis initiated synchronously in the same frame as monitored by the first sign of diminution of overall GFP fluorescence in the mating pair and the rounding-up of the vacuole indicative of a loss of turgor pressure. The cytoplasmic GFP slowly diffused from the mating pair over the next three minutes.

We also scored the synchrony of lysis between each cell of a mating pair by monitoring loss of turgor pressure in DIC images which results in high contrast vacuole profiles (Jin *et al.*, 2004). In this way, we were able to achieve a better time resolution of the lysis event because loss of turgor pressure happens instantaneously, compared to the slower leakage of GFP from a lysed mating pair. Figure 4C shows synchronous lysis of two cells of a *prm1Δ* x *prm1Δ* mating pair—synchronous loss of turgor pressure in both *MATa* and *MATα* cells is apparent in the 1-second frame, indicated by the vacuolar morphology, whereas neither cell appears to have lost turgor pressure in the 0-second frame. In each of eleven lysis events analyzed this way, lysis of both cells occurred within

a 2 second window.

A yeast synaptotagmin homolog, *TCB3*, dampens *prm1Δ* x *prm1Δ* mating pair lysis

Lysis of mating pairs is a result of plasma membrane disruption, and, as we have shown here, low extracellular Ca^{2+} concentrations enhance the penetrance of lysis, whereas higher concentrations suppress it. As shown in Figure 5A, *prm1Δ* x *prm1Δ* mating pairs in EGTA showed a remarkable abundance of membranes accumulating in the zone of cell-cell fusion/lysis, suggesting that membrane vesicles are recruited there yet in the absence of Ca^{2+} do not get consumed. These observations are reminiscent of repair mechanisms that have been described for damaged membranes in numerous systems and have been shown to require extracellular Ca^{2+} (Yawo and Kuno, 1985; Steinhardt *et al.*, 1994). In mammalian cells, for example, membrane wound repair can be mediated by Ca^{2+} -triggered exocytosis of lysosomes, and synaptotagmin VII has been suggested as a potential Ca^{2+} sensor for this regulated exocytosis event (Reddy *et al.*, 2001). A family of yeast proteins, Tcb1, Tcb2 and Tcb3, shares similar domain architectures with synaptotagmins (Schulz and Creutz, 2004). These proteins contain predicted transmembrane helices, followed by multiple C2 (Ca^{2+} -binding) domains.

To test if Tcb1, Tcb2 and/or Tcb3 have a role in suppressing lysis during yeast mating, we deleted the genes encoding these proteins in *prm1Δ* and isogenic wild-type cells and assayed unilateral and bilateral crosses for fusion defects as described above. Deletion of all three *TCB* genes in a *prm1Δ* background resulted in a greater than two-fold increase in mating pair lysis (Figure 5, bar 4), whereas it caused no significant defect in wild-type cells (Creutz *et al.*, 2004). The degree of the enhanced lysis defect in *prm1Δ* x *prm1Δ* *TCB*-deleted mating pairs (~ 50%) was equivalent to that observed in *prm1Δ* x *prm1Δ* mating pairs in the absence of Ca^{2+} (see Figure 2, bar 4). Moreover, it was exclusively due to the deletion of *TCB3* (Figure 5, bar 7), whereas deletion of *TCB1* and *TCB2* had no effect (Figure 5, bars 5 and 6). The enhanced lysis defect was undiminished

if only one of the *prm1Δ* cells was missing *TCB3*, regardless of which mating type lacked the gene (Figure 5, bar 8 and data not shown).

DISCUSSION

Prior to this work, Prm1 was the only protein known to act at the plasma membrane fusion step during yeast mating. Here we expand the cast of players in membrane fusion with the characterization of Fig1. Like *PRM1*, *FIG1* was identified bioinformatically as a pheromone-regulated gene encoding a multipass integral membrane protein (Heiman and Walter, 2000). Fig1 localizes to the zone of cell/cell contact, and deletion of *FIG1* results in a membrane fusion defect after cell wall removal, as indicated by ultrastructural analyses and the formation of cytoplasmic bubbles that are bounded by tightly apposed plasma membranes from both mating partners. *fig1Δ* x *fig1Δ* mating pairs have a delayed initiation of fusion, and bilateral *FIG1* deletion significantly enhances the fusion defects observed in *prm1Δ* x *prm1Δ* mating pairs. As a member of the Claudin superfamily, Fig1 may function analogously by bridging membranes in close proximity (Van Itallie and Anderson, 2004; Zhang *et al.*, 2006).

Albeit severely compromised, some residual fusion activity remains in the absence of Prm1 and Fig1. The low penetrance of the fusion defects suggests that either i) Prm1 and Fig1 are important yet non-essential components of the fusion machinery, or that ii) an alternate, Prm1 and Fig1-independent fusion pathway(s) can compensate for their absence. Currently available data do not allow us to distinguish between these possibilities.

Nonproductive mating pairs that fail to fuse in the absence of Prm1 and/or Fig1 can either lyse or remain unfused with their plasma membranes in close apposition. It was previously suggested that the observed cell lysis may be a direct result of engagement of the cell fusion machinery and possibly be intrinsically linked to the mechanism of lipid bilayer fusion (Jin *et al.*, 2004); the results presented here strongly

support this view. This notion implies that cells take a risk of dying when engaging in mating – if the fusion machinery is not working properly, the chances of death by lysis become significant. In Table 1, we express this risk as “fidelity”, defined as the probability that cells in a mating pair will survive after engagement of the fusion machinery. We have previously shown (Heiman and Walter, 2000) that surviving cells of an unfused mating pair eventually give-up on their mating partner, re-enter the cell cycle, and can productively bud as haploid cells to produce viable daughters. Note that the fidelity of the fusion machine declines from 96% in wild-type mating pairs to 63% and 43% in mating pairs missing *Prm1*, and *Prm1* and *Fig1* in both mating partners, respectively. The probability of engagement of the fusion machinery (leading to either fusion or lysis) is defined as “activity”. Thus only 37% of cells missing *Prm1* and *Fig1* engage the fusion machinery and of those that do only 43% survive.

The situation gets considerably worse when mating reactions are carried out in the absence of Ca^{2+} . Whereas we found no requirement for Ca^{2+} during mating of wild-type cells, fidelity values for mating reactions carried out in the absence of Ca^{2+} drop to 7% and 1.2% for *prm1* Δ x *prm1* Δ and *prm1* Δ *fig1* Δ x *prm1* Δ *fig1* Δ mating pairs, respectively. Thus Ca^{2+} masks the true extent of the mating defects in *prm1* and *fig1* mutant cells but is important only in the context of the defective fusion machine in the mutant cells.

Our results support in multiple ways a functional coupling of lysis to the engagement of the fusion machine: First, by removing Ca^{2+} to favor lysis, we observe that the timing of lysis events is the same as the timing of fusion. Second, we demonstrate that the two cells of a mating pair lyse synchronously, as expected for events at the interface between both cells in a mating pair. Third, mixing of cytoplasmic contents occurs concomitant with the initiation of lysis. This implies that lysis is initiated as fusion is catalyzed, most simply explained by hypothesizing a common machinery for the two outcomes. It is possible, for example, that a defective fusion machinery may not contain the fusion zone properly or correctly resolve unstable intermediates, leading to mating

pair lysis. Indeed, recent models of bilayer fusion (Muller *et al.*, 2003b) pose that membrane fusion is not a failsafe process: formation of the lipid stalk favors the formation of holes adjacent to the stalk in each of the two engaged membranes. Thus it is conceivable that the very act of bilayer membrane fusion can cause membrane rupture and cell lysis—unless the fusion zone is contained by accessory proteins of the fusion machinery. Prm1 and Fig1 could play such a role, for example by providing a molecular fence that corrals the fusion zone and prevents the catastrophic spread of local membrane damage. These accessory proteins could play positive roles as well, organizing the activity of the fusion machine to ensure correct membrane merger—thus explaining the accumulation of unfused mating pairs in matings lacking Prm1 and Fig1.

In this light, an attractive explanation for the Ca^{2+} effect in the mutant cells is that the mutations enhance lysis, which is counteracted by Ca^{2+} -dependent membrane repair mechanisms, thus influencing the fusion-lysis balance by rescuing potential lysis events. This would explain why Ca^{2+} is not required during wild-type mating reactions where Prm1 and Fig1 prevent lysis events from occurring. We provide evidence that Tcb3, a yeast synaptotagmin ortholog, may function as a Ca^{2+} sensor in a membrane repair pathway operating during this process. Deletion of *TCB3* mimics the lysis increase observed in *prm1* Δ x *prm1* Δ mating pairs upon Ca^{2+} depletion. This model would also explain the accumulation of membranes in *prm1* Δ x *prm1* Δ mating pairs upon Ca^{2+} depletion.

While attractive, this model leaves many interesting questions to be solved: For example it does not explain all of the observed effects that Ca^{2+} exerts on membrane fusion. In particular, the observation that high Ca^{2+} concentrations partially suppress the defects of *prm1* Δ x *prm1* Δ mating pairs suggests that Ca^{2+} at high concentrations may also promote the fusion of apposed membranes, perhaps by directly interacting with membrane lipids as seen in membrane fusions assays of pure lipid vesicles (Duzgunes *et al.*, 1981; Ellens *et al.*, 1985).

MATERIALS AND METHODS

Media and yeast strains.

Synthetic complete (SC), and complex (YPD) media were prepared and supplemented with 2% glucose using reagents from Difco Inc. and Sigma Chemical Company.

Synthetic growth media lacking calcium were prepared similarly using yeast nitrogen base (YNB) without calcium chloride (BIO 101, Inc.) and further treatment of the complete media with resin-bound BAPTA Calcium Sponge (Molecular Probes). All strains used in this study are derivatives of wild-type strain W303. Gene replacements were generated with the PCR transformation technique (Longtine et al., 1998) and confirmed by PCR.

Quantitative cell fusion assays

In a standard assay, cells of opposite mating types, with the *MAT α* strain expressing soluble cytosolic green fluorescent protein (GFP), were grown to mid-log phase. An equal number of cells of each mating type were mixed and vacuumed to a nitrocellulose filter. The filter was placed cell-side up on either YPD or supplemented YPD plates, and then incubated for 3 h at 30°C. Cells were scraped off the filter, fixed in 4% paraformaldehyde incubated at 4°C overnight, and inspected by fluorescence microscopy. To quantify cell lysis, mating mixtures were scraped and stained either with 0.02% methylene blue or 0.008% trypan blue for 15 min at 30°C. Methylene blue stained cells were directly imaged by light microscopy and trypan blue cell were washed and fixed in 4% paraformaldehyde prior fluorescence microscopy analysis. Both methods yielded indistinguishable results. For liquid media cell fusion assays cells of opposite mating types were grow as above described and then mixed (0.3 OD/mating type) prior filtering onto 12 mm transwells (Costar). Transwells were placed on chambers with 1 ml of synthetic media and covered with 300 ml of same media. After 3.5 hours at 30° C, mating

mixtures were treated for quantification of lysis and fixed as described above.

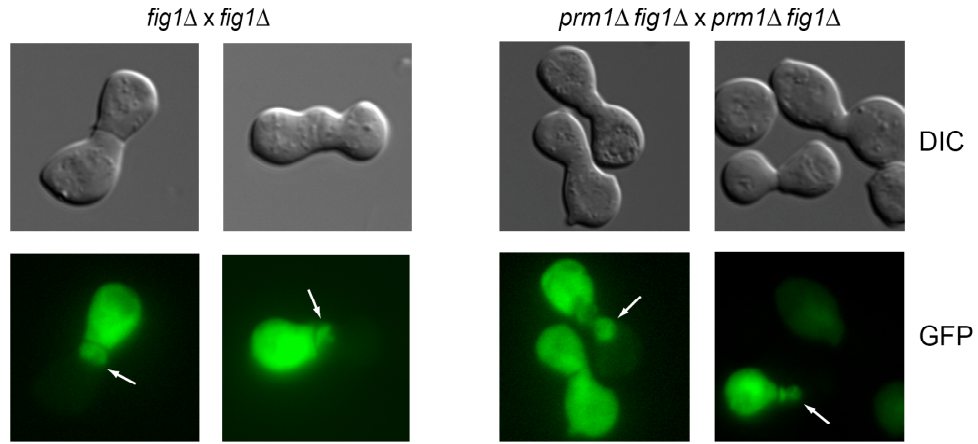
Fluorescence microscopy

Fluorescence and DIC microscopy was performed using an Axiovert 200M microscope (Zeiss), equipped with an X-cite 120 mercury arc lamp (EXFO), and an Orca ER camera (Hamamatsu). ImagePro or Metamorph were used for data collection. Time lapse microscopy was performed as previously described (Jin et al., 2004), with a few modifications. In brief, cells derived from preincubated mating mixtures were mounted on agarose pads, which contained 1.8% agarose in SC media. A cover slip was placed on top of this pad and sealed using VALAP or nail polish. Mating was followed at room temperature.

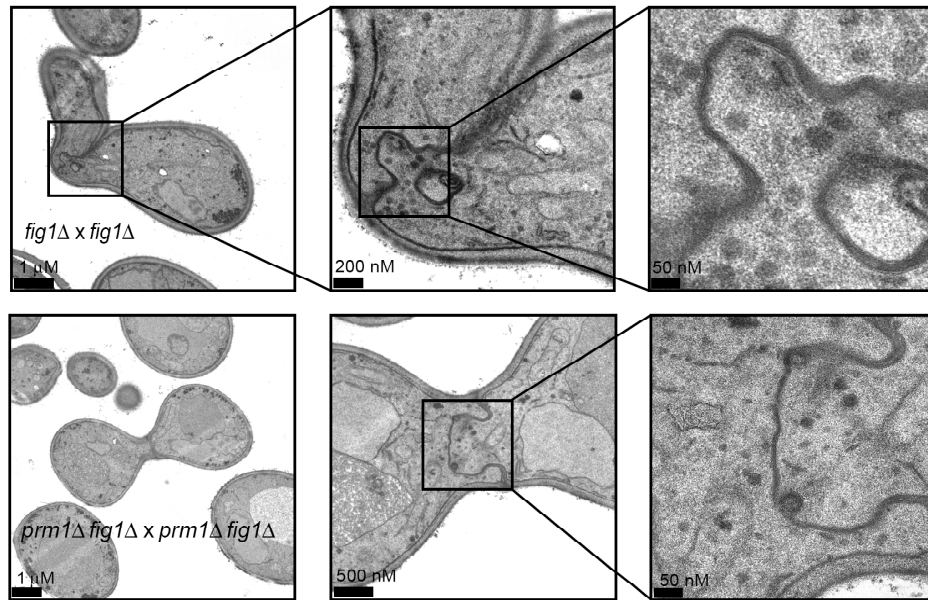
Electron microscopy

Cells of opposite mating type were treated as described above for quantitative cell fusion assays. Mating mixtures were scraped off, fixed, and processed as described previously (Heiman and Walter, 2000). Briefly, cells were fixed in 1% glutaraldehyde, 0.2% paraformaldehyde, 0.04 M potassium phosphate, pH 7, washed and then incubated in 2% KMnO_4 . After dehydration in ethanol, cells were prepared for embedding, replacing ethanol with propylene oxide. Embedding was performed using graded concentrations of resin (32% Epon, 18% Araldite, 34% DDSA, 16% NMA; Ted Pella Inc.) mixed with propylene oxide, followed by overnight infiltration with pure resin. Then, cells were transferred to resin containing 2% BDMA (Ted Pella Inc.), and incubated at 70°C for one day. Sections of 90 nm thickness were cut, stained with lead citrate (Ted Pella Inc.), and imaged with an electron microscope (EM400; Philips).

A



B



C

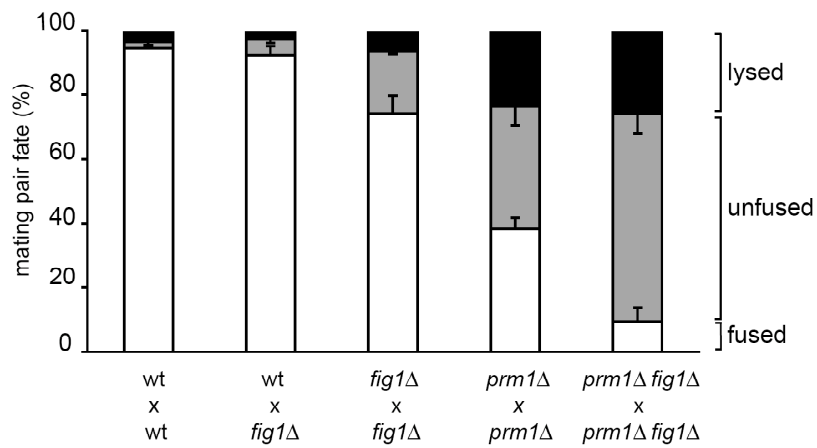


Figure 1. PRM1 and FIG1 promote the membrane fusion step during mating. (A) Unfused *fig1Δ x fig1Δ* mating pairs form bubbles. *MATα* cells carrying cytoplasmic GFP were mixed with *MATa* cells on nitrocellulose filters and incubated on YPD plates for 3 h at 30°C. Fixed mating mixtures were then imaged by DIC and fluorescence microscopy. Arrows point mating pair bubbles. (B) Bubbles in unfused *fig1Δ x fig1Δ* mating pairs contain closely apposed membranes. The ultrastructural detail of *fig1Δ x fig1Δ* mating pairs was determined as in Panel A with mating mixtures processed as described in Materials and Methods. The panels show three different magnifications for each mating pair. The lower magnification picture in the lower panel corresponds to a different section of the same mating pair. (C) *PRM1* and *FIG1* act through different pathways to promote cell fusion. Quantitative cell fusion and lysis assays were performed as described in Materials and Methods. All deletion genotypes were tested for both mating types; the results were indistinguishable. Error bars indicate standard errors for four independent experiments with 300 mating pairs scored for each case.

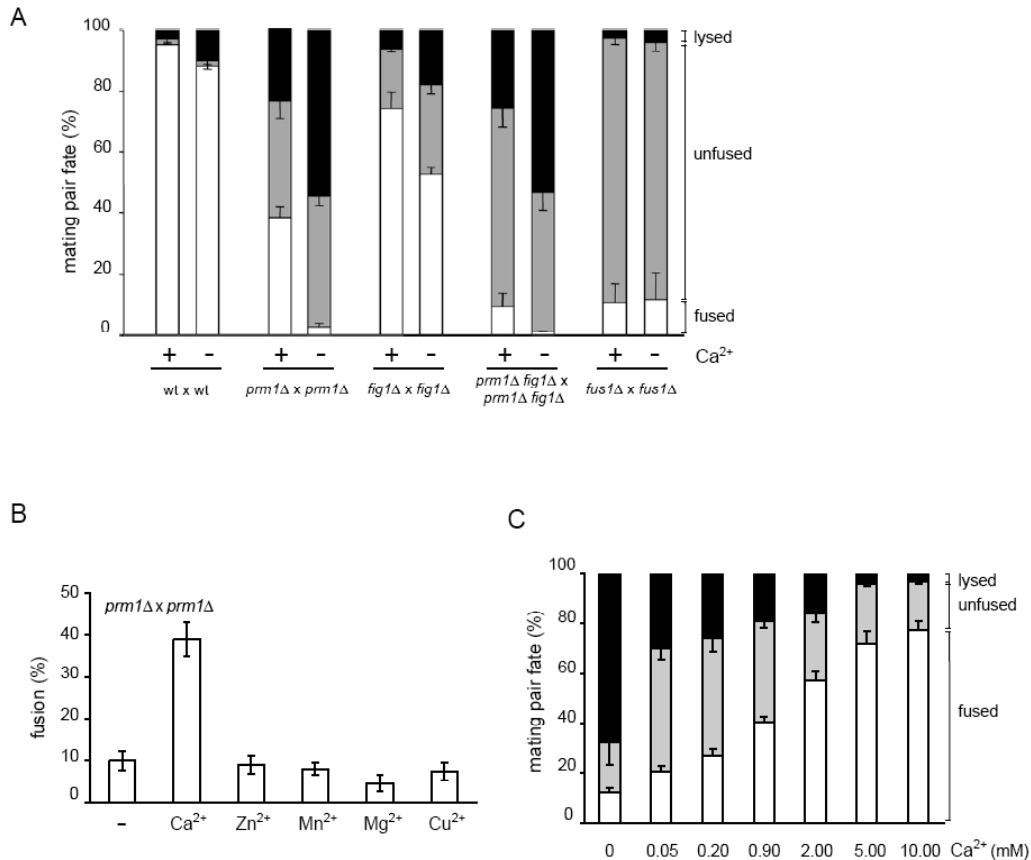


Figure 2. Extracellular Ca²⁺ suppresses cell lysis in *prm1Δ x prm1Δ* mating reactions. (A) Fusion of *prm1Δ x prm1Δ* mating pairs is highly sensitive to EGTA. Mating mixtures were incubated on YPD plates with (Ca²⁺: “-”) or without (Ca²⁺: “+”) 20 mM EGTA. (B) The sensitivity of *prm1Δ x prm1Δ* mating pairs to EGTA is due to a lack of Ca²⁺. Liquid media cell fusion assays were performed in synthetic media treated with resin-bound BAPTA and supplemented either with water (“-“) or divalent cation salts at concentrations found in synthetic complete media: calcium chloride (900 μM), zinc sulfate (1 μM), manganese sulfate (10 μM), magnesium sulfate (1 mM) and copper sulfate (1 μM). (C) Extracellular calcium suppresses the *prm1Δ x prm1Δ* mating defect. Liquid media cell fusion assays were performed as in B using media supplemented with calcium chloride as indicated. Error bars indicate standard errors for at least three independent experiments with 300 mating pairs scored per experiment.

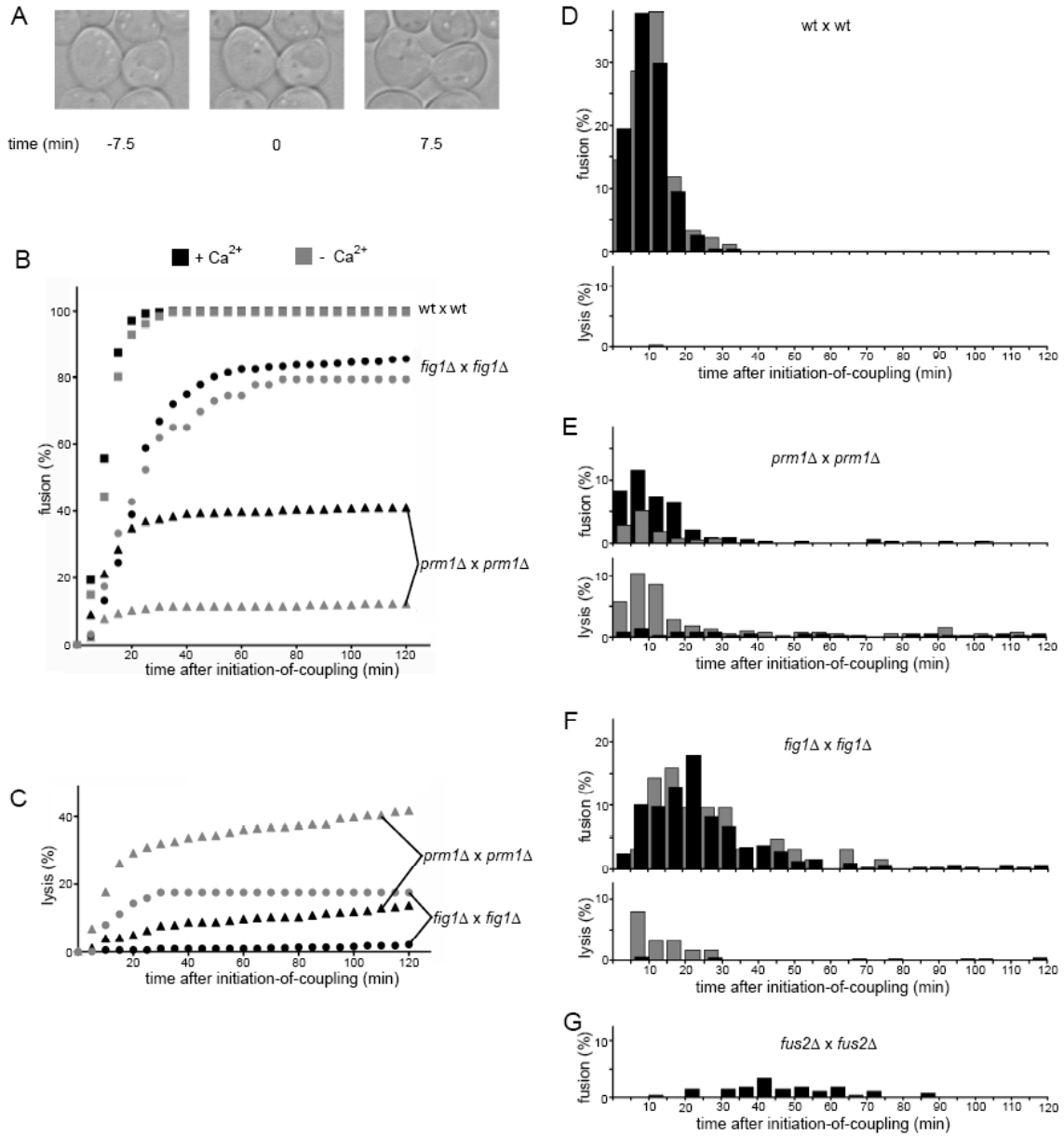


Figure 3. Kinetics of fusion and lysis initiation in mating populations. The fate of individual mating pairs in a mating mixture was followed by time-lapse microscopy. (A) Example of the determination of initiation-of-coupling. The picture in the center, showing the two cells initiating contact in a polarized manner, serves as a time zero reference point for the mating pair. (B) Plot showing the progression of the fusion outcome as a function of time in the presence (black symbols) or absence (gray) of Ca²⁺. (C) Plot showing the progression of the lysis outcome as a function of time. (D-G) Fusion

and lysis events were binned into five minute time windows and normalized to indicate the percentage of the mating pair population that would undergo the indicated event within these time windows. Black bars represent events in the presence of Ca^{2+} ; gray bars represent events in the absence of Ca^{2+} . All data shown are the result of three independent experiments. No lysis was observed for *fus2Δ* x *fus2Δ*. The lower rate of lysis (as compared to the endpoint assays shown in Figures 1 and 2) is likely due to performing the mating reaction at room temperature instead of at 30°C.

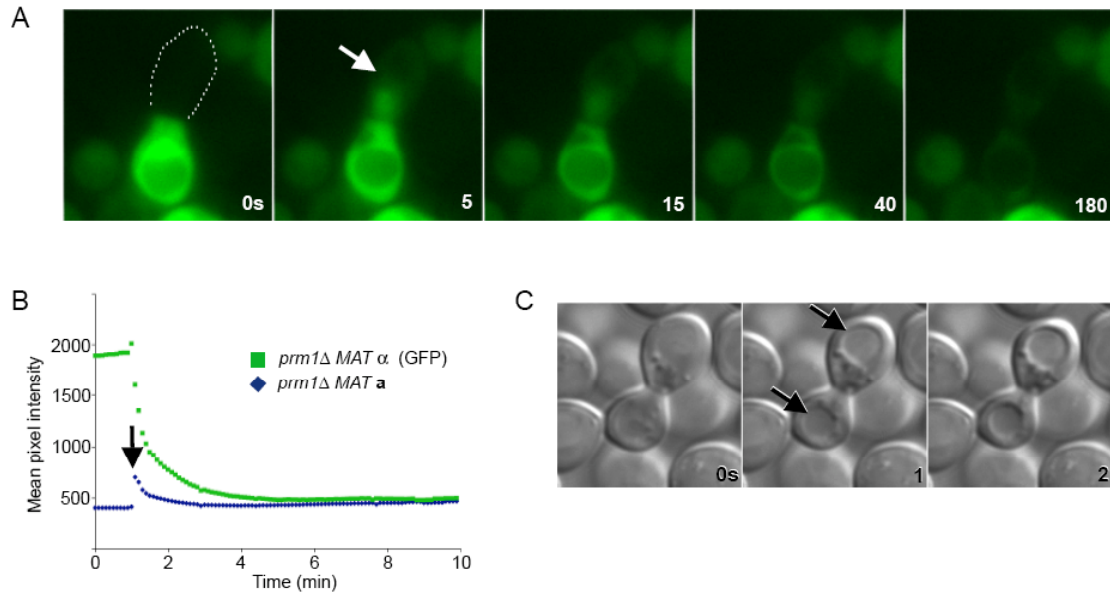


Figure 4. Lysis occurs simultaneously in each cell of a mating pair and is concomitant with cytoplasmic mixing. Lysis of *prm1Δ* x *prm1Δ* mating pairs in media lacking Ca^{2+} was imaged with fast time resolution. (A) Cytoplasmic GFP in a *MATα* cell spread into the *MATa* cell following initiation of lysis at 5 s (white arrow). Note that GFP has spread throughout the entire *MATa* cell in all frames subsequent to the 0 s frame, demonstrating cytoplasmic continuity. White dots represent the boundaries of the *MATa* cell. (B) Quantification of average pixel intensity in each mating partner over time; initiation of lysis is indicated by the black arrow. (C) DIC images of a lysing mating pair. Evidence of lysis is seen in the 1 s frame as rounded vacuoles (black arrows), indicating the loss of turgor pressure upon plasma membrane rupture.

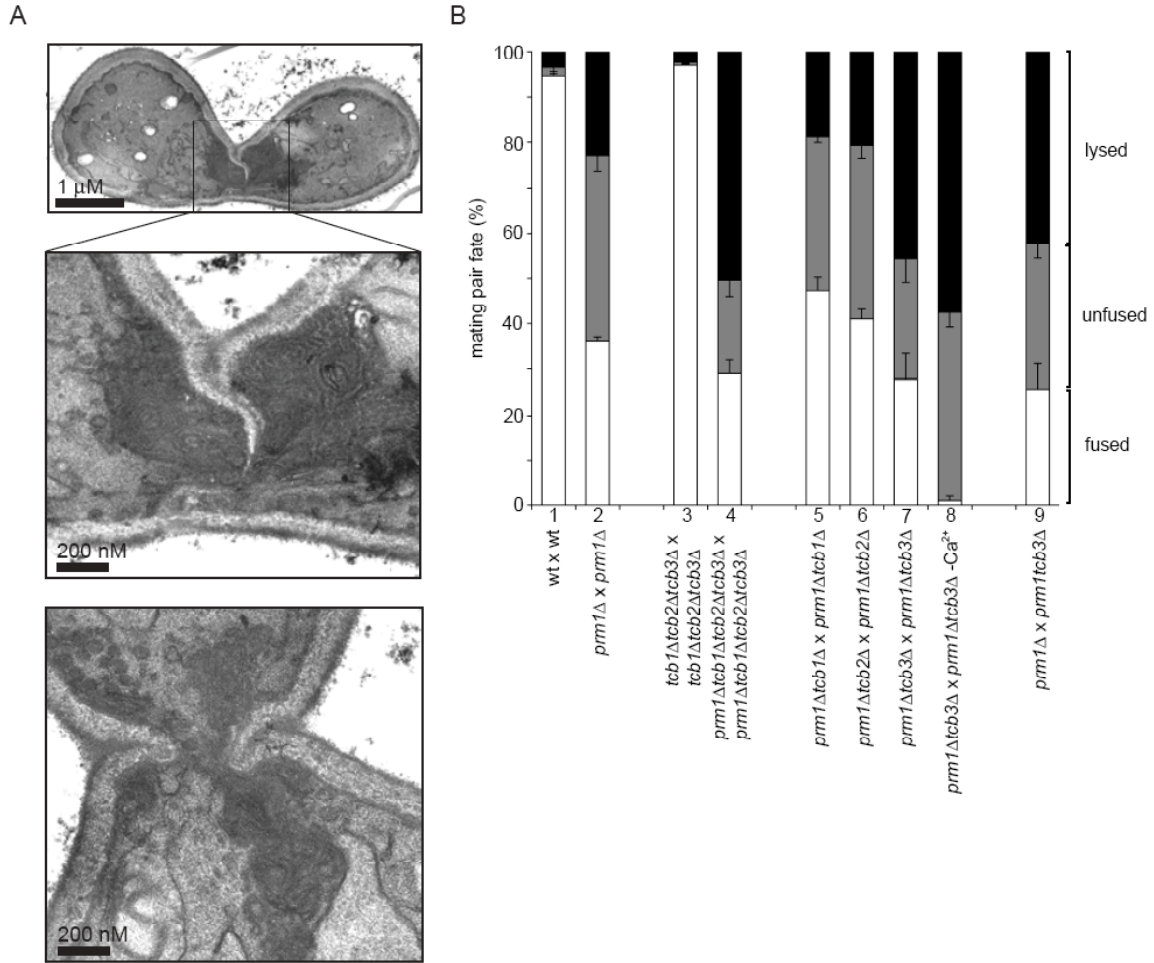


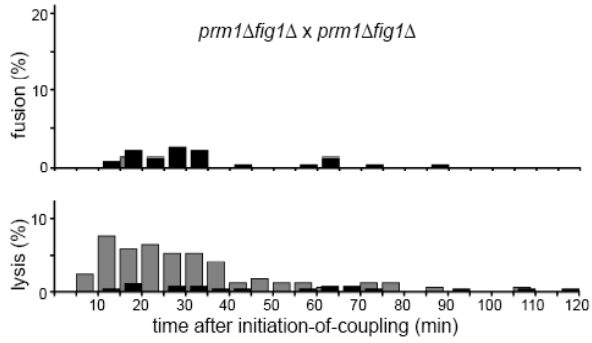
Figure 5. *TCB3* prevents mating pair lysis in the absence of *PRM1*.

(A) In the absence of Ca^{2+} , *prm1Δ* x *prm1Δ* mating pairs show extensive membrane accumulation where fusion should occur. Mating mixtures were processed as described in Materials and Methods. The panels show the zone of cell-cell contact for three different mating pairs. (B) Deletions of *TCB1*, *TCB2*, and *TCB3* were tested for their effect on cell fusion and lysis during mating. Crosses are labeled as *MATα* x *MATa*. Error bars indicate standard errors for at least three independent experiments with 300 mating pairs scored per experiment.

Table I. Influence of Ca²⁺ on Acitivity and Fidelity Values

	activity		fidelity	
	+ Ca ²⁺	- Ca ²⁺	+ Ca ²⁺	- Ca ²⁺
wt x wt	99.0	98.3	96.3	94.9
<i>prm1</i> Δ x <i>prm1</i> Δ	62.0	56.5	62.7	7.1
<i>fig1</i> Δ x <i>fig1</i> Δ	80.3	70.3	92.2	74.5
<i>prm1</i> Δ <i>fig1</i> Δ x <i>prm1</i> Δ <i>fig1</i> Δ	37.4	43.6	42.7	1.2

Activity is calculated as the percentage of total mating pairs that fuse or lyse. Fidelity represents the percentage of mating pairs that fuse among the number of mating pairs that fuse or lyse.



Supplemental Figure 1. Kinetics of fusion and lysis initiation of *prm1Δfig1Δ x prm1Δfig1Δ* mating pairs. Time lapse microscopy of a *prm1Δfig1Δ x prm1Δfig1Δ* mating mixture was performed on SDC agar slips. Fusion and lysis events were binned into five minute time windows and normalized to indicate the percentage of the mating pair population that would undergo the indicated event within these time windows.

Supplemental Movie 1. Cytoplasmic mixing occurs concomitant with mating pair lysis. Lysis of *prm1Δ* x *prm1Δ* mating pairs in media lacking Ca₂₊ was imaged at one frame per every 5 seconds. The *prm1Δ* MAT α cell is marked by cytoplasmic GFP expression. This movie plays 10 frames/sec, and thus represents 50x real time.

This movie may be viewed online at:

<http://www.molbiolcell.org/cgi/content/full/E06-09-0776/DC1>

CHAPTER 3

THE YEAST CELL FUSION PROTEIN PRM1P REQUIRES COVALENT DIMERIZATION TO PROMOTE MEMBRANE FUSION

INTRODUCTION

Lipid membranes allow cells to contain macromolecules and create many different specialized environments. However, these membranes are not simply static barriers and must accommodate the dynamic needs of life. Eukaryotic cells move vesicles between secretory compartments, excrete proteins and hormones, and maintain the identity of organelles; gametes must fuse their cell membranes to form embryos; and myoblast cells fuse during the development of skeletal muscle. Membrane fusion is also necessary for infection of enveloped viruses as a means of delivering the viral genome into the cell. For these processes a mechanism to merge membranes in a specific, fast, and non-leaky manner is required.

A protein family required for most intracellular fusion events, SNAREs (soluble *N*-ethylmaleimide-sensitive factor attachment protein receptors) use the energy of protein folding coupled to transmembrane anchors to pull membranes together and destabilize and fuse lipid bilayers (Jahn and Scheller, 2006). Similarly, class I and class II viral fusases refold from a metastable conformation to bring together a transmembrane anchor and a fusion peptide and achieve the same result (Weissenhorn et al., 2007). Though high-resolution structures of the soluble domains of individual SNARE complexes and viral fusase trimers have been solved, the stoichiometry and geometry of the fusases in membranes during fusion is not known.

Both SNARE and viral fusion proceed through a hemifusion intermediate in which *cis* leaflets of opposed membranes fuse to form a hemifusion stalk (Sollner, 2004). Expansion of the hemifusion stalk allows the *trans*-leaflets to form a bilayer. Rupture of this bilayer results in a fusion pore. This mechanism of membrane fusion maintains the

identity of the fusing compartments, never allowing leakage or membrane holes. However, the fidelity of membrane fusion as catalyzed by SNAREs and viral fuses appears not to be failsafe. Contents leakage has been observed in *in vitro* viral fusion systems (Blumenthal and Morris, 1999; Shangguan et al., 1996), and vacuoles containing high SNARE density lyse in a SNARE-dependent process (Starai et al., 2007). The mechanism by which compartmental specificity is maintained *in vivo* may therefore be more complicated than previously appreciated, involving the ordered assembly of fusases and possibly additional fusase cofactors.

Another membrane fusion event that exhibits loss of membrane integrity under altered circumstances is cell-cell fusion during yeast mating. Haploid yeast cells of opposite mating type fuse to form a diploid, gamete fusion event akin to sperm-egg fusion (Chen et al., 2007). In the process of yeast mating, cells polarize towards mating partners using pheromone gradients, agglutinate, locally remove cell wall material to allow for membrane contact, and fuse cell membranes.

A key regulator of the membrane fusion step of yeast cell fusion is Prm1p, a mating specific multipass membrane protein which localizes to the zone of cell fusion (Heiman and Walter, 2000). To promote fusion, Prm1p need only be expressed in one partner of the mating pair. However, if both cells of the mating pair lack Prm1p, less than half of mating pairs successfully fuse. Instead, many mating pairs accumulate with membranes unfused but in close apposition. Another outcome of *prm1 x prm1* mating pairs is simultaneous cell lysis (Jin et al., 2004). The extent of mating pair lysis is Ca^{2+} dependent—in the absence of Ca^{2+} lysis is enhanced and approximately half of *prm1 x prm1* mating pairs lyse (Aguilar et al., 2007). The rate of lysis of wild-type mating pairs

is very low, even in the absence of Ca^{2+} . As mating pair lysis requires membrane contact, occurs with the same timing as membrane fusion, and is a phenotype only observed in mutants of the cell membrane fusion step, lysis is thought to be caused by the misregulated activity of the cell fusase (Aguilar et al., 2007; Jin et al., 2004).

The mechanism by which Prm1p promotes membrane fusion and suppresses cell lysis is not known. In this study we demonstrate that Prm1p exists as a covalently linked homodimer. Furthermore, the covalent linkage is necessary for Prm1p activity, consistent with models in which Prm1p plays a structural role by surrounding the site of membrane fusion (Aguilar et al., 2007; Jin et al., 2004). These results begin to describe the organization of the yeast cell fusion machinery and may have implications for membrane fusion mechanisms beyond cell fusion.

RESULTS

Prm1p forms a covalent dimer in *cis*

Prm1p is intimately involved in the membrane fusion process during yeast mating, yet how Prm1p promotes fusion is not understood. Many fusion relevant proteins exist as multimers—enveloped virus fusases form homotrimers and the putative developmental fusase EFF-1 can oligomerize in *cis* (del Campo et al., 2005). We asked if Prm1p had the capacity to form higher order structures by forming homo- or heterodimers. In setting up *in vivo* purification trials we noticed that the mobility of α -factor induced Prm1p in SDS-PAGE was remarkably slower when the protein sample was not reduced (Fig 1A). When reducing agent was omitted from the sample buffer, Prm1p ran with an apparent mass greater than 250 kD. If the protein samples were reduced with DTT, Prm1p ran with an

apparent molecular mass of 125 kD, consistent with the sum of the masses of monomeric Prm1p (73 kD), sugar modifications, and the GFP tag (Heiman and Walter, 2000). The mobility of unreduced Prm1p was not affected when cell lysis was carried out in the presence of iodoacetamide to block non-specific oxidation (data not shown).

The reduction-sensitive behavior of Prm1p in SDS-PAGE suggested that Prm1p may exist as a covalent homo- or heterodimer. To see if the high molecular weight complex required expression of mating specific genes or pheromone-induced MAPK signaling, we expressed *PRM1* under the control of the *GALI* promoter (Fig 1B). In this non-mating context, Prm1p was still found as part of a high molecular weight complex. Finally, we purified Prm1p from mating mixtures under native conditions to see if we could identify non-Prm1p interacting partners. The same reduction-sensitive behavior was observed with colloidal blue staining (Fig 1C). Notably, reduction of the Prm1p sample did not reveal any other major protein species in addition to monomeric Prm1p. Analysis of the unreduced high molecular weight band by MALDI TOF/TOF MSMS identified many Prm1p peptides, but did not yield significant coverage for any other protein (data not shown). Taken together, these results suggest that the high molecular weight species is a covalently linked dimer of Prm1p molecules.

To test if Prm1p could self-associate as a homodimer, we coexpressed Prm1myc and Prm1GFP in both **a** and α cells under the control of the *PRM1* promoter. These cells were mated on YPD to induce Prm1p expression in the true mating context. Prm1myc was immunoprecipitated and the coprecipitation of Prm1GFP monitored by Western blot (Fig 2, top row of panels). Prm1myc was efficiently immunoprecipitated and was undetectable in the flow-through fraction. Though much of the Prm1GFP was contained

in the flow-through, coimmunoprecipitation of Prm1GFP was evident in the eluate. As seen by loading excess eluate, approximately 10% of Prm1GFP co-eluted with Prm1myc. If both fusion proteins are expressed at similar levels, this 10% co-IP efficiency is lower than expected for an unbiased, obligate partnership, for which 50% of Prm1GFP would be expected to coprecipitate. The reduced coprecipitation efficiency may represent a preference for associating with proteins translated from the same mRNA. If Prm1myc was not coexpressed with Prm1GFP, all of the Prm1GFP was found in the anti-myc flow-through and no detectable signal was apparent in the eluate (Fig 2, second row), indicating that the Prm1GFP was selectively retained by interacting with immobilized Prm1myc.

Next, we asked if Prm1 dimerization occurred immediately upon Prm1p biogenesis, or if dimers could be composed of Prm1p molecules made in opposite mating types, which associate upon membrane apposition and merger. We prepared samples for coimmunoprecipitation in two ways: (1) by mating wild-type *MAT α* cells to *MATa* cells coexpressing both Prm1myc and Prm1GFP, and (2) by mating *MAT α* cells expressing Prm1myc to *MATa* cells coexpressing Prm1GFP. When the epitope-tagged *PRM1* alleles were coexpressed, Prm1GFP coimmunoprecipitated with Prm1myc (Fig 1C, third row). However, when the expression of each *PRM1* allele was separated into opposite mating types, very little Prm1GFP was apparent in the anti-myc eluate (Fig 1C, bottom row). These results support a model in which Prm1p dimerization occurs in the ER and no interchange occurs at the cell surface. Such interchange would have been apparent even when the alleles were expressed *in trans* because almost half of the cells in the preparation had undergone cell fusion. In this population, the previously distinct

membranes in which Prm1myc and Prm1GFP were anchored had been merged. The small amount of Prm1GFP in the *trans*-expressed eluate likely represents dimerization of two newly synthesized Prm1 proteins in the same ER membrane after fusion, when mRNAs can diffuse throughout the mating pair.

Covalent dimerization is required for Prm1p activity

Because the Prm1p dimer was SDS-resistant and reduction-sensitive we predicted that the interaction between monomers is cemented by disulfide bridges. To test this possibility we mutated each of the twelve Prm1p cysteines to serines and assayed the ability of these mutants to form covalent dimers. Of these twelve mutants, two (*prm1(C120S)* and *prm1(C545S)*) were unable to form covalent dimers while the rest were unaffected (Fig 3A and data not shown). We tested the functionality of the *prm1(C120S)GFP* and *prm1(C545S)GFP* alleles by expressing them in a *prm1 MATa* background and mating to a *prm1 MATα* strain. Fusion was scored microscopically by monitoring diffusion of cytoplasmic GFP expressed in the *MATα* strain (Heiman and Walter, 2000). To enhance the penetrance of the *prm1* phenotype mating was performed on media supplemented with 20mM EGTA (Aguilar et al., 2007). Under these conditions almost 60% of mating pairs successfully fuse when the *PRM1* deletion is covered by *PRM1GFP* (Fig 3B). However only 10% of mating pairs fuse when the *PRM1* deletion is covered by *prm1(C120S)GFP*, and an even greater fusion defect was seen for *prm1(C545S)GFP*. These alleles retain some activity as *prm1* x *prm1* mating mixtures yield only 2% fused mating pairs. None of the 10 cysteine-substituted alleles, which did not affect covalent dimerization, had reduced fusion activity (data not shown). Because

cys-120 may reside within the second predicted transmembrane domain of Prm1p we also constructed substitutions with alanine and leucine to ensure that the polar nature of the serine was not interfering with *prm1(C120S)* activity. Both of these alleles behaved identically to *prm1(C120S)* (data not shown). Despite the failure of *prm1(C120S)GFP* and *prm1(C545S)GFP* to support cell fusion, the bulk of the protein product of these alleles was delivered to the cell surface (Fig 3C). Thus, a failure to deliver the cysteine-substituted proteins to the zone of cell fusion cannot explain their defect.

As *prm1(C120S)* and *prm1(C545S)* fail to form covalent dimers, we tested if they could still self-associate and form non-covalent dimers. When both wild-type *PRM1* and *prm1(C120S)* or *prm1(C545S)* were coexpressed from low copy plasmids, a significant fraction of the mutant proteins were integrated into covalent dimers (Fig 4A, top two right panels). This may represent wild-type-mutant dimers forming an asymmetrical disulfide linkage *in trans* (i.e., cys-120 of Prm1p to cys-545 of *prm1(C120S)*) that normally occurs between wild-type molecules. However, these mutants may also form non-native disulfide linkages, as overexpression of *prm1(C120S)* and *prm1(C545S)* alone can rescue the formation of covalent dimers (Fig 4B). Despite resulting in the formation of covalently linked species, overexpression of *prm1(C120S)* or *prm1(C545S)* does not rescue fusion activity, further suggesting that these linkages are non-physiological (data not shown). Substituting all three cysteines predicted to reside in the luminal/extracellular space prevented covalent dimerization when coexpressed with wild-type Prm1p or overexpressed (*prm1C(120,277,545)S*; Fig 4A, B).

Both *prm1(C120S)* and *prm1(C545S)* retained their ability to interact with wild-type Prm1p (Figure 4A). No bias is observed in interaction efficiency between covalently

linked proteins compared to non-covalently associated proteins, demonstrating that these cysteines are not influencing the ability of Prm1p to dimerize. Consistent with this, even triply substituted *prm1C(120,277,545)S* could interact with itself, in addition to wild-type Prm1p (Figure 4A). Interestingly, coexpression of *prm1C(120,277,545)S*, but not *prm1(C120S)* or *prm1(C545S)*, prevented a fraction of wild-type Prm1p from forming a covalent dimer (Figure 4A, third row). Presumably the triply substituted mutant interacts with and sequesters wild-type Prm1p, but, unlike the singly substituted mutants, does not contain the cysteine(s) to covalently pair.

Charged residues in the second transmembrane domain influence Prm1p dimerization

The two cysteines required for covalent dimerization are located within the most conserved stretches of Prm1p. cys-120 is located within or adjacent to the second predicted transmembrane domain, the most conserved transmembrane domain of Prm1p; cys-545 is in the middle of the most conserved non-transmembrane stretch on the large second extracellular loop. Curiously, the second transmembrane domain contains two charged residues (glu-104 and asp-112), which are fairly well conserved among fungal homologs (Fig 5A). Due to their proximity to cys-120, and given the likelihood that cys-120 forms a disulfide linkage *in trans*, we predicted that these residues would be important for interaction between Prm1p molecules. Nonconservative substitution of glu-104 with leucine only partially compromised covalent dimer and fusion activity; however, leucine substitution for asp-112 prevented covalent linkage (Fig 5 B). As the *prm1(D112L)* phenotype was more completely defective, we chose to characterize this

mutant further. To test if *prm1(D112L)* fails to form covalent dimers because *prm1(D112L)* monomers do not interact as well as wild-type, we coexpressed *prm1(D112L)myc* and *prm1(D112L)GFP* and immunoprecipitated *prm1(D112L)myc* from the lysate of a mating mixture (Fig 5C). As with the cysteine substituted alleles, we found that covalent dimerization could be somewhat rescued by higher expression, though the majority of *prm1(D112L)myc* was not present as a covalent dimer. Only a very small fraction of *prm1(D112L)GFP* coprecipitated with *prm1(D112L)myc*, and this fraction was exclusively the covalently associated form. These results suggest that *prm1(D112L)* mutants do not bind each other well, but if their expression is increased they may dimerize and form covalent interactions. However, we cannot rule out the possibility that the second transmembrane domain is required for intramolecular folding, and only a small fraction of *prm1(D112L)* correctly folds.

We observed that covalent dimerization was necessary for Prm1p activity based on the loss of fusion activity of the cysteine substituted alleles, and thus expected that *prm1(D112L)* would be similarly hypomorphic. Indeed, mating pairs of *prm1 MAT α* and *prm1 MATa* cells expressing *prm1(D112L)GFP* exhibited a strong fusion defect (9.2% fused mating pairs +/- 2.8% S.D.). Additionally the *prm1(D112L)GFP* mutant failed to localize to the zone of cell fusion, instead being retained in the ER (Fig 5D). The mislocalization of *prm1(D112L)* suggests that dimerization is a prerequisite for ER exit.

DISCUSSION

Prm1 plays an important role in the fusion of cell membranes during yeast mating.

Without Prm1p, mating pairs arrest with membranes in close apposition or undergo cell

lysis. It is not understood how Prm1p promotes membrane fusion and prevents cell lysis. In this study we show that Prm1p forms a covalent dimer, and that this covalent linkage is important for Prm1p function.

There is strong evidence that Prm1p exists predominantly as a dimer covalently linked via disulfide bridges: First, Prm1p migrates with an apparent mass of greater than 250kD in the absence of reducing agent. This is most likely due to homodimerization or oligomerization, as we have demonstrated Prm1p self-interaction. Second, the high molecular weight species is disassembled into Prm1p monomers by reducing agent and does not form when cys-120 or cys-545 of Prm1p are mutated, implicating *trans* disulfide bridges between Prm1p molecules. Though we were unable to observe corresponding crosslinked peptides by MSMS, the most likely linkages are either C120-C120 and C545-C545, or two C120-C545 bridges. Prm1p dimers probably form soon after synthesis in the ER. The interaction of Prm1p monomers may be driven by TM2 *trans*-interactions with other transmembrane domains. Once two Prm1p molecules dimerize, their interaction is preserved by the formation of intermolecular disulfide bonds. At the cell surface, Prm1p dimers do not interchange.

Prm1p dimerization fits well within a membrane fusion model where Prm1p plays a structural role (Aguilar et al., 2007; Jin et al., 2004). In this model, Prm1 oligomers surround cell-cell fusase proteins and membrane fusion intermediates in a circular array. By forming such a structure, Prm1 may be able to influence membrane fusion by positioning fusase molecules in a cooperative arrangement. Covalent linkage of dimers would keep one interface of the Prm1 ring from dissociating, which could be necessary due to the high energies needed for membrane fusion and the vigorous protein folding

events described for the canonical fusases (Li et al., 2007). Another proposed function of this ring is to limit the expansion of membrane holes by corralling lipids within the membrane fusion microenvironment. These holes could be an off-pathway outcome of membrane fusion, or, as predicted by molecular simulations, a true intermediate (Muller et al., 2003). The intermolecular disulfide bridges could increase the effectiveness of a Prm1p barrier to lipid diffusion, especially considering the hydrophobic environment in which cys-120 is located (Fig 5A).

Such functions have been either hypothesized or demonstrated for other classes of membrane fusion. In the case of SNARE-mediated membrane fusion, the prevailing model is that multiple *trans*-SNARE pairs assemble into a ring-like structure. This structure has been observed in reconstituted SNARE protein membrane docking by atomic force microscopy (Cho et al., 2002). Unknown factors have been hypothesized to organize the fusases in this configuration, as this complex is unlikely to form spontaneously (Rizo et al., 2006). In support of the Prm1p-corrall model, the restriction of lipid flow by the assembled fusion machine has been observed during HA-catalyzed membrane fusion (Chernomordik et al., 1998). A ring-shaped oligomer consisting of many HA trimers is believed to surround the hemifusion stalk and prevent diffusion of lipids between merged *cis* leaflets.

A few predictions can be made if Prm1p indeed can organize fusase complexes or prevent lipid diffusion during the membrane fusion process. First, Prm1p would need to physically interact with the fusion machine. Thus, Prm1p remains a promising handle for the biochemical identification of the yeast cell fusase. Second, Prm1p dimers should be

able to form higher order oligomers, either by themselves or in concert with other proteins of the cell fusion machinery.

It is also possible that Prm1p can directly act as a fusase alone or in conjunction with other proteins. If this were the case, the disulfide bonds suggested in this study may serve to lock Prm1p in a metastable state, akin to HA in its neutral pH conformation. Refolding from this metastable state upon fusase activation would provide the energy for membrane fusion.

Further elucidation of Prm1p's role in membrane fusion will build our knowledge of how biological membrane fusion is achieved with high fidelity, moving from the minimal fusion machinery with its elegant mechanism to the complete fusase machine and its fascinating engineering.

MATERIALS AND METHODS

Media and Yeast Strains

Synthetic complete (SC), and complex (YPD) media were prepared and supplemented with 2% glucose using reagents from Difco Inc. and Sigma Chemical Company.

All strains used in this study are derivatives of wild-type strain W303, the *prm1* mutant strains were generated in a previous study (Heiman and Walter, 2000), and the genomic fusion of *GAL_{PRO}-HA* was generated with the PCR transformation technique (Longtine et al., 1998).

Plasmid construction

PRMIGFP, including 507bp of the 5' promoter region and the *ADHI* terminator 3' of the GFP sequence, was amplified from genomic DNA of a *PRMIGFP* strain and cloned into pRS315 by gap repair. Cysteine substitution was achieved by site directed mutagenesis. Myc-tagged *PRMI* constructs were generated by gap repair of the corresponding *PRMIGFP* plasmid digested with *AscI*/*PacI* using PCR product amplified from genomic DNA of a *PRMI**myc* strain. *PRMI* alleles were subcloned into pRS314 and pRS425 as a *SacI*/*XhoI* fragment. Plasmids constructed for this study are listed in Table 1.

Immunoprecipitations

50 OD units of each mating type were filtered onto 85mm 0.45µm HATF membranes (Millipore) and incubated for 3 h at 30°C. Cells were collected from the filters by vortexing in 10ml YPD and pelleted at low speeds in an IEC clinical centrifuge. Pellets were resuspended in IP buffer (50mM HEPES, 100mM KOAc, 2mM Mg(OAc)₂, 1mM PMSF, 1mM EDTA, supplemented with the Complete protease inhibitor (Roche)), and cells were disrupted by bead beating with 0.5mm glass beads (BioSpec Products, Inc.) for a total of 5 min in one min intervals alternating with ice incubations. After unlysed cells and large debris were removed by a 1000RPM microcentrifugation step, the cell lysate was spun at 20K x g for 20 min. The membrane pellet was resuspended in IP buffer + 1% Triton X-100 (Pierce) for 2 h rotating at 4°C. Unsolublized membrane was pelleted in another 20K x g centrifugation step. The supernatant was applied to 30µl of equilibrated agarose-coupled 9E10 anti-c-myc antibody slurry (Santa Cruz Biotechnology) and

rotated for 2 h at 4°C. The beads were washed with 25ml IP buffer + 1% Triton X-100 and bound proteins were eluted in after shaking at 50°C in PBS with 2% SDS for 5 min.

Quantitative cell fusion assay

Mating pair fate was scored microscopically as previously described (Heiman and Walter, 2000).

Microscopy

Fluorescence and DIC microscopy was performed using an Axiovert 200M microscope (Zeiss), equipped with an X-cite 120 mercury arc lamp (EXFO), and an Orca ER camera (Hamamatsu). Metamorph was used for data collection.

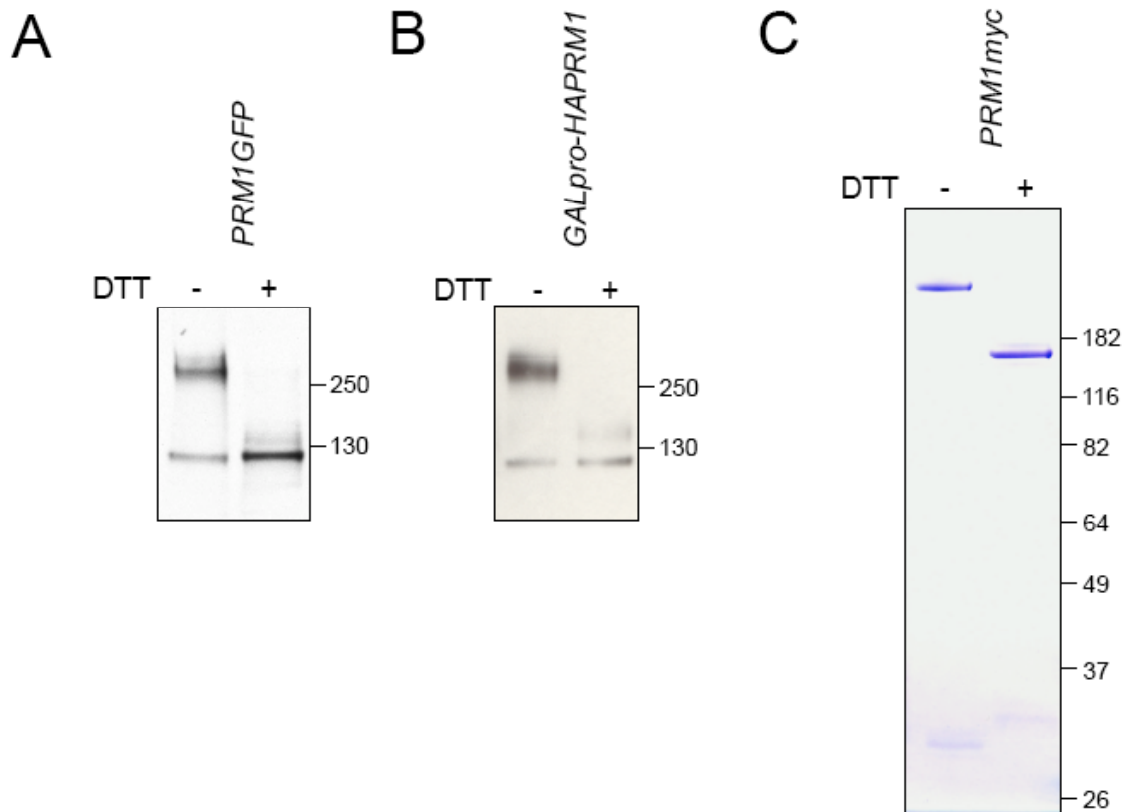
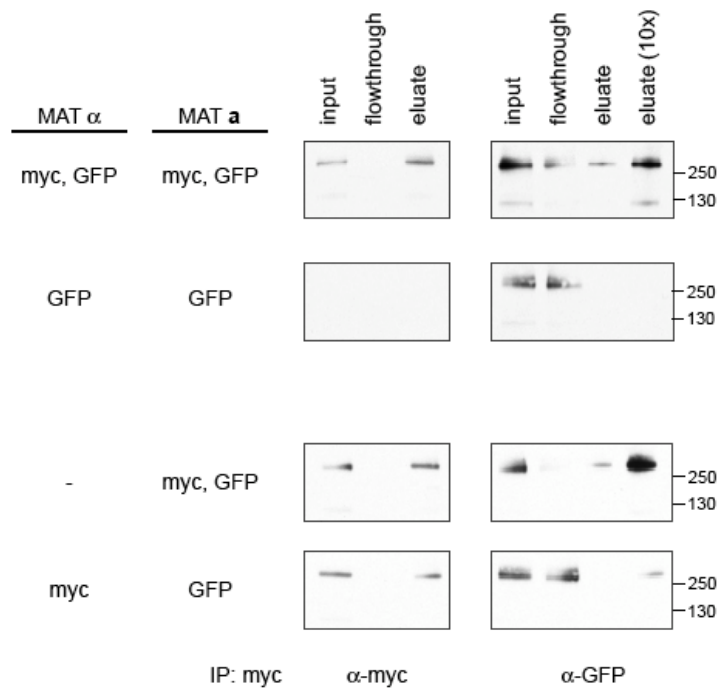


Figure 1. Prm1p reduction-sensitive high molecular weight complex. (A) Anti-GFP Western blot on whole cell lysate of *PRM1GFP MAT a* cells induced with 10µg/ml α-factor for 90 min. (B) Anti-HA Western blot on whole cell lysate after galactose induction of *HAPRM1*. (C) Prm1p was purified from a population of mating cells by α-myc-Agarose immunoprecipitation, eluted with 2% SDS, run on a 10% bis-Tris polyacrylamide gel, and visualized by colloidal blue staining. Protein samples were reduced with 100mM DTT.



*Figure 2. Prm1p homo-oligomerizes in cis. MAT **a** and MAT α cells expressing epitope tagged PRM1 as indicated were mated on YPD plates at 30°C for 3 h. After cell disruption, membrane proteins were solubilized in 1% Triton X-100 and immunoprecipitated using α -myc-Agarose. Western blotting with α -myc and α -GFP antibodies was used to assay pull-down efficiency and co-immunoprecipitation.*

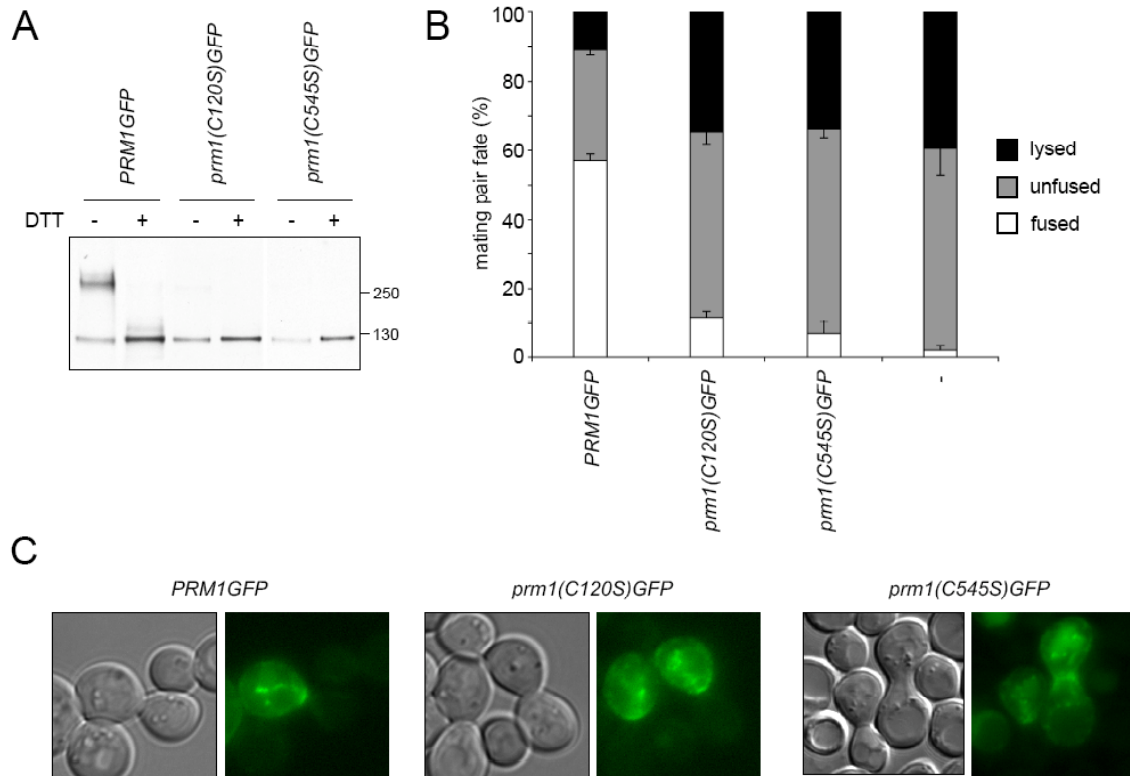


Figure 3. Two cysteines are required for formation of functional covalent Prm1p dimers. (A) Anti-GFP Western blot on whole cell lysate after expression of *PRM1GFP* or cysteine-substituted mutants was induced with 10 μ g/ml α -factor for 90 min. (B) *prm1 MAT* α cells expressing cytoplasmic GFP and *prm1 MAT a* cells bearing the indicated *PRM1* alleles on low copy plasmids were mated on YPD + 20mM EGTA plates at 30°C for 3 h. Mating pairs were fixed with 4% paraformaldehyde and mating pair fate was scored microscopically by observing diffusion of cytoplasm throughout the mating pair (fusion) or loss of GFP signal and abnormal morphology (lysis). (C) Transmitted light and epifluorescence images of Prm1GFP and mutant proteins in live mating pairs shortly after coupling.

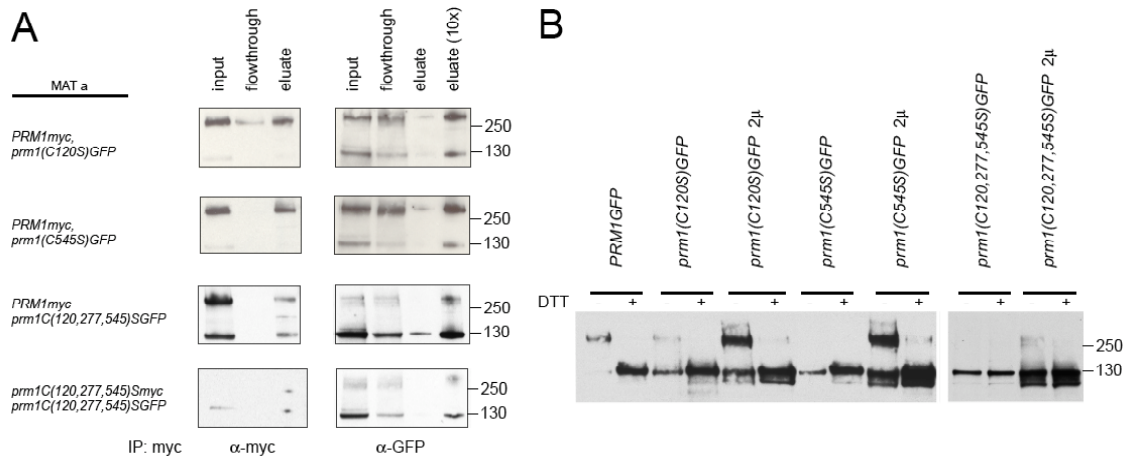


Figure 4. Interaction between Prm1p monomers is not affected by cysteine substitution.

(A) *MAT a* cells expressing epitope tagged *PRM1* or mutant alleles as indicated were mated to wild-type *MAT α* cells on YPD plates at 30°C for 3 h. Myc-tagged fusion proteins were immunoprecipitated using α-myc-Agarose. Western blotting with α-myc and α-GFP was used to assay pull-down efficiency and co-immunoprecipitation. (B) Anti-GFP Western blot on whole cell lysates of *MAT a* cells induced with 10μg/ml α-factor for 90 min. Indicated alleles of GFP-tagged *PRM1* were maintained on CEN-ARS plasmids or on high copy plasmids (indicated as 2μ). Protein samples were reduced with 100mM DTT.

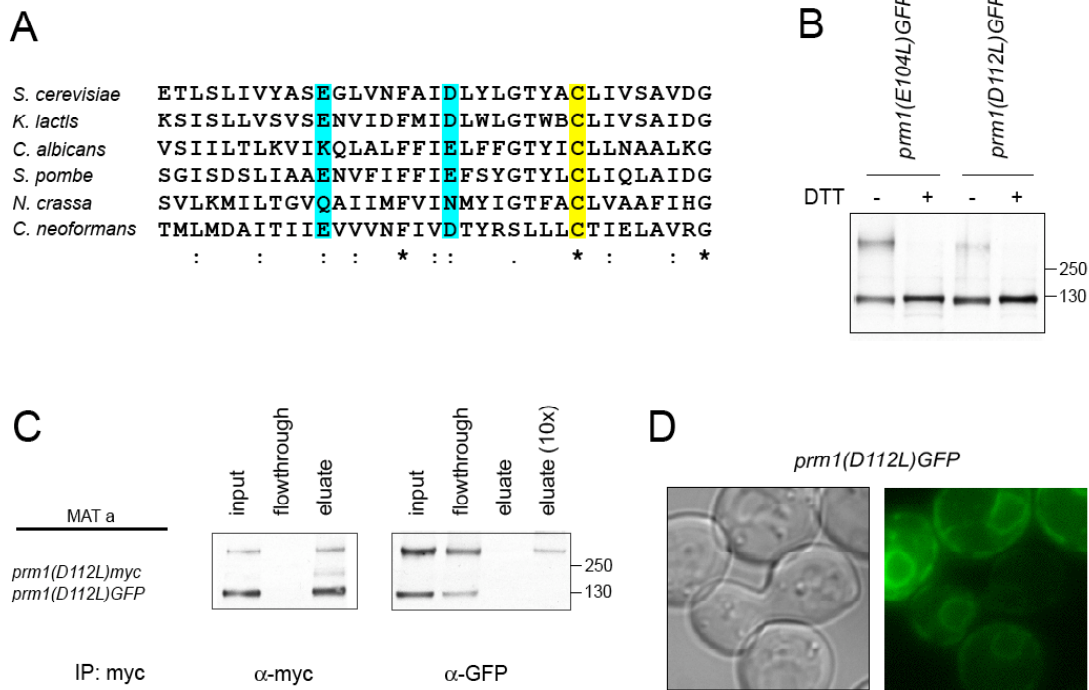


Figure 5. Influence of charged residues in the second transmembrane domain of Prm1p on dimerization. (A) ClustalW alignment of the Prm1p TM2 region. (B) Anti-GFP Western blot on whole cell lysate after expression of *prm1E104LGFP* or *prm1D112LGFP* was induced with 10 μ g/ml α -factor for 90 min. (C) *MAT a* cells coexpressing *prm1D112LGFP* and *prm1D112Lmyc* were mated to wild-type *MAT a* cells on YPD plates at 30°C for 3 h. Myc-tagged fusion proteins were immunoprecipitated using α -myc-Agarose. Western blotting with α -myc and α -GFP was used to assay pull-down efficiency and co-immunoprecipitation. (D) Transmitted light and epifluorescence images of *prm1D112LGFP* in a live mating pair.

Table 1. Plasmids constructed for this study

Plasmid name	<i>PRM1</i> allele	Parental plasmid
pAE18	<i>PRM1GFP</i>	pRS315
pAE28	<i>prm1(C6S)GFP</i>	pRS315
pAE29	<i>prm1(C55S)GFP</i>	pRS315
pAE20	<i>prm1(C120S)GFP</i>	pRS315
pAE21	<i>prm1(C277S)GFP</i>	pRS315
pAE30	<i>prm1(C302S)GFP</i>	pRS315
pAE31	<i>prm1(C308S)GFP</i>	pRS315
pAE32	<i>prm1(C329S)GFP</i>	pRS315
pAE33	<i>prm1(C377S)GFP</i>	pRS315
pAE34	<i>prm1(C424S)GFP</i>	pRS315
pAE35	<i>prm1(C436S)GFP</i>	pRS315
pAE36	<i>prm1(C438S)GFP</i>	pRS315
pAE22	<i>prm1(C545S)GFP</i>	pRS315
pAE37	<i>prm1(C120,277,545S)GFP</i>	pRS315
pAE38	<i>prm1(C120,277,545S)myc</i>	pRS314
pAE39	<i>prm1(C120S)GFP</i>	pRS425
pAE40	<i>prm1(C545S)GFP</i>	pRS425
pAE41	<i>prm1(C120,277,545S)GFP</i>	pRS425
pAE42	<i>prm1(E104L)GFP</i>	pRS315
pAE27	<i>prm1(D112L)GFP</i>	pRS315
pAE43	<i>prm1(D112L)myc</i>	pRS314

Chaper 4 is reproduced from The Journal of Cell Biology, 2006, 176:209-222. Copyright
2006 the Rockefeller University Press.

CHAPTER 4

THE GOLGI-RESIDENT PROTEASE KEX2 ACTS IN CONJUNCTION WITH PRM1 TO FACILITATE CELL FUSION DURING YEAST MATING

**The Golgi-resident protease Kex2 acts in conjunction with Prm1
to facilitate cell fusion during yeast mating**

Maxwell G. Heiman*, Alex Engel, and Peter Walter

Howard Hughes Medical Institute
and Department of Biochemistry and Biophysics
University of California at San Francisco
San Francisco, CA 94158

(415) 476 5017 (phone)

(415) 466 5233 (FAX)

pwalter@biochem.ucsf.edu

* Present address: Rockefeller University
 1230 York Avenue
 New York, NY 10021

ABSTRACT

The molecular machines that mediate cell fusion are unknown. Previously, we identified a multispinning transmembrane protein, Prm1, that acts during yeast mating. Without Prm1, a significant fraction of mating pairs arrest with their plasma membranes tightly apposed yet unfused. Here, we show that lack of the Golgi-resident protease Kex2 strongly enhances the cell fusion defect of Prm1-deficient mating pairs and causes a mild fusion defect in otherwise wild-type mating pairs. Lack of the Kex1 protease but not the Ste13 protease results in similar defects. $\Delta kex2$ and $\Delta kex1$ fusion defects were suppressed with osmotic support, similar to mutants defective in cell wall remodeling. By contrast, other cell wall mutants do not enhance the $\Delta prm1$ fusion defect. Electron microscopy of $\Delta kex2$ -derived mating pairs revealed novel extracellular blebs at presumptive sites of fusion. Kex2 and Kex1 may promote cell fusion by proteolytically processing substrates that act in parallel to Prm1 as an alternative fusion machine, as cell wall components, or both.

INTRODUCTION

Cell fusion is an important developmental event, from sperm-egg fusion during fertilization to syncytium formation in the development of placenta, muscle, and certain hematopoietic cell types. While detailed mechanistic characterizations have been carried out for virus-cell fusion and vesicle-organelle fusion, the molecular events mediating cell-cell fusion are poorly understood. In virus and vesicle fusion, a protein machine – a fusase – assembles between the fusing bilayers, such that it spans both membranes (Hernandez et al., 1996). For influenza virus the fusase is the hemagglutinin protein which is anchored in the viral membrane and inserts itself into the target membrane (Ramalho-Santos and de Lima, 1998; Skehel and Wiley, 2000) while for vesicle-organelle fusion the interaction of cognate SNARE-family transmembrane proteins results in the assembly of a multiprotein complex anchored in both vesicle and target membranes (Weber et al., 1998). Hemagglutinin and the SNARE complex each adopt a coiled-coil structure that undergoes a series of conformational changes to winch the two bilayers into close proximity (Sutton et al., 1998; Wilson et al., 1981). During this process, the bilayer structure becomes distorted and water separating the apposing membranes is squeezed out, initiating fusion (Harbury, 1998; Hughson, 1995).

A similar fusase mediates cell fusion during placental development: syncytin, a protein encoded by a retrovirus-derived gene, is necessary and sufficient for placental cell fusion (Mi et al., 2000). However, no analogous fusases have been identified in muscle precursors, sperm or egg, or other cells that fuse. Over a dozen proteins required for myoblast or osteoclast/macrophage fusion have been identified, but many of these proteins promote early steps including cell migration and adhesion rather than the later

step of cell fusion (Dworak and Sink, 2002; Han et al., 2000). Likewise, in sperm-egg fusion, the fertilin complex was initially recognized as bearing hallmarks of a fusase – it contains a hydrophobic peptide capable of inserting into a membrane and experimentally blocking fertilin function prevents fusion – yet fertilin knockout mice are primarily defective in sperm migration into the oviduct and binding to the zona pellucida that surrounds the egg, with a much weaker defect at the final step of cell fusion (Blobel et al., 1992; Cho et al., 1998; Cho et al., 2000).

A few proteins likely to act late in cell fusion, possibly at the ultimate step of membrane fusion, have been identified. EFF-1, a single-pass transmembrane protein, is required for syncytia formation in the hypodermal cells of *C. elegans* (Mohler et al., 2002) and when ectopically expressed is sufficient to fuse cells that do not normally fuse (Shemer et al., 2004, del Campo et al., 2005, Podbilewicz et al., 2006), thus making it an excellent candidate fusase. Two proteins, CD9 and CRISP-1, are important for sperm-egg fusion and seem to act after the initial steps of cell adhesion. CD9 is a multispinning membrane protein in the oocyte plasma membrane, and oocytes from mice lacking CD9 adhere normally to sperm but do not fuse with them (Kaji et al., 2000; Le Naour et al., 2000; Miyado et al., 2000). CRISP-1 is a peripherally associated membrane protein on the surface of sperm that, when blocked, prevents sperm-egg fusion but not adhesion (Cuasnicu et al., 2001).

Yeast mating offers a genetically powerful system in which to identify factors controlling the late steps of cell fusion. During yeast mating, haploid cells of mating types MAT_a and MAT_α secrete pheromone (MAT_a cells make a-factor; MAT_α cells make α-factor) which is detected by a G-protein-coupled receptor on the complementary

cell type, initiating a MAPK signaling cascade which results in G1 cell cycle arrest, polarized growth in the direction of highest pheromone concentration, and transcriptional upregulation of about 100 genes (Herskowitz, 1995). The mating partners adhere to one another through interactions in the cell wall to produce a mating pair. Finally, in a process whose molecular details have only begun to come to light, a small region of the cell wall at the interface between the mating partners is degraded, the mating partners' plasma membranes become apposed, and finally cell fusion occurs.

Numerous attempts to identify the cell fusion machinery have identified factors required for cell wall degradation at multiple steps, from regulating cell wall remodeling and secretory vesicle trafficking to the maintenance of osmotic integrity (Brizzio et al., 1998; Kurihara et al., 1994; Philips and Herskowitz, 1997; Philips and Herskowitz, 1998; Trueheart et al., 1987). None of these genetic screens, however, have identified genes that seem to act at the final step in cell fusion, the merging of plasma membrane bilayers. Previously, we designed a reverse genetic approach aimed at uncovering the fusion machinery (Heiman and Walter, 2000). We reasoned that the cell fusion machinery that acts during mating probably includes a transmembrane protein expressed specifically in response to mating pheromone. We began studying pheromone-regulated membrane proteins (PRM proteins) and, using the data mining program Webminer (<http://genome-www.stanford.edu/webminer>), we identified the membrane protein most induced by pheromone, Prm1, and characterized its role in membrane fusion (Heiman and Walter, 2000).

Prm1 is a multispanning membrane protein not expressed under standard growth conditions but induced in both mating types in response to pheromone (Heiman and

Walter, 2000). It localizes to the site of cell fusion. If either mating partner lacks Prm1, about 10% of mating pairs fail to fuse but if both mating partners lack Prm1 then about 50% of mating pairs fail to fuse (Heiman and Walter, 2000). When we examined *Δprm1* x *Δprm1* mating pairs by electron microscopy, we observed a morphology never before seen. In some mating pairs the cell wall had been degraded and the plasma membranes had become apposed yet failed to fuse (Heiman and Walter, 2000). This result indicates that Prm1 facilitates the final step in cell fusion, that of plasma membrane fusion (White and Rose, 2001).

But Prm1 cannot constitute the complete machinery. Even in its absence about half of all mating pairs still fuse, indicating that Prm1 either facilitates the action of a yet unidentified fusase or that Prm1 is itself a fusase and one or more alternative fusases exist. Intriguingly, *Δprm1* mating pairs frequently lyse when attempting to fuse, suggesting the remaining presence of an active but dysregulated fusase (Jin et al., 2004). Among *Δprm1* mating pairs that are capable of fusion, the initial permeance and expansion rate of the fusion pore are slightly decreased, indicating a role for Prm1 in fusion pore opening; however, the subtlety of this defect again points to the presence of a redundant fusion activity (Nolan et al., 2006). The notion of additional fusion machinery that is regulated by or acts in parallel to Prm1 implies that disruption of additional components should create more severe blocks to membrane fusion than can be achieved by disrupting *PRM1* alone. Here, we have exploited this prediction to design a genetic screen that led to the identification of a gene acting in conjunction with *PRM1* to promote cell fusion.

RESULTS

A genetic screen for enhancers of the *Δprm1* mating defect identifies mutations in *KEX2*

To identify factors required for Prm1-independent cell fusion, we screened for mutants that enhance the *Δprm1* × *Δprm1* mating defect. We performed random mutagenesis of a *Δprm1* MAT α strain bearing a selectable marker. We then plated the mutants, allowed them to form small colonies, and replica plated them to a lawn of *Δprm1* MAT α cells bearing a different selectable marker. We allowed mating to occur and replica-plated to medium selective for auxotrophic markers of both parent strains, thus allowing growth only of diploids that arose during the mating. Each mutant colony from the original plate resulted on the final selective plate in a small patch with many diploid micro-colonies emerging from it as papillae (Fig. 1A). The density of diploid papillae within each patch reflected the mating efficiency of the mutant that gave rise to it. Using this “replica mating” assay, we screened for mutants in the *Δprm1* background that mated poorly to a *Δprm1* partner.

In addition to mutants in the *PRM1*-independent fusion pathway, we expected to find sterile mutants not relevant to this study. To distinguish these classes, we tested the ability of each mutant to mate to a wild-type partner. Mutants that mated poorly to a wild-type partner were considered sterile and discarded.

To further characterize the remaining mutants, we performed a backcross to ensure that the observed phenotypes segregated as single mutations. To our surprise, 4 out of 10 mutants revealed a new phenotype after backcrossing. MAT α progeny bearing these mutations, but not MAT α progeny, displayed complete sterility whether mated to a wild-type or *Δprm1* partner. Therefore, we assumed that a set of mutations that enhance the *Δprm1* phenotype in MAT α cells

causes sterility in MAT α cells. Because sterility was easier to score, we used complementation cloning to isolate the gene responsible for the MAT α -specific sterility in one of the mutants. The remaining mutants were not characterized further. We recovered 4 genomic fragments that restored mating to this mutant. These fragments overlapped in a region containing the coding sequence of *KEX2*.

Kex2 functions as a protease in the Golgi apparatus that processes several proteins traversing the secretory pathway, including the α -factor mating pheromone (Fuller et al., 1989; Julius et al., 1983). This essential role of *Kex2* in the processing of prepro- α -factor readily explains why MAT α $\Delta kex2$ mutants are sterile. In contrast, *Kex2* does not process the a-factor mating pheromone and MATa $\Delta kex2$ mutants do not display pheromone response defects, making it unlikely that the observed mating defect results from impairment of the pheromone signaling pathway (Leibowitz and Wickner, 1976).

As expected, a MAT α $\Delta kex2 \Delta prm1$ mutant was sterile in our assay (not shown). In contrast, a MATa $\Delta kex2 \Delta prm1$ mutant mated efficiently to a wild-type partner but poorly to a $\Delta prm1$ partner. While we could not detect the weakly penetrant $\Delta prm1 \times \Delta prm1$ phenotype by replica mating, the more severe phenotype of a $\Delta prm1 \Delta kex2 \times \Delta prm1$ mating was readily apparent (Fig. 1B).

Loss of *Kex2* synergizes with loss of *Prm1* to impair mating at the cell fusion step

To learn whether *Kex2* acts in cell fusion, we used a quantitative cell fusion assay as previously described (Heiman and Walter, 2000). Mating partners carrying deletions in *PRM1*, *KEX2*, both, or neither were mixed and allowed to mate. One partner expressed soluble cytoplasmic GFP to serve as a marker for cytoplasmic mixing. Mating pairs were examined by fluorescence

microscopy. Mating pairs with GFP throughout their volume were scored as fused, while mating pairs in which GFP remained restricted to one partner were scored as unfused (Fig. 2A). By counting the ratio of fused to total mating pairs, we quantitated the efficiency of cell fusion. This assay differs from replica mating in that it scores only the cell fusion step of mating rather than the entire mating process.

In agreement with our previous results, we observed in control mating reactions that deletion of *PRM1* from both mating partners creates a substantial block to cell fusion compared to wild-type (Fig. 2B, compare bars 1 and 7), while deletion of *PRM1* from either mating partner alone produces a barely perceptible decrease in fusion efficiency (Fig. 2B, compare bars 1, 3 and 5) (Heiman and Walter, 2000).

Interestingly, the loss of *KEX2* in the MAT α partner alone decreases fusion by 15% compared to wild-type (Fig. 2B, bars 1 and 2) thereby demonstrating a role in cell fusion of Kex2 in MAT α cells. While the defect was small, it was highly reproducible. Due to the role of Kex2 in α -factor processing, we could not reciprocally assay MAT α Δ *kex2* mutants.

We observed a significantly greater Kex2-dependency of cell fusion in mating reactions in which both partners lacked Prm1. The efficiency of cell fusion in Δ *kex2* Δ *prm1* x Δ *prm1* mating pairs is 70% lower than that in Δ *prm1* x Δ *prm1* mating pairs (Fig. 2B, bars 7 and 8). The Δ *kex2* mutation thus unilaterally and potently enhances the otherwise weakly penetrant Δ *prm1* fusion phenotype.

The Kex2 dependency of mating reactions in which only one partner expresses Prm1 proved more complicated. Mating pairs in Δ *kex2* x Δ *prm1* mating reactions fuse with a much reduced efficiency compared to WT x Δ *prm1* mating reactions (Fig. 2B, bars 3 and 4). In contrast, Δ *kex2* Δ *prm1* x WT mating reactions do not differ greatly from Δ *prm1* x WT matings

(Fig. 2B, bars 5 and 6). In other words, the $\Delta kex2$ mutation produces a much stronger effect when placed in *trans*, rather than in *cis*, to the $\Delta prm1$ mutation.

Processing by Kex2 and Kex1 but not Ste13 synergizes with Prm1 in cell fusion

The Kex2 protease has been extensively characterized (Rockwell et al., 2002). In brief, Kex2 acts as a furin-type endopeptidase that cleaves substrate proteins at dibasic sequence “LysArg” sites as the proteins traverse the Golgi apparatus. For many substrates, such as α -factor, the initial Kex2 cleavage is followed by the action of two exopeptidases, which trim the newly exposed ends: Kex1, a carboxypeptidase, removes the “LysArg” sequence from the C-terminus of the N-terminal fragments, while Ste13, an aminopeptidase, removes pairs of residues (preferring “X-Ala” sequences) from the N-terminus of the C-terminal fragments.

To test whether Kex1 or Ste13 also affect cell fusion, we subjected $\Delta kex1$ and $\Delta ste13$ mutants to the same genetic analysis we used with $\Delta kex2$ mutants. We conducted mating reactions in which the partners lacked either Prm1 or Kex1 in all combinations, or Prm1 or Ste13 in all combinations and assayed the resulting mating pairs for fusion using the GFP-mixing assay.

As shown in Figure 3, a $\Delta kex1$ mutant displays a slight but significant fusion defect when crossed to a wild-type partner (Fig. 3A, bars 1 and 2). This defect was enhanced when we introduced a $\Delta prm1$ mutation in *trans* but not in *cis* (Fig. 3A, bars 3 and 4, and bars 5 and 6, respectively). Finally, the most severe defect occurred when we introduced a $\Delta kex1$ mutation into a $\Delta prm1 \times \Delta prm1$ cross, which reduced the number of successful fusions by more than half (Fig. 3A, bars 7 and 8). Thus, the effects of the $\Delta kex1$ mutation qualitatively phenocopy those of the $\Delta kex2$ mutation, although the $\Delta kex1$ mutation produces slightly milder fusion defects.

In contrast, deletion of *STE13* from a WT x WT mating reaction produced no significant difference in cell fusion (Fig. 3B, bars 1 and 2). Furthermore, Δ *ste13* did not enhance the Δ *prm1* fusion phenotype when placed in *trans* or in *cis* (Fig. 3B, bars 3 and 4, and bars 5 and 6). Finally, when introduced into a Δ *prm1* x Δ *prm1* mating, the Δ *ste13* mutation did not reduce mating significantly (Fig. 3B, bars 7 and 8). These results demonstrate that the complement of proteases required to promote cell fusion in MATa cells is distinguishable from that required for α -factor processing.

The Δ *kex2* fusion defect is not due to inactivation of a previously known substrate or either of two novel substrates

The dependency of cell fusion on Kex2 and Kex1 suggests the existence of a proteolytically-activated protein that facilitates fusion. To try to identify such a protein, we generated strains carrying deletions of known Kex2 substrates and assayed their fusion efficiencies.

Among known Kex2 substrates are cell wall glucosidases such as Scw4 and Scw10 (Basco et al., 1990; Mrsa et al., 1997; Cappellaro et al. 1998) and cell wall structural components such as Hsp150 (Russo et al., 1992). We systematically generated deletions in eight known Kex2 substrates and mated each mutant to a wild-type or Δ *prm1* mating partner (Fig. 4A). If proteolytic activation of a given substrate is required for fusion, we expected the loss of that substrate to phenocopy the loss of Kex2: it should display a mild decrease in fusion when crossed to a wild-type partner and a more severe decrease when crossed to a Δ *prm1* partner. As shown in Figure 4A, none of the mutants

displayed such a fusion defect. Thus, the $\Delta kex2$ fusion defect does not result from inactivation of any one of these substrates singly.

Some of these Kex2 substrates may act redundantly, and only show a phenotype when removed in combination. For example, it has been shown that lack of Scw4 or Scw10 alone causes a very mild cell wall defect, but loss of both results in extreme weakening of the cell wall and a mating defect (Cappellaro et al., 1998). We tested the $\Delta scw4 \Delta scw10$ double mutant in our fusion assays, and saw no effect with a wild-type or $\Delta prn1$ mating partner (Fig. 4A) or with a $\Delta scw4 \Delta scw10$ mating partner (not shown). It remains possible that inactivation of some other combination of known Kex2 substrates would recapitulate the $\Delta kex2$ fusion defect.

We hypothesized that there might be an additional, unidentified Kex2 substrate that mediates Kex2-dependent fusion. We designed a bioinformatics screen to attempt to identify such a substrate. Briefly, we developed a scoring matrix based on the cleavage site sequences of known substrates and used it to rank potential cleavage sites in all other *S. cerevisiae* proteins, discarding high-scoring candidate sites that are not conserved among closely related yeasts or that are predicted to be cytoplasmic (Supplementary Table 1). We tested 11 proteins with the highest-ranked candidate sites by generating epitope-tagged alleles of each in wild-type and $\Delta kex2$ backgrounds and performing SDS-PAGE and Western blotting of cell lysates. With this approach, we identified two new Kex2 substrates: Prm2 and Ykl077w (Fig. 4B).

Prm2 is predicted to be a pheromone-regulated multispinning membrane protein with topology similar to Prm1, and was identified in the bioinformatics screen that led to characterization of Prm1 (Heiman and Walter, 2000). Ykl077w is an uncharacterized

protein predicted to have a large (~300 amino acid) extracellular/luminal domain and a single transmembrane segment. Both proteins showed a shift in apparent molecular weight in a $\Delta kex2$ mutant background consistent with Kex2-dependent proteolysis (Fig. 4B).

We generated $\Delta prm2$ and $\Delta ykl1077w$ mutants and tested them in our fusion assays. Neither mutant showed a defect with wild-type or $\Delta prm1$ mating partners (Fig. 4A). Thus, although we were able to identify two novel Kex2 substrates, neither appears to be the hypothetical substrate relevant to fusion. It may be that another, yet unidentified substrate or a combination of redundant Kex2 substrates acts during cell fusion.

$\Delta kex2$ shares a spectrum of phenotypes with other cell wall mutants but uniquely enhances the $\Delta prm1$ cell fusion defect

We asked whether the sum of physiological effects resulting from a lack of processing of Kex2 substrates might explain the $\Delta kex2$ fusion defect. For example, cells lacking Kex2 display a weakened cell wall phenotype, as assayed by upregulation of cell integrity pathway target genes and hypersensitivity to the cell-wall-binding dye Congo Red (Tomishige et al., 2003). Cell wall stress is known to induce the PKC signaling pathway, which can inhibit cell fusion (Philips and Herskowitz, 1997). Thus we next asked whether cell wall stress could explain the cell fusion defect caused by loss of Kex2.

To this end, we first established whether the PKC cell integrity pathway is activated in $\Delta kex2$, $\Delta kex1$, and $\Delta prm1$ mutant cells. Cell wall stress and low osmolarity signals activate Pkc1 through the Bck1 MAPK module, eventually leading to activation of the transcription factor Rlm1, which activates transcription of many genes including

MPK1 (Banuett, 1998). An *MPK1-lacZ* reporter gene has thus been used to detect activation of the PKC cell integrity pathway (Jung and Levin, 1999; Muller et al., 2003). We grew strains bearing the *MPK1-lacZ* reporter overnight with or without 1M sorbitol added as osmotic support, harvested cultures in exponential phase, and assayed for reporter activity during vegetative growth or following exposure to α -factor pheromone (Fig. 5A).

Wild-type cells show enhanced *MPK1* activation upon α -factor treatment, as expected from the cell wall remodeling that accompanies the pheromone response. The presence of osmotic support slightly decreased *MPK1* activation in wild-type cells (Fig. 5A, black bars). Note that $\Delta prm1$ mutant cells were indistinguishable from wild type in the absence and presence of α -factor, strongly suggesting deletion of *PRM1* does not affect cell wall structure (Fig. 5A). In contrast, $\Delta kex1$ and $\Delta kex2$ mutants showed enhanced baseline *MPK1* activation (2.5-fold and 6-fold greater than wild-type levels, respectively), consistent with a cell wall structural defect. The enhanced *MPK1* activation was exacerbated by pheromone treatment and weakly mitigated by the presence of osmotic support (Fig. 5A). $\Delta ste13$ mutants did not show these effects (not shown).

As a further measure of cell wall integrity, we assayed each mutant for Congo Red sensitivity. Mutants with compromised cell walls generally do not grow on media containing Congo Red. Consistent with previously reported results, $\Delta kex2$ growth was severely inhibited on plates containing 100 μ g/ml Congo Red (Tomishige et al., 2003, Fig. 5B), similar to the phenotype of the Kex2 substrate mutant $\Delta scw4 \Delta scw10$ (Cappellaro et al., 1998., Fig. 5B). In contrast, viability of neither $\Delta kex1$ nor $\Delta prm1$ was

affected by Congo Red. Thus, as assayed by *MPK1* activation and Congo Red sensitivity, cell wall defects are severe in $\Delta kex2$ mutant cells, mild in $\Delta kex1$ mutant cells, and undetectable in $\Delta prm1$ mutant cells.

Most cell wall defects manifest themselves due to a failure of the cell wall to provide a rigid support counteracting the outward force on the cell membrane caused by the osmotic imbalance between cytoplasm and the growth medium. Thus we asked next whether osmotically stabilized medium (i.e., growth medium formulated at an osmolarity closer to that of cytoplasm) which relieves many phenotypes resulting from cell wall defects, could suppress the $\Delta kex2$ cell fusion defect. Mating reactions were performed under standard conditions with or without 1M sorbitol and fused mating pairs counted in the quantitative cell fusion assay. As controls, we showed that bilateral crosses of the classical cell wall remodeling mutants $\Delta fus1$ and $\Delta fus2$ were partially suppressed by mating on osmotic support (Fig. 5C). Surprisingly, we found $\Delta prm1$ cells displayed a decreased fusion efficiency in the presence of osmotic support (Fig. 5C, a similar observation was reported by Jin et al., 2004). The explanation for this decrease is not clear, but it suggests that the $\Delta prm1$ defect is distinct from cell wall stress. In contrast, the mild $\Delta kex2$ x WT defect was suppressed by osmotic support (Fig. 5C), as was the $\Delta kex1$ x WT defect (not shown). The strongly deficient $\Delta kex2$ x $\Delta prm1$ mating was partially suppressed but, importantly, fusion was not restored to wild-type levels. Thus, $\Delta kex2$ and $\Delta kex1$ behave similarly to other fusion mutants known to affect cell wall degradation, while $\Delta prm1$ does not.

If cell wall defects caused by loss of Kex2 are responsible for strongly enhancing the $\Delta prm1$ fusion defect then we expect other mutants with similar cell wall defects also

to synergize with $\Delta prml$ in a fusion assay; alternatively, if the failure to process Kex2 substrates that act specifically with Prm1 causes the enhanced fusion defect then other cell wall mutants will not synergize with $\Delta prml$. To distinguish these possibilities, we mated strains bearing a $\Delta fus1$, $\Delta fus2$, or $PKC1-R398P$ (a gain-of-function allele which mimics constitutive cell wall stress; Nonaka et al., 1995) mutation to a $\Delta prml$ partner and scored mating pairs with the cell fusion assay. Unlike $\Delta kex2 \times \Delta prml$, no combination of mutants in these mating reactions showed a synergistic defect (Fig. 5D). Mating reactions with the cell wall structure mutant $\Delta scw4 \Delta scw10 \times \Delta prml$ (Fig. 4B) similarly did not produce a synergistic defect. Thus, taken together, $\Delta kex2$ mutant cells experience cell wall stress and concomitantly increase *MPK1* activation. Those defects are not sufficient, however, to explain the unique synergy we observe between $\Delta kex2$ and $\Delta prml$ mating partners. These results therefore strongly suggest that the synergistic effect of the $\Delta kex2$ and $\Delta prml$ mutations on cell fusion results from combined defects in the cell fusion machinery.

$\Delta kex2$ mutants produce cytoplasmic blebs embedded in the cell wall

To characterize ultrastructurally the cell fusion intermediate at which $\Delta kex2 \times$ WT mating reactions arrest, we examined fusion-arrested mating pairs using electron microscopy. In the majority (80%) of unfused $\Delta kex2 \times$ WT mating pairs, we observed novel, bleb-like structures in the cell wall separating the two mating partners. Such cell wall-embedded blebs appear disconnected from both cells (Figs. 6 and 7). The blebs are bounded by a visible lipid bilayer (see especially Figs. 6E, 7F and 7M; in other views the bilayer is harder to discern owing to the angle of the section relative to the plane of the bilayer). A gap of a relatively consistent width of

about 8 nm separates the blebs from the plasma membrane that they appear adhered to (see especially Figs. 6A, 6C, 6E, 7F, 7J and 7M). About 90% of the blebs appear preferentially linked to one mating partner, but about 10% of the blebs closely approach the plasma membrane of the other mating partner as well (see Figs. 6B, 6C, 7F and 7M). In any given section, we observed numbers ranging from one bleb (see Figs. 6A and 6C), to one primary bleb with others clearly above or below it (see Figs. 6B and 6E), to two blebs side-by-side with their surfaces tightly apposed (see Fig. 6D), to a cascade of blebs spread out across the diameter of the cell-cell interface (Fig. 6F). About 75% of unfused mating pairs have one to five blebs, with 5% having more and 20% having none. In serial sections, we never detected a clear cytoplasmic continuity between a bleb and either mating partner. The texture of the staining inside the blebs often appears fibrous, unlike the regular punctate staining of ribosomes observed in normal cytoplasm (see especially Fig. 6D).

We examined the three-dimensional structure and arrangement of blebs in more detail by serial section analysis. A representative set of serial sections is shown in Figure 7. At one end of the series, the cell-cell interface appears restricted and secretory vesicles are sparse, indicating the sections come from a region where the cells are just beginning to make contact off-center of the long axis of the mating pair (Figs. 7A and 7B). As the sections approach the center of the mating pair, the contact zone widens, the number of secretory vesicles in the cytoplasm increases, and a cell wall-embedded bleb appears (Figs. 7C and 7D). Moving more to the center of the cell-cell interface, the bleb broadens and appears to push slightly into the mating partner on the left (Figs. 7E and 7F) before disappearing from view (Fig. 7G). A second bleb appears in a lower section and widens (Figs. 7G-K); a third and possibly a fourth bleb appear still farther along the stack of sections (Figs. 7J and 7K). The bleb in Figures 7C-F almost contacts both

plasma membranes; in Fig. 7F (magnified in Fig. 7M) it appears only about 10 nm from the partner on the right.

Other structures of unknown function are also frequently observed in these images. A dark unclosed circle—reminiscent of the formation of autophagic structures by the fusion of small vesicles (Kim and Klionsky, 2000)—appears to begin enclosing a region of cytoplasm (Fig. 7G, magnified in Fig. 7N). Similarly, a spherical lipid bilayer enclosed in a second, equidistant bilayer contains dark-staining cytoplasm (Fig. 7I, magnified in Fig. 7O) and suggests a mature form of the first structure. Both structures are surrounded by a zone of ribosome exclusion. Similar structures appear often in sections of *Δkex2* mutant derived mating pairs (see for example Fig. 6D).

***Δprm1 Δkex2* x *Δprm1* mating pairs exhibit blebs, bubbles, and enormous barren bubbles**

We had previously described the formation of ‘bubbles’ as characteristic features of fusion-arrested *Δprm1* x *Δprm1* mating pairs (Heiman and Walter, 2000). Bubble formation appeared to result from a block in fusion of the mating partners after intervening cell wall had been removed and plasma membranes had tightly adhered to each other, often buckling as a double membrane into either cell. Based on the morphologically distinguishable phenotypes of the *Δkex2* x WT and *Δprm1* x *Δprm1*-derived mating pairs, we wished to explore whether the ultrastructure of *Δprm1 Δkex2* x *Δprm1* mating pairs would reflect the order of *KEX2* and *PRM1* function in the fusion pathway. Rather than observing a single epistatic phenotype, however, we saw a more complex, heterogeneous mixture of three classes of structures.

First, we observed bubbles in *Aprm1 Δkex2* x *Aprm1* mating pairs, similar to those seen in *Aprm1* x *Aprm1* mating reactions. A characteristic bubble in such mating pairs is shown in Figures 8A and 8B. In this example, the mating partner on the bottom forms an extension past the midline of the mating pair and well into the space previously occupied by the mating partner on the top. The plasma membranes appear tightly apposed but unfused. The cytoplasmic continuity between the bubble and the bottom cell is obvious, and the texture of the staining within the bubble matches that of normal cytoplasm.

Second, we observed cell wall-embedded blebs, similar to *Δkex2* x WT mating reactions. Serial sections of a *Aprm1 Δkex2* x *Aprm1* bleb are shown in Figure 9. Several blebs extend over the full width of the cell-cell interface. No cytoplasmic continuity between the blebs and either mating partner can be found. Additionally, a double-bilayer-bound structure appears in the upper mating partner of this pair. In some mating pairs, blebs of an enormous size accumulated (both mating pairs in Fig. 8C, magnified in Figs. 8D and 8E).

Third, some *Aprm1 Δkex2* x *Aprm1* mating pairs display a unique morphology not previously observed, here referred to as “enormous barren bubbles” (EBBs). EBBs appear similar to *Aprm1* x *Aprm1* bubbles yet are essentially devoid of the staining of ribosomes and vesicles that populate normal cytoplasm (serial sections, Figs. 8F-I). These structures also lack the fibrous pattern typical of *Δkex2* blebs. Instead, they present the appearance of empty, organelle-free cytoplasm, despite the presence of clear continuities to one mating partner (see Fig. 8H). One section shows an EBB that may be folded back onto itself thus giving the appearance of two separate structures (Fig. 8I). The lack of cytosol might reflect a lysis event, which a fraction of *Aprm1* mating pairs undergo (Jin et al., 2004). Similarly barren areas have been observed in ultrastructural studies of myoblast fusion pores and within membrane sacs

subsequent to cell-cell fusion (see Fig. 2 in Doberstein et al., 1997). It remains an intriguing mystery how a portion of the cytoplasm could become so distinctly different without a visibly delimiting barrier.

DISCUSSION

The molecular machine that fuses cells during yeast mating has remained elusive. We describe here the discovery of a role of Kex2 during cell fusion. To date, Kex2's only known function in mating involved an earlier step, namely the proteolytic processing of the pheromone α -factor in MAT α cells (Rockwell et al., 2002). In contrast, Kex2 is not required in MAT α cells for pheromone processing, which allowed the discovery of its role in cell fusion. This duality mirrors the Ax11 protease, which processes α -factor pheromone in MAT α cells and is required in MAT α cells for efficient fusion (Adames et al., 1995; Elia and Marsh, 1998); however, as Ax11 activity is cytoplasmic and Kex2 activity is luminal/extracellular, it is unlikely that this curious parallel reflects a shared mechanism. MAT α cells lacking the exopeptidase Kex1 display a cell fusion defect similar to that of cells lacking Kex2, strongly suggesting that it is the luminal/extracellular proteolytic activities of Kex2 and Kex1 that are required in this process. We therefore propose that Kex2 and Kex1 proteolytically activate at least one yet to be identified substrate protein that comprises part of the fusion machinery. By analogy, furin, a Kex2-family protease, proteolytically activates the fusases of several viruses. Mechanistically, the postulated Kex2 substrate could form a complex with Prm1 and possibly other components to constitute the membrane fusion machine.

Alternatively, the Kex2 substrate and Prm1 could act at distinct, yet mechanistically coupled sites in the membrane to promote fusion.

Genetic analysis of *KEX2* and *PRM1* shows a synergistic interaction between these genes. To achieve efficient cell fusion, at least one mating partner must carry active *KEX2* and *PRM1*. Cell fusion suffers greatly in mating efficiency when both mating partners lack one or both of the two genes ($\Delta prm1 \times \Delta prm1$, $\Delta kex2 \times \Delta prm1$, $\Delta prm1 \Delta kex2 \times \Delta prm1$), whereas only mild defects are observed whenever one mating partner is wild-type (WT \times WT, $\Delta prm1 \times$ WT, WT \times $\Delta prm1$, $\Delta kex2 \times$ WT, $\Delta kex2 \Delta prm1 \times$ WT). Thus a simple model emerges from the genetic data: i) Prm1 and Kex2 (the latter likely acting by proxy through a substrate) are both important for the same step in cell fusion, and ii) this step can be carried out by either mating partner. This model also accounts for the finding that *Aprm1* and *Δkex2* mutations synergize in *trans* but not in *cis*

This definition of *KEX2*'s role in cell fusion therefore illuminates another layer of genetic redundancy in the process. Originally, *PRM1* eluded detection in traditional screens because a *Aprm1* mutant only displays a cell fusion phenotype when mated to a partner also lacking *PRM1*. A *Δkex2* mutant likewise displays a strong cell fusion phenotype only when mated to a *Aprm1* partner. Consequently, *kex2* mutants would be isolated for their cell fusion phenotype only in a sensitized screen, such as the one described here. This strategy can now be extended to identify other genes in the pathway, including —but by no means limited to— the postulated and eagerly sought-after Kex2 substrate.

Although the Kex2 substrate relevant to cell fusion remains unknown, one especially interesting candidate is Prm2. Prm2, a protein of unknown function, is

topologically similar to Prm1, is expressed only during mating, and is a Kex2 substrate. However, deletion of Prm2 causes no fusion defect. It is possible that Prm2 acts redundantly with another Kex2 substrate or that deletion of Prm2 fails to mimic the presence of unprocessed Prm2. On the other hand, it also remains possible that Kex2 acts indirectly during fusion, for example through general effects on the stability of the cell wall. Consistent with this hypothesis, the magnitude of the $\Delta kex2$ fusion defect is reduced by osmotic support. However, other mutants that affect cell wall integrity ($\Delta scw4 \Delta scw10$), cell wall remodeling ($\Delta fus1$ and $\Delta fus2$) or hyperactivate the cell wall stress pathway ($PKC1-R398P$) do not synergize with $\Delta prm1$, arguing that the $\Delta kex2$ defect is uniquely linked to the Prm1-dependent step of membrane fusion. Likewise, the EM phenotype of unfused zygotes resulting from matings of $\Delta kex2$ MATa cells suggests a specific and novel defect resulting from attempted fusion.

While it is unlikely that the morphological features observed in arrested mating pairs reflect *bona fide* intermediates in the fusion pathway, the morphological consequences of blocking the fusion reaction are nevertheless intriguing. Rather than arresting at the same end-point as one might naively have expected, $\Delta kex2$ and $\Delta prm1$ mating pairs show unique morphologies at the electron microscope level. Yet in many respects, the *blebs* observed here resemble *bubbles* seen previously in $\Delta prm1 \times \Delta prm1$ matings, consistent with the notion that *KEX2* and *PRM1* act at similar steps. Like bubbles, blebs are membrane-bounded structures often found apposed to a nearby plasma membrane separated by a regular gap of about 8 nm, and both bubbles and blebs appear to push into the space occupied by one mating partner. In contrast to bubbles, however, blebs are extracellular entities that show no continuity to either parent cell. This

difference shows that loss of Prm1 and loss of Kex2 are not equivalent. If both Prm1 and the postulated Kex2 substrate are components of a single fusion machine, which becomes partially inactivated when either component is compromised, then the residual machines in the respective mutant cells preferentially stall in the pathway at different points, thus leading to the characteristic and distinct morphological phenotypes. Consistent with this notion, stalling can occur at either end-point when both Prm1 and Kex2 are missing in mating cells. Unfortunately, the effects of *KEX2* disruption can currently only be observed in MATa cells because of the requirement for Kex2 processing of α -factor.

One possible mechanism for the formation of blebs is that a Δ *prm1*-like bubble forms first but then becomes severed from the partner that forms it (Fig. 10A); an intermediate suggesting this state is seen in mutants deficient in the a-factor transporter Ste6 (Elia and Marsh, 1996). Alternatively, delivery of exocytic vesicles may be misregulated thus producing the blebs (Fig. 10B), or blebs could derive from the unusual circular structures observed (Fig. 10C). According to both of these latter possibilities, Δ *kex2* blebs would not be derived from Δ *prm1* bubbles, because in either case the membrane surrounding the bleb would come from the same cell that provides the apposing plasma membrane. Precedence for the mechanism shown in Figure 10B comes from our knowledge of the sperm acrosome reaction. In this system, a repository of fusogenic material is delivered to the sperm surface in a burst of exocytosis. As part of this process, membrane-bounded, cytoplasmic fragments are excised from the sperm due to rapid exocytosis at many points along the plasma membrane (Talbot et al., 2003). To distinguish between these models, it will be helpful to determine in future studies from which of the two parental cells the blebs originate.

METHODS

Yeast strains, plasmids, and growth media

Strains used in this study are listed in Table 1. Gene replacements were generated with the PCR-transformation technique (Longtine et al., 1998). Strains MHY398 and MHY427 were derived from KRY18, a gift of Robert Fuller (Komano and Fuller, 1995). The plasmid pDN291, as previously described, was used to express soluble cytosolic GFP and contains the *URA3* gene (Ng and Walter, 1996). The plasmid pRS314 is a standard vector containing the *TRP1* gene, and was used in conjunction with pDN291 to create a set of mating-type-specific selectable markers (Sikorski and Hieter, 1989). The plasmid pJP67 is used to express the hyperactive allele PKC1(R398P) (Nonaka et al., 1995; Philips and Herskowitz, 1997)

Congo Red plates were prepared as previously described (Tomishige *et al.*, 2003) by adding a 20 mg/ml stock solution of Congo Red to <70°C autoclaved YPD agar to a final concentration of 100 µg/ml.

Genetic screen for enhancers of *Aprm1*

Aprm1 TRP1 MATa cells were grown to log phase, and 4 A₆₀₀ units were washed once in a buffer of 10 mM potassium phosphate pH 7.4 (Sigma; 10 ml) and then resuspended in same solution. The mutagen ethyl methane sulfonate (Sigma; 300 µl) was added. Cells were vortexed and incubated for 30 min at 30°C. At that point, a solution of 10% sodium thiosulfate (Sigma; 15 ml) was added to quench the reaction. Cells were washed twice in YPD medium and allowed to recover in YPD for 90 min at 30°C to fix any mutations that

were induced. Serial dilutions of this stock were plated to medium lacking tryptophan and the titer of colony forming units was calculated; meanwhile the stock was kept at 4°C. For screening, the stock was plated to 100 plates lacking tryptophan at a density of about 120 colonies per plate. Colonies were allowed to grow for 40 h at 30°C. After about 25 h, a stationary overnight culture of *Aprm1 URA3 MAT α* was plated to 100 plates of YPD at 100 μ l/plate and incubated at room temperature for the remaining 15 h to form lawns. These lawns were re-spread with 100 μ l/plate water to a dull matte appearance indicative of homogeneity. Colonies of the mutagenized MAT α cells were replica-plated to mating lawns and incubated for 8 h at 30°C. The plates were then replica-plated to medium lacking tryptophan and uracil to select for diploids. Phenotypes were scored on plates incubated for 2 days at 30°C. The clarity of the phenotypes depended critically on having homogeneous lawns of the proper density.

Complementation of the *Aprm1* enhancer mutation

MAT α -specific sterility appeared in several of the enhancer mutants. We aimed for complementation of this phenotype because it was easier to score. Following backcross to a *Aprm1* strain, the sterile *Aprm1 MAT α* was transformed with a pRS316-based library, a generous gift of Sean O'Rourke (O'Rourke and Herskowitz, 2002). Transformants (15,000) were subjected to a replica mating assay as described above, with a tester strain as partner.

Quantitative assay of cell fusion

The cell fusion assay was performed as described previously (see also Philips and Herskowitz, 1997). Cells of opposite mating types, with the *MAT α* strain expressing soluble cytosolic GFP, were grown overnight to log phase, 1 A₆₀₀ unit of each were mixed, and vacuumed to a nitrocellulose filter. The filter was placed cell-side up on a YPD plate, and the plate incubated for 3 h at 30°C. Cells were then scraped off the filter, fixed in 4% paraformaldehyde, and incubated at 4°C overnight. This mixture was then spotted on a slide and observed with a fluorescent microscope (Zeiss Axiovert 200M) using a 63x oil-immersion objective (Zeiss Plan-Apochromat). First, a field was selected randomly using transmission optics. Then, groups of zygotes and mating pairs within that field were identified by bright-field microscopy and subsequently scored as fused zygotes or unfused mating pairs by switching between bright-field and fluorescence. This procedure was continued until all the zygotes and mating pairs in the field were scored, at which point a new field was chosen and the procedure was repeated. To capture images, a single optical section was taken by both bright-field and fluorescence microscopy using a confocal microscope (Leica TCS NT) with a 100x oil-immersion objective, a 488 nm excitation laser and a 510-550 nm band pass emission filter to visualize GFP. These images were then superimposed and contrast-enhanced.

β -Galactosidase Assays

Yeast strains containing the *MPK1-LacZ* reporter were grown to log phase in SC-URA with or without 1M sorbitol. For pheromone induction, log phase cultures were incubated with 10 μ g/ml α -factor for 2 h. Reporter activity was quantified as previously described (Papa *et al.*, 2003) using 0.8 mg/ml *o*-nitrophenol β -D-galactoside (ONPG) (Sigma).

Reactions were incubated at 32°C for 10 min and stopped by adding an equal volume of 1M NaCO₃.

Bioinformatic search for novel Kex2 substrates

A scoring matrix to predict Kex2 cleavage sites was generated based on previously reported Kex2 substrates (Kex2 (Rockwell et al., 2002); Mf α 1, Mf α 2 (Kurjan and Herskowitz, 1982; Singh et al., 1983); Ccw6/Pir1, Ccw7/Hsp150 (Russo et al., 1992); Ccw8/Pir2, Ccw11, Scw3/Sun4, Scw4 (Cappellaro et al., 1998); Scw6/Exg1 (Basco et al., 1990); Scw10, Scw11, killer toxin (Bostian et al., 1984; Zhu et al., 1992)). The scoring matrix consisted of ten protein sequence positions centered on the cleavage site, with the score for each residue at each position reflecting its prevalence among the known substrates at that position (Supplementary Table 1). To obtain an overall score for a candidate sequence, the scores at each position were multiplied. For comparison purposes we took the negative natural log of this value. Using a perl script, we searched the yeast genome for high-scoring potential cleavage sites. From the list of proteins that contained high-scoring sites, we discarded those which did not have a predicted transmembrane domain or signal sequence. Finally, candidates were selected which had high-scoring sites and in which the P2 and P1 positions were conserved among fungal homologs.

Electron microscopy

Mating reactions were performed identically to the method described for quantitative fusion assays, but at room temperature. During the mating, plates were taken to the University of California Berkeley electron microscopy lab and subjected to high-pressure

freezing after about 3 h total incubation (McDonald, 1999; McDonald and Müller-Reichert, 2002). Samples were fixed, stained and embedded (McDonald, 1999). High-pressure freezing was found to yield superior contrast between membranes and surrounding areas and a smoother curvature to membranes than we had observed by conventional fixation (Heiman and Walter, 2000; see also McDonald and Müller-Reichert, 2002). Sections of about 60 nm thickness were cut, post-stained with uranyl acetate and lead citrate (Ted Pella Inc, Redding CA), and imaged with an electron microscope (Philips Tecnai-F20) equipped with a 200 kV LaB6 cathode and a bottom-mounted four-quadrant 16-million pixel CCD (Gatan UltraScan 4000).

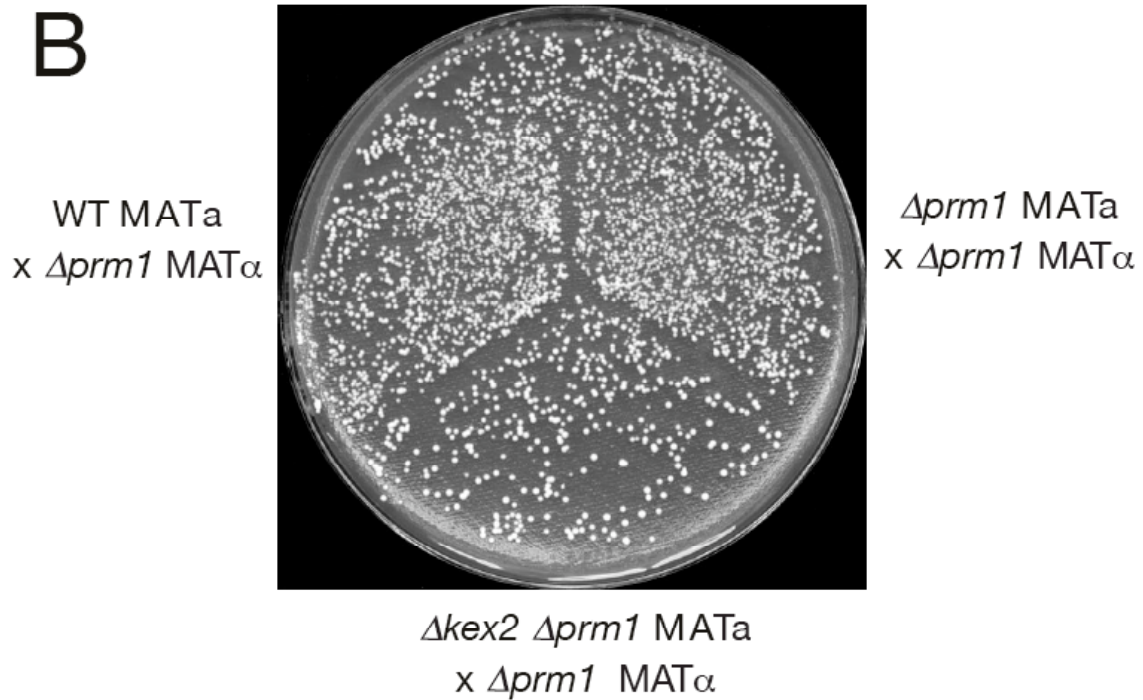
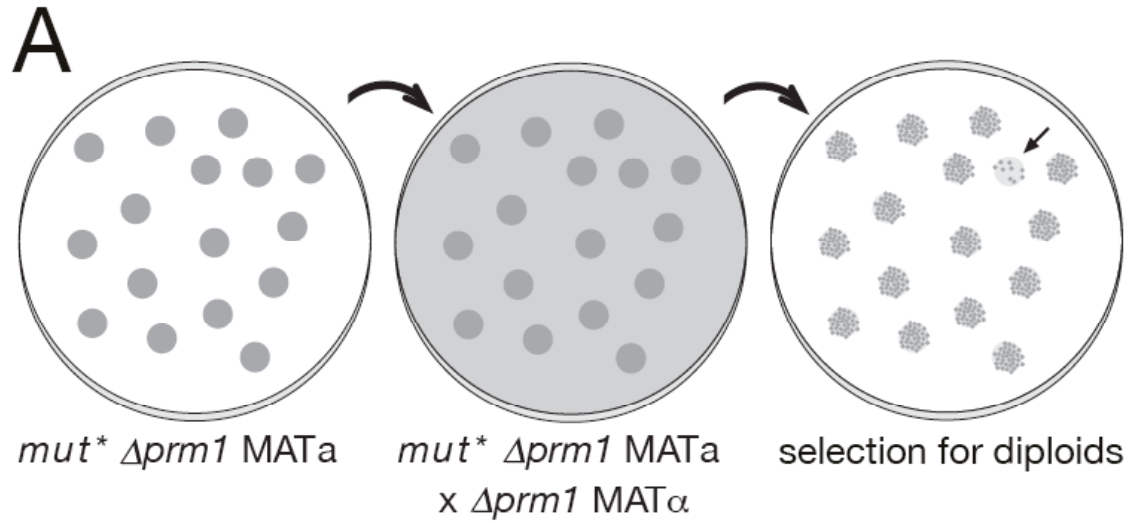


Figure 1. Replica mating strategy to isolate enhancers of *Δprm1*. **(A)** A *Δprm1* MATa strain was mutagenized and plated to form colonies. Colonies were replica plated to a lawn of *Δprm1* MATα mating partner on a YPD plate and incubated at 30° for 8 h. The mating was then replica plated to medium selective for diploids. Mutant colonies yielding a low density of diploid papillae were identified. **(B)** Patches of wild-type,

Δprm1, and *Δprm1 Δkex2* MATa haploids were ‘replica-mated’ as above to a lawn of *Δprm1* MATα mating partner. The resulting diploid papillae are shown.

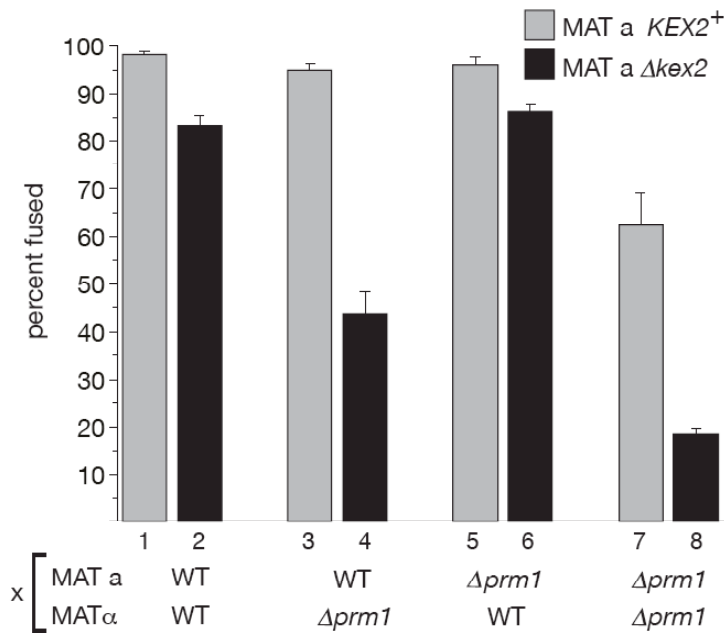
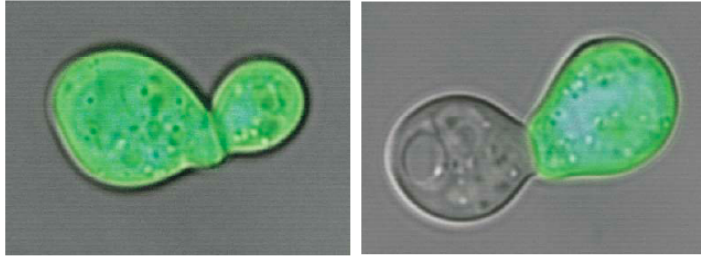


Figure 2. *Δkex2* enhances the *Δprm1* cell fusion defect. **(Top)** *Δkex2* MATa cells were mixed with WT MATα cells expressing soluble cytosolic GFP as a reporter of cytoplasmic mixing between mating partners. This mixture was applied to a nitrocellulose filter and incubated at 30° for 3 h on a YPD plate. Fluorescent micrographs showing the GFP-stained cytoplasm were super-positioned over bright-field images of the mating pairs. **(Bottom)** Mating mixes in which mating partners carried deletions of *PRM1*, *KEX2*, both, or neither were prepared as described above. In all cases the MATα partner carried soluble cytosolic GFP. Mating pairs were visually identified and then scored with regard to cell fusion by microscopy. Bars represent the average percent of mating pairs that scored as fused in three independent experiments. During each

experiment, 300 mating pairs per mating mix were counted. All matings are written in the form MAT α x MAT α : WT x WT, $98.2 \pm 0.6\%$; $\Delta kex2$ x WT, $83.2 \pm 2.3\%$; WT x $\Delta prm1$, $94.8 \pm 1.4\%$; $\Delta kex2$ x $\Delta prm1$, $43.6 \pm 4.6\%$; $\Delta prm1$ x WT, $95.9 \pm 1.6\%$; $\Delta prm1$ $\Delta kex2$ x WT, $86.3 \pm 1.6\%$; $\Delta prm1$ x $\Delta prm1$, $62.4 \pm 6.8\%$; $\Delta prm1$ $\Delta kex2$ x $\Delta prm1$, $18.5 \pm 1.2\%$.

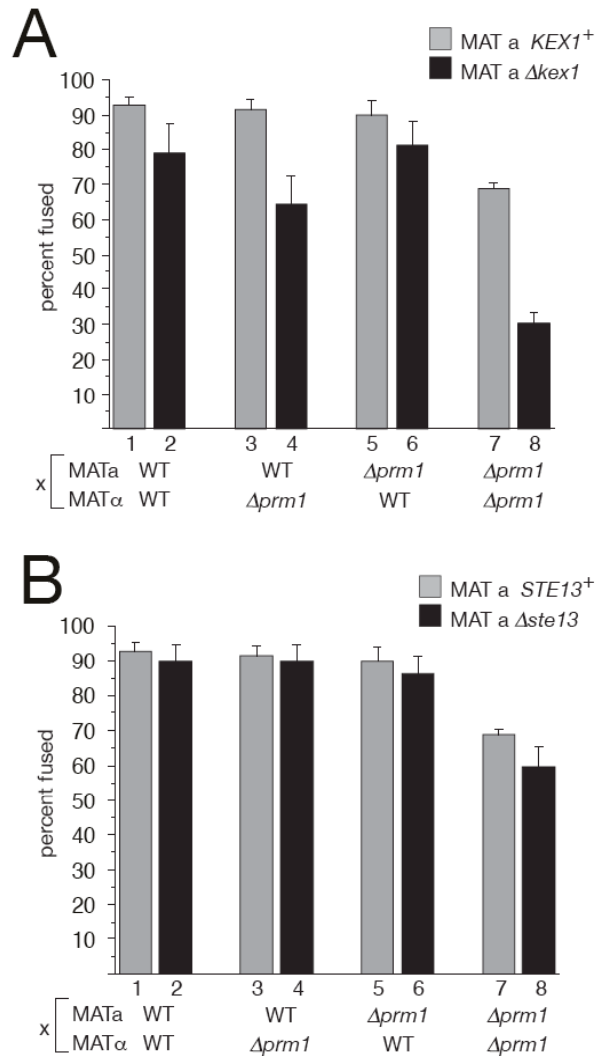


Figure 3. *Δkex1*, but not *Δste13*, enhances the *Δprm1* cell fusion defect. Mating mixes in which mating partners carried deletions of *PRM1*, *KEX1*, or *STE13* singly or in combination were subjected to filter matings followed by microscopic inspection of mating pairs, and fusion efficiencies were quantitated using the GFP-mixing assay as described in Figure 2. All matings presented in this figure were conducted in parallel and three independent trials were performed, with 300 mating pairs per mating mix counted each time. All matings are written in the form MATa x MATα. **(A)** Matings with deletions of *KEX1*: WT x WT, 92.9 ± 2.3 %; *Δkex1* x WT, 78.8 ± 8.6 %; WT x *Δprm1*, 91.5 ± 2.8 %; *Δkex1* x *Δprm1*, 64.5 ± 7.7 %; *Δprm1* x WT, 90 ± 4.2 %; *Δprm1* *Δkex1* x WT,

81.3 ± 6.9%; *Aprm1* x *Aprm1*, 68.7 ± 1.6%; *Aprm1 Δkex1* x *Aprm1*, 30.4 x 3.0%. **(B)**

Matings with deletions of *STE13*: WT x WT, 92.9 ± 2.3 %; *Δste13* x WT, 90.1 ± 4.5%;

WT x *Aprm1*, 91.5 ± 2.8%; *Δste13* x *Aprm1*, 90.1 ± 4.5%; *Aprm1*x WT, 90 ± 4.2%;

Aprm1 Δste13 x WT, 86.1 ± 5.2%; *Aprm1* x *Aprm1*, 68.7 ± 1.6%; *Aprm1 Δste13* x

Aprm1, 59.7 ± 5.6%.

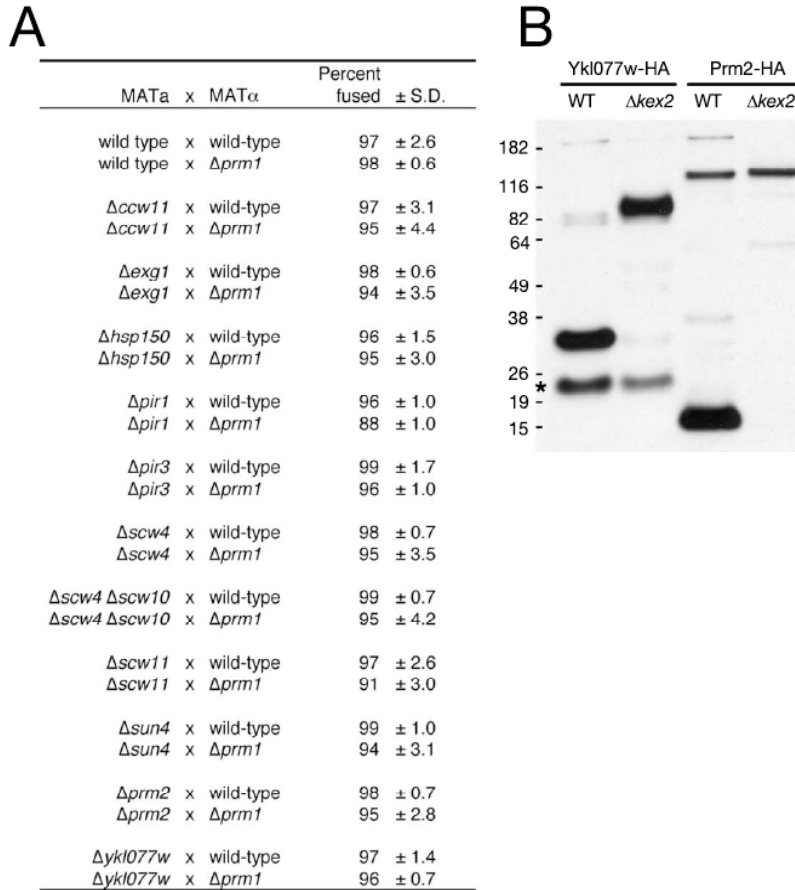


Figure 4. Deletion of known Kex2 substrates fails to enhance the $\Delta prm1$ fusion defect in *trans*. **(A)** MAT α strains bearing deletions of genes for known Kex2 substrates were crossed to WT or $\Delta prm1$ MAT α strains. Following filter mating and fixation, 100 mating pairs per experiment were scored for cytoplasmic mixing; data shown are derived from three independent experiments. **(B)** Kex2-dependent mobility shift of Ykl077w and Prm2 was assayed by Western blot. Protein was prepared from whole cell lysates of vegetatively growing cultures (Ykl077w-HA strains) or α -factor induced cultures (Prm2-HA strains, 10 μ g/ml α -factor for 30 min). A likely degradation product of Ykl077w-HA (asterisk) is independent of Kex2.

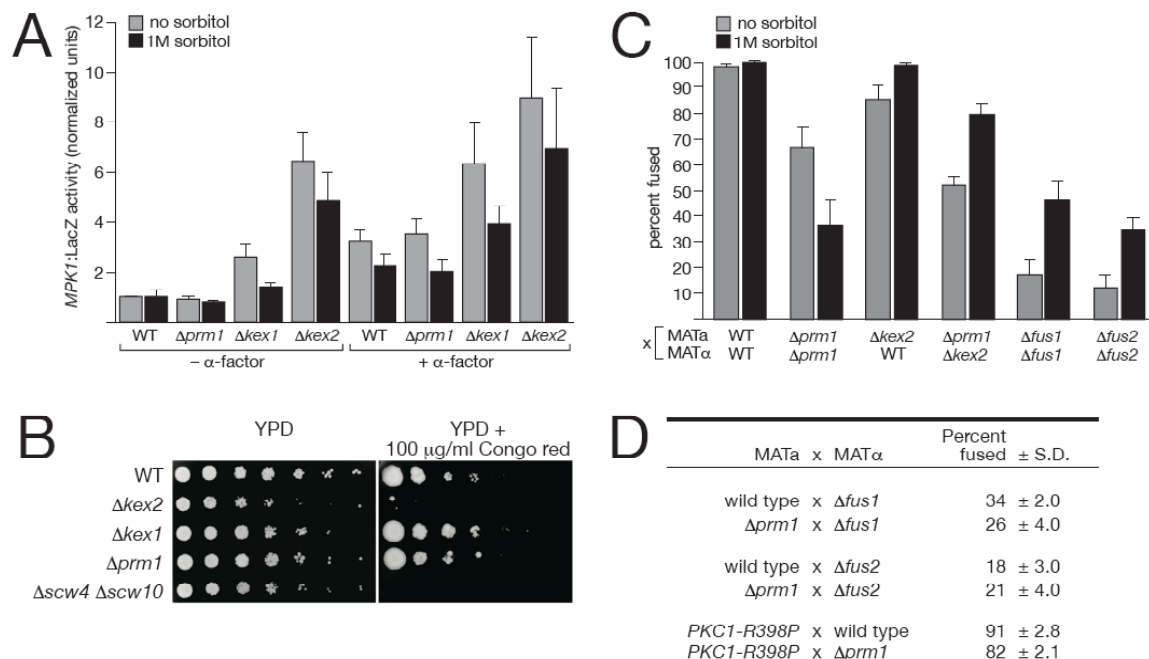


Figure 5. $\Delta k e x 1$ and $\Delta k e x 2$ mutants exhibit cell wall phenotypes similar to other mutants but are unique in synergizing with $\Delta pr m 1$. **(A)** To assay activation of the cell integrity pathway WT, $\Delta pr m 1$, $\Delta k e x 1$, and $\Delta k e x 2$ strains bearing an *MPK1:LacZ* reporter were grown to log phase without pheromone ($- \alpha$ -factor) or treated with 10 μ g/ml α -factor ($+ \alpha$ -factor) for 2 h and β -galactosidase activity was quantified. Values were normalized to that of uninduced WT. Bars represent the average \pm S.D. of three experiments. **(B)** Cells were grown to OD 1.0, and spotted onto YPD plates with or without 100 μ g/ml Congo Red in 1:5 serial dilutions and cultured for 2 days at 30°C. **(C)** Indicated crosses were performed by filtering mating mixtures onto nitrocellulose filters and incubating for 3 h on YPD or YPD supplemented with 1M sorbitol. Bars indicate the average \pm S.D. of three experiments. **(D)** Strains bearing deletions of *FUS1* or *FUS2* or expressing an activated allele of PKC1 (*PKC1-R398P*) were mated to a $\Delta pr m 1$ partner for 3h and assayed for cytoplasmic mixing.

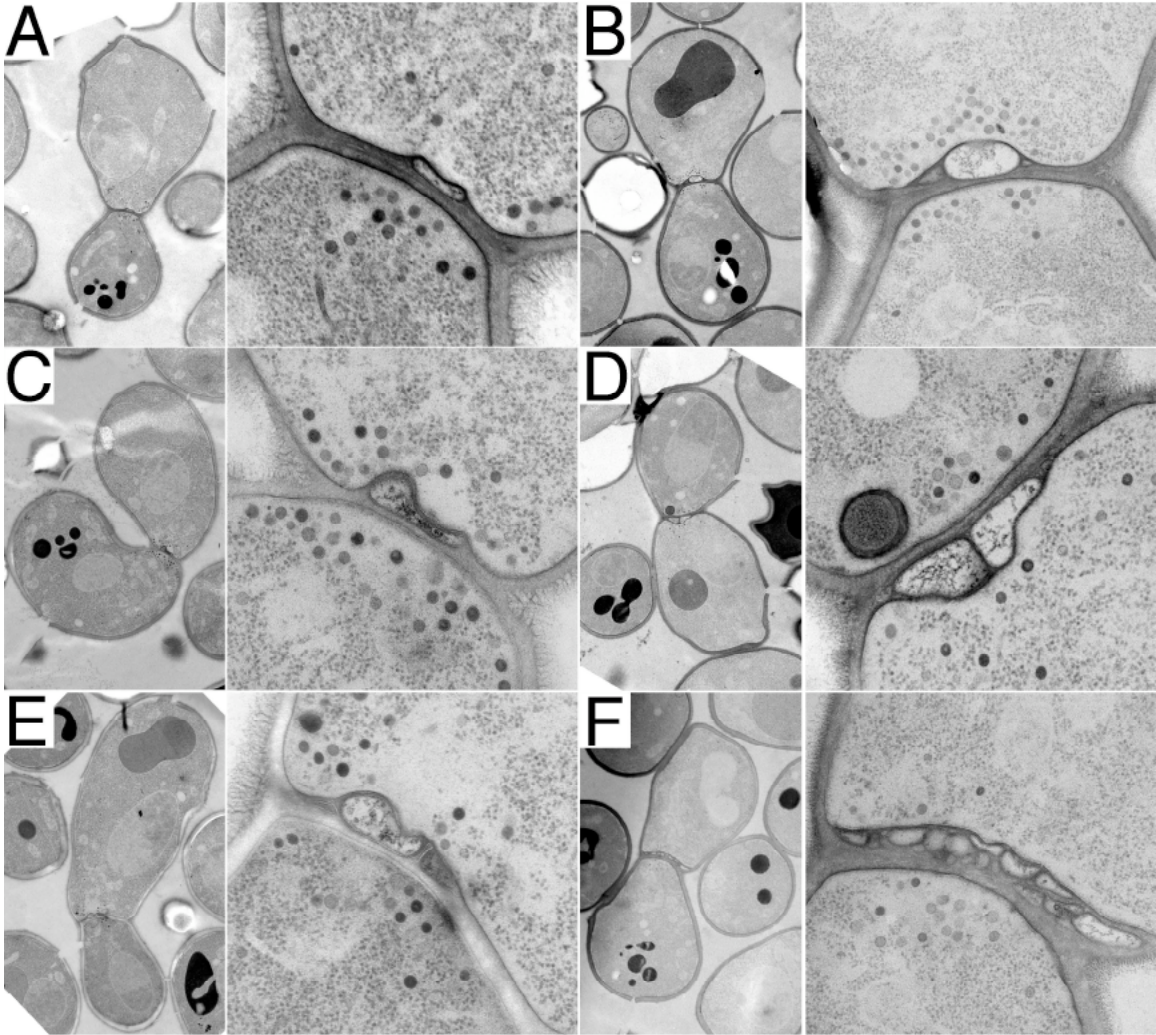


Figure 6. $\Delta kex2$ x WT mating pairs fail to fuse and develop cell wall-embedded blebs. Mating mixes of $\Delta kex2$ x WT partners were prepared on filters as described above and incubated for about 3 h at ambient temperature. The cells were then subjected to high-pressure freezing, fixed, stained, and imaged by transmission electron microscopy. Two different magnifications are shown for each image. (A-F) Mating pairs showing one, two, or more blebs trapped within the cell wall near the center of the cell-cell interface.

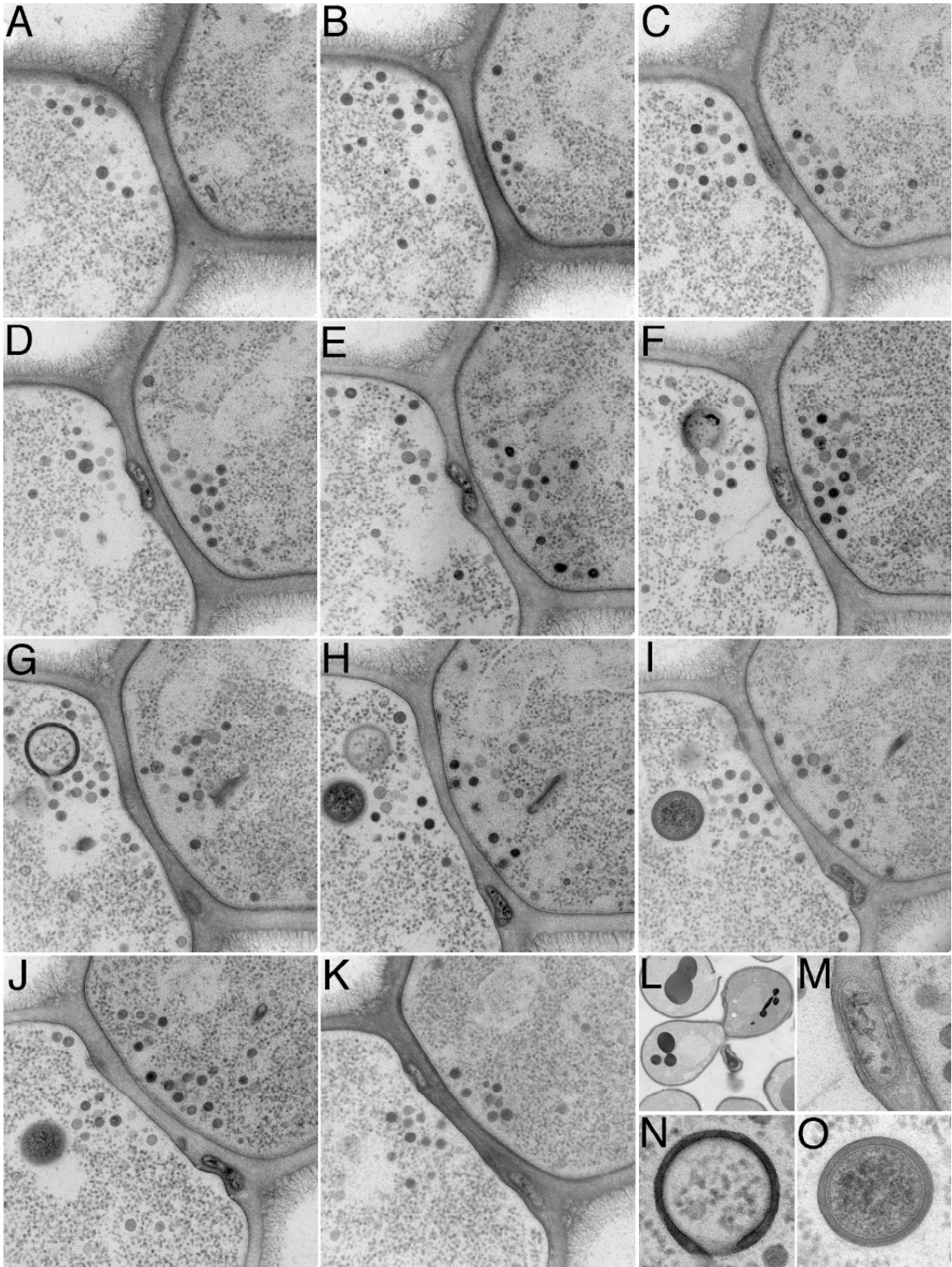


Figure 7. Serial section analysis of a $\Delta kex2$ x WT mating pair. (A-K) Transmission electron micrographs of serial sections through the cell-cell interface of a $\Delta kex2$ x WT

mating pair prepared as in Fig. 6. **(L)** Low-magnification view of the mating pair. **(M)** High-magnification view of the bleb seen in panel F. **(N)** High-magnification view of an intracellular structure from panel G. **(O)** High-magnification view of an intracellular structure from panel I.

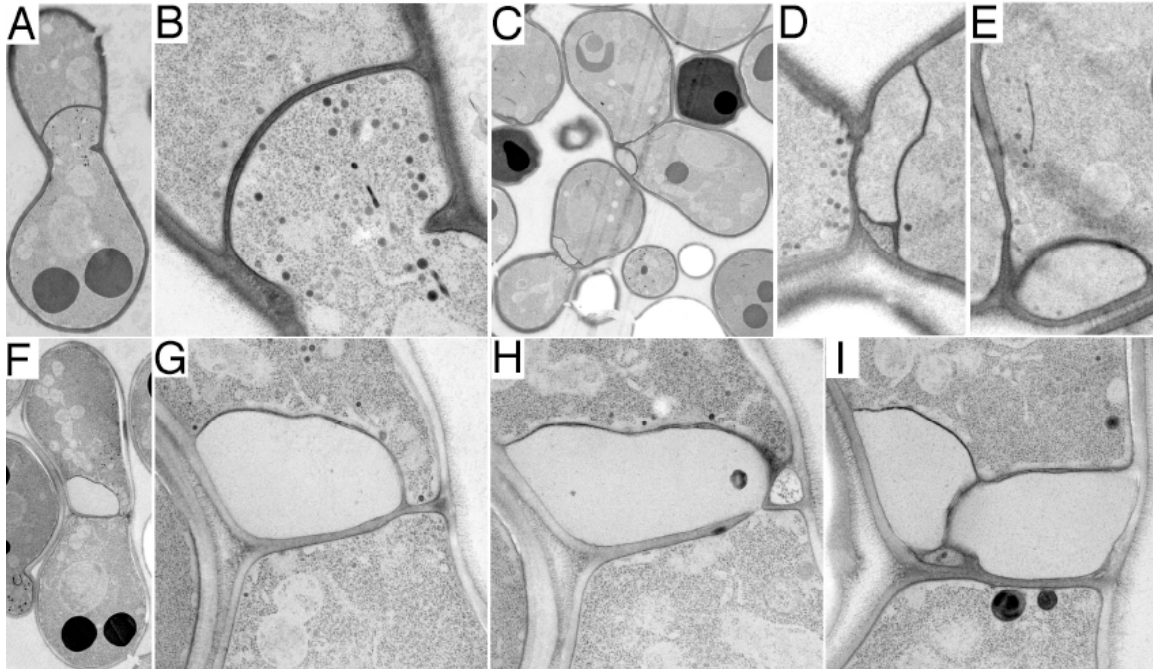


Figure 8. $\Delta prm1 \Delta kex2 \times \Delta prm1$ mating pairs fail to fuse and develop a variety of structures. Mating mixes were prepared as in Fig. 6. **(A, B)** A mating pair, in low- and high-magnification views, with a region of cytoplasm extending across the midline from one partner to the other. **(C-E)** Two mating pairs, in low- and high-magnification views, containing membrane-bounded inclusions with staining textures consistent with that of cytoplasm. **(F-I)** A mating pair, in low-magnification view and three serial sections in high-magnification view, with a membrane-bounded structure that extends across the midline from one partner to the other and that has a staining texture different than cytoplasm.

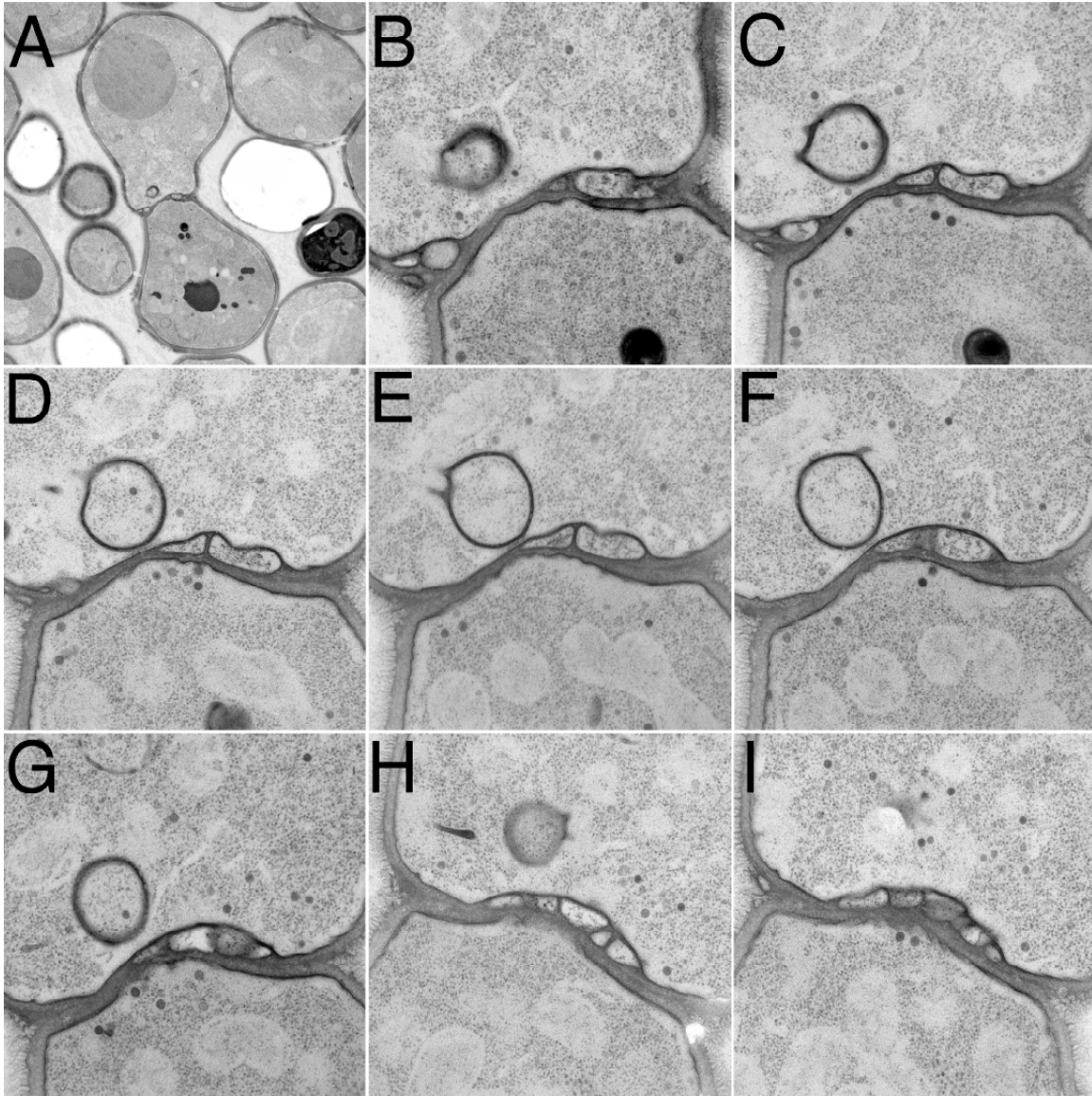


Figure 9. Serial section analysis of a $\Delta prm1 \Delta kex2 \times \Delta prm1$ mating pair. **(A)** Low-magnification transmission electron micrograph of a $\Delta prm1 \Delta kex2 \times \Delta prm1$ mating pair prepared as in Fig. 6. **(B-F)** High-magnification serial sections across the cell-cell interface of the mating pair shown in panel A.

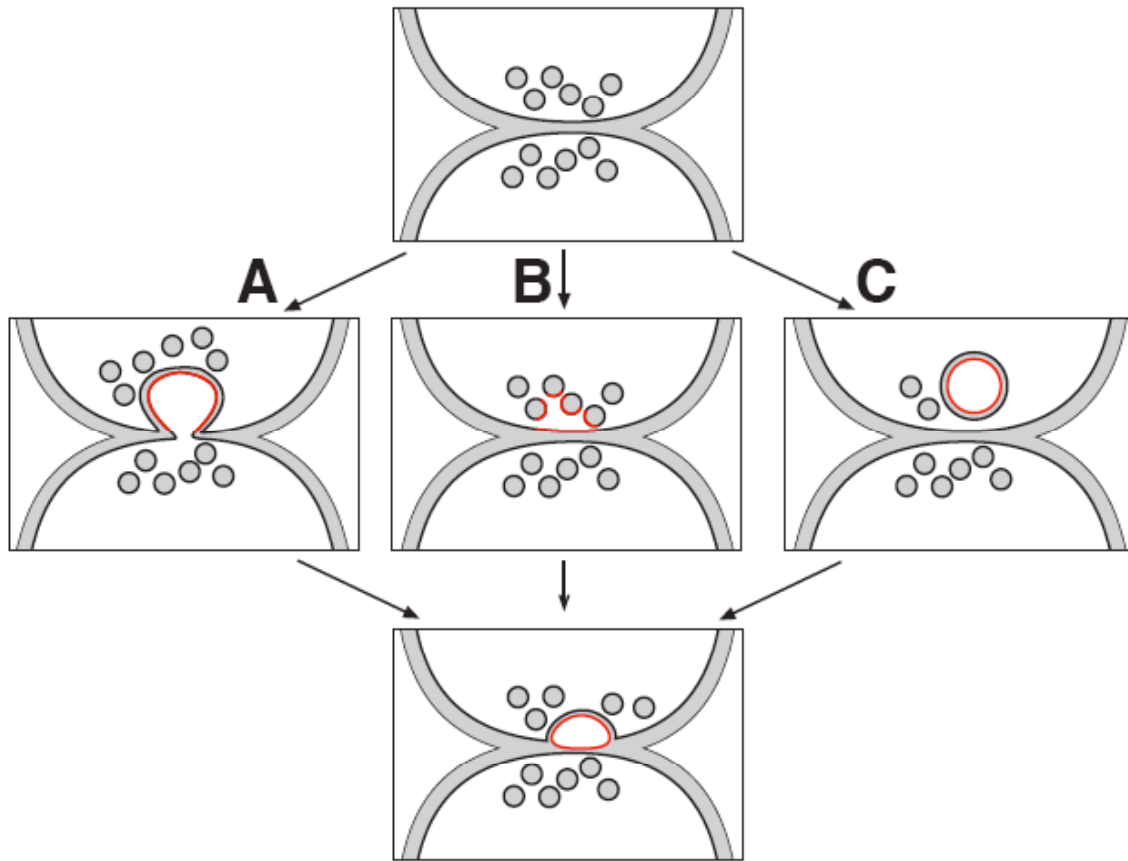


Figure 10. Possible models for the mechanism of bleb formation. Three possibilities for how defective attempts at cell fusion could produce cell wall-embedded blebs at the cell-cell interface. **(A)** A cytoplasmic extension reaches across the midline and then is severed. **(B)** Extensive fusion of vesicles to each other and to the plasma membrane excises a pocket of cytoplasm. **(C)** An intracellular inclusion forms and is delivered to the surface.

Table 1

The following strains were used. All were constructed in the W303 background.

MHY425	MATa, <i>his3-Δ200, ura3-Δ99, leu2-Δ1, trp1-Δ99, ade2-101^{ochre}</i> , pRS314
MHY189	MATα, <i>his3-Δ200, ura3-Δ99, leu2-Δ1, trp1-Δ99, ade2-101^{ochre}</i> , pDN291
MHY426	MATa, <i>Δprm1::S.kluyveri HIS3⁺, his3-Δ200, ura3-Δ99, leu2-Δ1, trp1-Δ99, ade2-101^{ochre}</i> , pRS314
MHY191	MATα, <i>Δprm1::S.kluyveri HIS3⁺, his3-Δ200, ura3-Δ99, leu2-Δ1, trp1-Δ99, ade2-101^{ochre}</i> , pDN291
MHY398	MATa, <i>Δkex2::TRP1, his3-Δ200, ura3-Δ99, leu2-Δ1, trp1-Δ99, ade2-101^{ochre}</i>
MHY461	MATa, <i>Δkex1::kan^R, his3-Δ200, ura3-Δ99, leu2-Δ1, trp1-Δ99, ade2-101^{ochre}</i> , pRS314
MHY462	MATa, <i>Δste13::kan^R, his3-Δ200, ura3-Δ99, leu2-Δ1, trp1-Δ99, ade2-101^{ochre}</i> , pRS314
MHY427	MATa, <i>Δprm1::S.kluyveri HIS3⁺, Δkex2::TRP1, his3-Δ200, ura3-Δ99, leu2-Δ1, trp1-Δ99, ade2-101^{ochre}</i>
MHY445	MATa, <i>Δprm1::S.kluyveri HIS3⁺, Δkex1::kan^R, his3-Δ200, ura3-Δ99, leu2-Δ1, trp1-Δ99, ade2-101^{ochre}</i> , pRS314
MHY447	MATa, <i>Δprm1::S.kluyveri HIS3⁺, Δste13::kan^R, his3-Δ200, ura3-Δ99, leu2-Δ1, trp1-Δ99, ade2-101^{ochre}</i> , pRS314
MHY189	MATα, <i>his3-Δ200, ura3-Δ99, leu2-Δ1, trp1-Δ99, ade2-101^{ochre}</i> , pDN291
MHY387	MATa, <i>Δscw4::S.kluyveri HIS3⁺, his3-Δ200, ura3-Δ99, leu2-Δ1, trp1-Δ99, ade2-101^{ochre}</i> , pRS314
MHY388	MATα, <i>Δscw10::S.kluyveri HIS3⁺, his3-Δ200, ura3-Δ99, leu2-Δ1, trp1-Δ99, ade2-101^{ochre}</i> , pDN291
MHY389	MATa, <i>Δscw4::S.kluyveri HIS3⁺, Δscw10::S.kluyveri HIS3⁺, his3-Δ200, ura3-Δ99, leu2-Δ1, trp1-Δ99, ade2-101^{ochre}</i> , pRS314
MHY390	MATα, <i>Δscw10::S.kluyveri HIS3⁺, Δscw10::S.kluyveri HIS3⁺, his3-Δ200, ura3-Δ99, leu2-Δ1, trp1-Δ99, ade2-101^{ochre}</i> , pDN291
AEY142	MATa, <i>Δpir3::kan^R, his3-Δ200, ura3-Δ99, leu2-Δ1, trp1-Δ99, ade2-101^{ochre}</i>
AEY143	MATa, <i>Δhsp150::kan^R, his3-Δ200, ura3-Δ99, leu2-Δ1, trp1-Δ99, ade2-101^{ochre}</i> , pRS314
AEY144	MATa, <i>Δsun4::kan^R, his3-Δ200, ura3-Δ99, leu2-Δ1, trp1-Δ99, ade2-101^{ochre}</i> , pRS314
AEY145	MATa, <i>Δccw11::kan^R, his3-Δ200, ura3-Δ99, leu2-Δ1, trp1-Δ99, ade2-101^{ochre}</i> , pRS314
AEY146	MATa, <i>Δexg1::kan^R, his3-Δ200, ura3-Δ99, leu2-Δ1, trp1-Δ99, ade2-101^{ochre}</i>
AEY147	MATa, <i>Δscw11::kan^R, his3-Δ200, ura3-Δ99, leu2-Δ1, trp1-Δ99, ade2-101^{ochre}</i> , pRS314
AEY148	MATa, <i>Δpir1::kan^R, his3-Δ200, ura3-Δ99, leu2-Δ1, trp1-Δ99, ade2-101^{ochre}</i> , pRS314
AEY14	MATa, <i>Δykl077w::kan^R, his3-Δ200, ura3-Δ99, leu2-Δ1, trp1-Δ99, ade2-101^{ochre}</i> ,
pRS314	
MHY524	MATa, <i>Δprm2::S.kluyveri HIS3⁺, his3-Δ200, ura3-Δ99, leu2-Δ1, trp1-Δ99,</i>
<i>ade2101^{ochre}</i> ,	
	pRS314
AEY7	MATa, <i>YKL077W-HA::kan^R, his3-Δ200, ura3-Δ99, leu2-Δ1, trp1-Δ99, ade2-101^{ochre}</i> ,
	pRS314
AEY8	MATa, <i>YKL077W-HA::kan^R, Δkex2::TRP1, his3-Δ200, ura3-Δ99, leu2-Δ1, trp1-Δ99, ade2-101^{ochre}</i> , pRS314
MHY546	MATa, <i>PRM2-HA::S.kluyveri HIS3⁺, his3-Δ200, ura3-Δ99, leu2-Δ1, trp1-Δ99, ade2101^{ochre}</i> , pRS316
MHY548	MATa, <i>PRM2-HA::S.kluyveri HIS3⁺, Δkex2::TRP1, his3-Δ200, ura3-Δ99, leu2-Δ1, trp1-Δ99, ade2101^{ochre}</i> , pRS316
AEY67	MATa, <i>his3-Δ200, ura3-Δ99, leu2-Δ1, trp1-Δ99, ade2-101^{ochre}</i> , pMPK1-LacZ::URA3
AEY69	MATa, <i>Δkex2::TRP1, his3-Δ200, ura3-Δ99, leu2-Δ1, trp1-Δ99, ade2-101^{ochre}</i> , pMPK1-LacZ::URA3
AEY71	MATa, <i>Δkex1::kan^R, his3-Δ200, ura3-Δ99, leu2-Δ1, trp1-Δ99, ade2-101^{ochre}</i> , pMPK1-

LacZ::URA3
 AEY72 MATa, $\Delta prml::S.kluyveri$ HIS3⁺, his3- Δ 200, ura3- Δ 99, leu2- Δ 1, trp1- Δ 99, ade2-101^{ochre}, pMPK1-LacZ::URA3
 AEY92 MATa, $\Delta ste13::kan^R$, his3- Δ 200, ura3- Δ 99, leu2- Δ 1, trp1- Δ 99, ade2-101^{ochre}, pMPK1-LacZ::URA3
 AEY1 MAT α , $\Delta fus1::kan^R$, his3- Δ 200, ura3- Δ 99, leu2- Δ 1, trp1- Δ 99, ade2-101^{ochre}, pDN291
 AEY17 MATa, $\Delta fus1::kan^R$, his3- Δ 200, ura3- Δ 99, leu2- Δ 1, trp1- Δ 99, ade2-101^{ochre}, pRS314
 AEY2 MAT α , $\Delta fus2::kan^R$, his3- Δ 200, ura3- Δ 99, leu2- Δ 1, trp1- Δ 99, ade2-101^{ochre}, pDN291
 AEY18 MATa, $\Delta fus2::kan^R$, his3- Δ 200, ura3- Δ 99, leu2- Δ 1, trp1- Δ 99, ade2-101^{ochre}, pRS314
 AEY58 MATa, his3- Δ 200, ura3- Δ 99, leu2- Δ 1, trp1- Δ 99, ade2-101^{ochre}, pJP67

Supplementary Table 1

The strong preference for a lysine, arginine or proline residue at position P2 and the requirement for an arginine residue at position P1 are indicated. For other positions, if a given amino acid never occupies the position among the sample set then a value of 0.01 was used. Arrow indicates position of proteolytic cleavage.

	P ₅	P ₄	P ₃	P ₂	P ₁	↓	P' ₁	P' ₂	P' ₃	P' ₄	P' ₅
Ala	.05	.01	.35	0	0		.25	.50	.10	.35	.10
Arg	.01	.01	.01	.05	1		.01	.01	.01	.01	.05
Asn	.01	.10	.01	0	0		.01	.01	.05	.01	.01
Asp	.05	.01	.10	0	0		.15	.05	.10	.01	.15
Cys	.01	.01	.01	0	0		.01	.01	.01	.01	.01
Glu	.05	.01	.01	0	0		.40	.01	.15	.01	.20
Gln	.01	.05	.01	0	0		.01	.01	.01	.10	.05
Gly	.05	.01	.01	0	0		.01	.01	.01	.01	.01
His	.10	.05	.05	0	0		.01	.01	.01	.01	.01
Ile	.05	.01	.01	0	0		.01	.05	.05	.05	.10
Leu	.01	.25	.05	0	0		.05	.01	.01	.01	.01
Lys	.05	.25	.05	.90	0		.01	.01	.01	.01	.01
Met	.01	.20	.01	0	0		.01	.01	.01	.01	.05
Phe	.01	.01	.05	0	0		.01	.01	.01	.01	.01
Pro	.20	.01	.05	.05	0		.01	.05	.05	.10	.01
Ser	.30	.01	.01	0	0		.05	.01	.15	.05	.05
Thr	.10	.01	.01	0	0		.01	.01	.05	.15	.05
Trp	.01	.01	.01	0	0		.01	.01	.01	.05	.05
Tyr	.01	.05	.20	0	0		.10	.05	.05	.05	.05
Val	.01	.10	.05	0	0		.01	.30	.25	.05	.05

CHAPTER 5

MEMBRANE LYSIS DURING BIOLOGICAL MEMBRANE FUSION: COLLATERAL DAMAGE BY ALTERED FUSION MACHINES

INTRODUCTION

Membrane fusion is a ubiquitous process in biology that allows for delivery, mixing, and sorting of soluble and membrane integrated macromolecules across membrane barriers. Despite enormous diversity of fusion reactions, the job description remains simple: tether, destabilize, and fuse membranes without allowing contents leakage across the bilayer (Jahn et al., 2003; Sollner, 2004). In the prevailing model of membrane fusion, fusase activity induces the formation of a hemifusion stalk, a non-bilayer intermediate that joins the apposed leaflets of the fusing membranes (Figure 1A). Lateral expansion of the stalk leads to a single bilayer separating compartments consisting of the other two leaflets—termed a hemifusion diaphragm. Rupture of the hemifusion diaphragm results in a fusion pore. At no point in this process are the contents of the two fusing membrane exposed to the environment between the membranes; thus, compartmental identity is preserved. This characteristic of the fusion pathway is vital to biological membrane fusion because leakiness in the fusion pathway would have disastrous consequences for the cell. Uncontained membrane holes would allow the dissipation of ion gradients, escape of potentially harmful hydrolases, and result in cell lysis. Thus it comes as a surprise that recent work has shown that vacuole fusion and yeast mating are prone to lysis when the balance of fusion players is altered, and some reports suggest that viral fusases may also cause membrane holes. Here we review what perturbations cause fusases to make holes instead of non-leaky fusion pores and speculate on what these observations might tell us about the mechanism and regulation of biological membrane fusion.

LYSIS DURING BIOLOGICAL MEMBRANE FUSION

SNARE-driven vacuole lysis. Analogous to lysosomes, yeast vacuoles are an acidified compartment specialized for protein and membrane degradation. These large (1-3 μ m in diameter) organelles undergo fusion and fission and are maintained at 1-5 vacuoles per cell (Wang et al., 2002). The SNARE dependent fusion of yeast vacuoles has been extensively studied *in vitro*. Prior to fusion, Rab-dependent docking results in expansive membrane contact between neighboring vacuoles. The vertices at the edges of this boundary domain accumulate many fusion-relevant proteins, including the Rab GTPase Ypt7p, the Rab effector HOPS complex, and the vacuolar SNAREs (Wang et al., 2002). Fusion initiates along the vertex ring, resulting in fused vacuoles with the boundary membranes released into the luminal space.

By monitoring the release of luminal GFP in the *in vitro* vacuole fusion assay, Wickner and colleagues were able to assess vacuole lysis during the fusion reaction (Starai et al., 2007). They observed a low background of vacuole lysis, likely a result of handling the purified vacuoles. Surprisingly, when the s-SNARE Vam7p was added in excess, which results in increased trans-SNARE complex formation, vacuole lysis increased (Vam7p has a PX domain for membrane association, but no transmembrane anchor). The Vam7p-induced lysis was concentration-dependent and required full-length Vam7p capable of SNARE pairing; furthermore, vacuole lysis and vacuole fusion followed identical kinetics.

As an alternative means of assessing the consequences of increased trans-SNARE pairing, vacuoles were isolated from strains overexpressing all four vacuolar SNARE proteins. Upon addition of Sec18p (NSF) to disassemble cis-SNARE pairs, these

SNARE-laden vacuoles underwent vacuole fusion. Similar to conditions with excess Vam7p, these reactions were prone to vacuole lysis: now over 60% of luminal GFP escaped the vacuole, significantly higher than the background of 25% non-sedimentable GFP. The high lysis rate of these vacuoles was blocked by antibodies that inhibit cis-SNARE disassembly, vacuole docking, and trans-SNARE pairing, and again the lysis followed similar kinetics to vacuole fusion.

Overexpression of vacuolar SNAREs not only induced trans-SNARE-dependent lysis, it allowed vacuole fusion to bypass a requirement for Ypt7p. Interestingly, extraction of Ypt7p causes vacuole lysis to fall to background levels despite being expendable for fusion. Thus a model emerges in which excess trans-SNARE pairing results in vacuole lysis. In the absence of Ypt7p fewer trans-SNARE pairs are formed so no SNARE-dependent lysis occurs, but because of the increased SNARE levels this number is sufficient to drive vacuole fusion.

Lysis of yeast mating pairs. Lysis is also observed during cell fusion of mating yeast. Fusion of haploid cells of opposite mating type yields diploid zygotes (Chen et al., 2007; White and Rose, 2001). The mating reaction begins with pheromone sensing, which results in cell cycle arrest, polarized growth towards a mating partner (“shmooing”), and induction of a mating specific transcriptional program. When a polarized shmoo meets a mating partner, their cell walls are woven together and a small channel at the center of the mating pair is cleared, such that the plasma membranes may come into contact (Gammie et al., 1998). Membrane fusion rapidly ensues, and further cell wall remodeling

and fusion pore expansion allow for widening of the mating pair neck to allow for nuclear congression and fusion (“karyogamy”).

Efficient membrane fusion requires the mating specific, multipass membrane protein Prm1p (Heiman and Walter, 2000). Prm1p localizes to the zone of contact between cells of a mating pair, and its activity is required in only one partner. When *PRM1* is deleted in both α and α cells only 40% of mating pairs correctly complete membrane merger and cell fusion. Of the remaining mating pairs, most arrest at the step of membrane fusion. Cell wall removal continues such that large areas of membrane are in direct apposition, with only 8 nm separating the outer leaflets of the facing plasma membranes. Due to the absence of cell wall at the interface to separate the mating partners, the opposed membranes grow and retract such that the cytoplasm of one partner invades the space of the other, forming a membrane-contained structure (“cytoplasmic bubbles”). These prezygotes remain arrested for up to 2 hours, by which point individual cells resume the cell cycle and begin budding, or repolarize in an attempt to mate with another cell nearby.

In addition to fusion failure and extension of cytoplasmic bubbles, some *prm1* x *prm1* mating pairs undergo simultaneous cell lysis (Jin et al., 2004). Many lines of experimentation support the hypothesis that mating pair lysis is caused by the cell fusion machinery. The simplest explanation for the lysis and membrane fusion defects is that both are caused by misregulation of the fusase. First, lysis requires membrane contact, as deletion of *FUS1* and *FUS2*, which results in arrest of mating pairs at the upstream step of cell wall removal, suppress the *prm1* lysis phenotype (Jin et al., 2004). Second, mutants with enhanced mating pair lysis, *prm1* and *fig1*, accumulate arrested mating pairs

with membranes apposed but unfused (Aguilar et al., 2007), yet these cytoplasmic bubble structures are not inherently unstable and lead to lysis. They can grow and retract for hours without losing integrity. Instead, lysis events initiate with the same timing as opening of fusion pores and are rarely preceded by the extension of a cytoplasmic bubble (Aguilar et al., 2007). Concomitant with mating pair lysis, a small amount of cytoplasmic mixing is observed, consistent with fusion pores opening simultaneously with the appearance of membrane holes that result in mating pair lysis (Aguilar et al., 2007).

The extent of *prm1 x prm1* mating pair lysis was greatly increased when the mating reaction is performed in the absence of extracellular Ca^{2+} , jumping from 20% to 50% of the mating pairs (Aguilar et al., 2007). The increase in mating pair lysis in the absence of extracellular Ca^{2+} is balanced by a similar decrease in mating pair fusion, again suggesting the engagement of the fusion machine can have two possible outcomes: productive fusion or lysis. Conversely, *prm1 x prm1* mating pair lysis can be suppressed by high concentrations of Ca^{2+} . Calcium may play a direct role in the fusion step by interacting with lipid head groups of the opposed bilayers or the proteins which comprise the fusion machinery (Papahadjopoulos et al., 1990). However, wild-type mating pairs do not require calcium to avoid extensive lysis, suggesting that the mechanism of fusion is less robust for *prm1* mutants. More distantly, Ca^{2+} could prevent mating pair lysis by initiating a wound repair process to fix membrane defects initiated by the fusase. In cell culture wound-healing models, membrane holes are repaired by fusion of lysosomal membrane delivery via a Ca^{2+} -dependent mechanism that involves the C2 domain containing membrane protein synaptotagmin VII. Intriguingly, deletion of yeast *TCB3*, which codes for a C2 domain containing membrane protein, increases *prm1 x prm1*

mating pair lysis to 50% of mating pairs (Aguilar et al., 2007). Thus, wound repair processes may mask the true lytic extent of mating in the absence of Prm1.

Viral fusase-induced lysis. Enveloped viruses must fuse with host cells to transfer their genomes. These fusion events are catalyzed by virally encoded single pass transmembrane proteins. A few studies have found that viral fusases create membrane holes concurrent with fusion pore opening.

The influenza fusase hemagglutinin (HA) is the most thoroughly studied fusion molecule. During HA-mediated virus-liposome fusion, large membrane holes were generated with identical kinetics to lipid mixing, as monitored by the release of large dextran molecules (Shangguan et al., 1996). Similarly, video microscopy revealed contents leakage after hemifusion diaphragm formation during fusion of HA expressing fibroblasts with erythrocytes (Blumenthal and Morris, 1999). However, conductance measurements during virus-planar bilayer fusion were not consistent with membrane holes during the reaction (Young et al., 1983).

Infection of CD4-positive lymphocytes with human immunodeficiency virus type 1 (HIV-1) results in cell death as a consequence of lethal syncytium formation and single-cell lysis. Single-cell lysis requires coexpression of the HIV-1 fusase, gp41, and its receptor CD4 (Cao et al., 1996). Low molecular weight compounds directed against gp41, but not soluble CD4 or neutralizing antibodies, are capable of inhibiting single-cell lysis, indicating that the lethal fusase-receptor interaction occurs intracellularly (Madani et al., 2007). In the experimental system, maximal expression of envelope glycoproteins was reached three days after induction by removing tetracycline, but single-cell lysis was

not evident until 5-12 days after induction. Taken together, these results suggest that gp41-dependent single-cell lysis of lymphocytes is caused by accumulated insults to membrane integrity in the secretory system (Cao et al., 1996). Whether these insults are leaky fusion pores remains an open question.

FUSION MACHINES AND THE PATHWAY OF MEMBRANE FUSION

In the prevailing model, membrane fusion does not risk the integrity of compartmental identity (Figure 1A, left pathway). Yet, as described above, leakiness in fusion has been observed in three separate classes of membrane fusion when the balance of fusion players or identity of fusing membranes is altered. These findings raise two important questions: Where in the pathway of membrane fusion is lysis initiated and how is the fusion machinery designed to prevent this outcome?

Mechanism of biological membrane fusion. The pathway to membrane fusion must include non-bilayer intermediates; generating or resolving these intermediates may be the step where the above lysis examples diverge. Recently, a new model for membrane fusion has been proposed in which compartmental identity is temporarily lost (Muller et al., 2003). Simulations of membrane fusion using coarse grained models predicted that the stalk intermediate promotes the formation of adjacent holes in the bilayers (Figure 1A, 3a and 3b). These holes are then surrounded by the stalk to form a fusion pore (3c). This pathway is less energetically costly than the traditional, non-leaky hemifusion hypothesis (Katsov et al., 2006). Lysis could emerge from this pathway if these membrane holes expand before the stalk can encircle them to form the fusion pore. A

similar leaky structure would be created if, instead of bilayer rupture within the hemifusion diaphragm (Figure 1A, 3), a hole opens in one of the four bilayers adjacent to the hemifusion diaphragm.

Alternatively, lysis may occur before formation of the hemifusion stalk as a consequence of trying to transition to the non-bilayer intermediate. Strongly bending membranes may be a mechanism for forming the stalk intermediate (Kozlov and Chernomordik, 1998). This could be a risky endeavor—without correctly setting up an opposing bilayer to relieve bending stress through stalk formation, generation of unstable, highly curved membranes could result in membrane rupture.

Assembling a fusion machine. Viral fusases and SNAREs are sufficient to fuse lipid bilayers and biological membranes, yet this feat is not achieved by a single viral fusase or trans-SNARE pair. Instead, these molecules are assembled into a greater fusion machine, consisting of multiple core fusases (ie. HA, gp41, a trans-SNARE pair) and, in some cases, regulatory proteins (ie. synaptotagmin, complexin) (Tang et al., 2006). Some of these regulators have been described to govern specificity and timing of the fusion event, might others ensure membrane integrity during lipid rearrangement? The characteristics of this fusion machine realize the fusogenic, and may limit the lytic, potential of individual fusases.

An exciting explanation for SNARE-dependent vacuole lysis is that trans-SNARE pairs are balanced with regulatory proteins that govern membrane integrity during membrane fusion. These integrity factors are not capable of handling the many trans-SNARE complexes formed when SNAREs are overexpressed. Integrity promoting

proteins could exert their effects by controlling and organizing fusases or by preventing off-pathway lipidic rearrangements.

Both viral and intracellular fusion utilize the concerted action of multiple fusases to achieve the energy required for membrane fusion. Kinetic analysis of fusion by cells expressing HA with different surface densities estimated a minimum of three HA trimers mediate membrane fusion (Danieli et al., 1996), and modeling has suggested that the concerted action of at least 8 HA trimers, including 2 in the activated state, are required to open a fusion pore (Bentz, 2000b). In addition to recruiting multiple fusases, the geometry of their association is likely important for efficacy of the fusion machine. The geometry of the HA fusion machine is thought to be circular and surround the hemifusion stalk and nascent fusion pore (Chernomordik et al., 1998). Multiple *trans*-SNARE pairs are required to achieve fusion and atomic force microscopy showed that SNAREs also associate in a ring-like fashion (Cho et al., 2002; Hofmann et al., 2006; Hua and Scheller, 2001). If a fusion machine were haphazardly assembled, the membrane destabilizing activities of the core fusases may result in membrane lysis instead of a fusion pore. The geometrical information behind HA oligomerization is likely inherent in the molecule but this may not be the case for SNAREs and the as yet unidentified yeast fusase. Prm1p could regulate cell fusion by interacting with and orienting core fusase molecules (Figure 2A; Rizo et al., 2006). In the absence of Prm1p, a decreased ability to assemble active fusion machines results in apposed but unfused membranes. Incorrectly assembled fusion machines may destabilize membranes but not in a productive stalk-promoting manner, resulting in cell lysis (Figure 2A, arrow).

Instead of regulating protein fusases, integrity promoting accessory factors could control lipid diffusion to control dangerous fusion intermediates such as the hypothetical membrane holes described above (Figure 2B). HA-mediated cell-cell fusion has been arrested in a state of hemifusion without lipid mixing; clustered HA trimers are believed to cause this restriction (Chernomordik et al., 1998). Modeled on these observations, Prm1 may act by preserving the lipidic environment set up by the core fusase or by stopping expansion of membrane holes (Jin et al., 2004; Shangguan et al., 1996). Consistent with this corral-like structural role, Prm1 forms covalent homodimers, but it is not known if these dimers further oligomerize (A.E. unpublished results).

CONCLUSION

Convergence of molecular simulations and experimental data is making it more difficult to ignore lysis as an irrelevant experimental artifact of membrane fusion assays.

Accordingly, we must revisit the classical model of merger. The experimentally verified stalk structure is not in question, but different rearrangements that risk loss of compartmental identity may occur before fusion pore formation. Specific factors may be involved containing these risks, and identifying such factors would be an extremely valuable advance in our understanding of how the activity of fusases is controlled to fuse membranes with high fidelity. Finding proteins that can suppress vacuole lysis without lowering SNARE activity could help establish such late stage regulation.

Moving from the other direction, identifying proteins that interact with Prm1p is likely to yield a fusase responsible for cell fusion. When available, comparing this class

of fusion to viral and intracellular fusion will describe the breadth of strategies for joining membrane encapsulated compartments.

Recently, a new class of fusion proteins has been described to mediate cell fusion (Salsman et al., 2005; Top et al., 2005). Given their small size (14kD) and simple domain structure, these reovirus FAST proteins would be another great system to ask questions about membrane integrity during the fusion event (see Chapter 1).

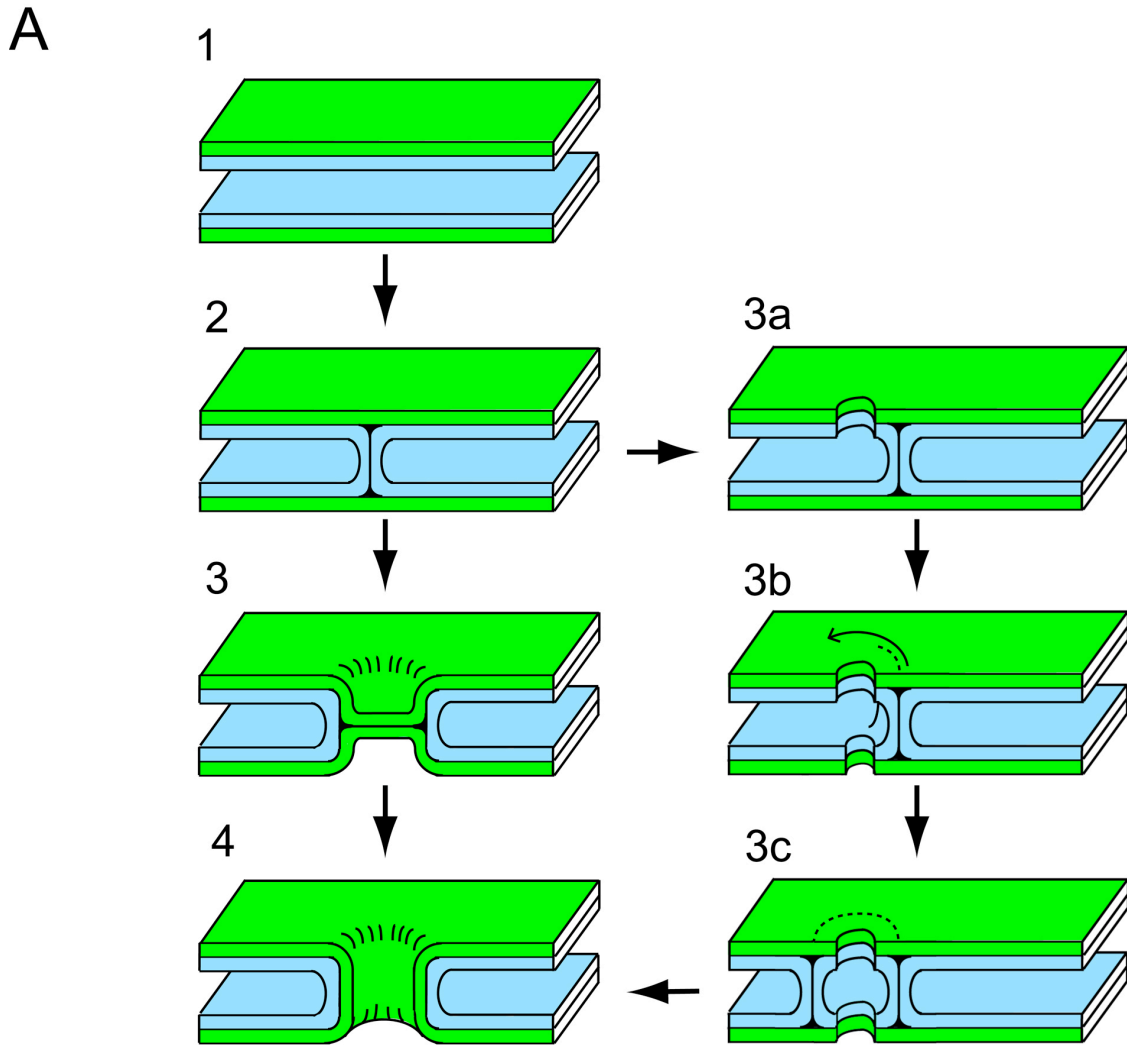


Figure 1. Models for lipid rearrangements leading to the formation of a fusion pore. The left pathway depicts the classical model for membrane fusion via rupture of a hemifusion diaphragm. The alternative pathway (3a-c) does not maintain compartmental identity.

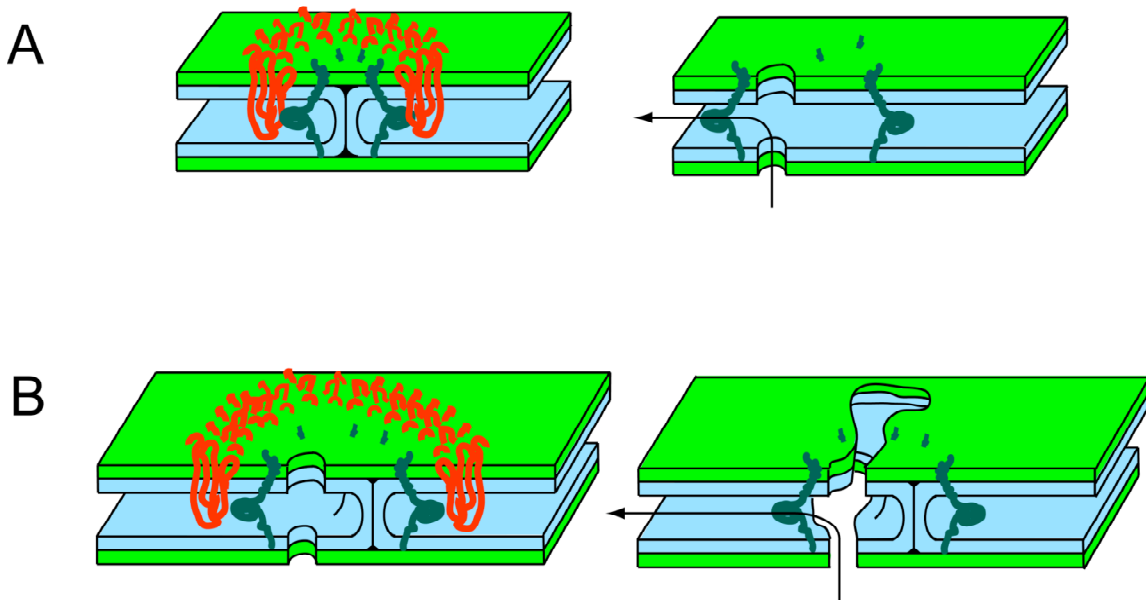


Figure 2. Models for regulation of fusion integrity by non-fusase factors. Fusase molecules are drawn in green, integrity promoting factors in red. (B) Regulation of lytic potential by organizing fusase molecules. (C) Restriction of membrane hole expansion by a ring of membrane proteins.

REFERENCES

- Adames, N., K. Blundell, M.N. Ashby, and C. Boone. 1995. Role of yeast insulin-degrading enzyme homologs in propheromone processing and bud site selection. *Science*. 270:464-7.
- Aguilar, P.S., A. Engel, and P. Walter. 2007. The plasma membrane proteins Prm1 and Fig1 ascertain fidelity of membrane fusion during yeast mating. *Mol Biol Cell*. 18:547-56.
- Baba, M., N. Baba, Y. Ohsumi, K. Kanaya, and M. Osumi. 1989. Three-dimensional analysis of morphogenesis induced by mating pheromone alpha factor in *Saccharomyces cerevisiae*. *J Cell Sci*. 94 (Pt 2):207-16.
- Bagnat, M., and K. Simons. 2002. Cell surface polarization during yeast mating. *Proc Natl Acad Sci U S A*. 99:14183-8.
- Bai, J., and E.R. Chapman. 2004. The C2 domains of synaptotagmin--partners in exocytosis. *Trends Biochem Sci*. 29:143-51.
- Banuet, F. 1998. Signalling in the yeasts: an informational cascade with links to the filamentous fungi. *Microbiol Mol Bio Rev*. 62:249-274.
- Barkai, N., M.D. Rose, and N.S. Wingreen. 1998. Protease helps yeast find mating partners. *Nature*. 396:422-3.
- Basco, R.D., G. Gimenez-Gallego, and G. Larriba. 1990. Processing of yeast exoglucanase (beta-glucosidase) in a KEX2-dependent manner. *FEBS Lett*. 268:99-102.

Baumert, M., P.R. Maycox, F. Navone, P. De Camilli, and R. Jahn. 1989. Synaptobrevin: an integral membrane protein of 18,000 daltons present in small synaptic vesicles of rat brain. *Embo J.* 8:379-84.

Beckers, C.J., M.R. Block, B.S. Glick, J.E. Rothman, and W.E. Balch. 1989. Vesicular transport between the endoplasmic reticulum and the Golgi stack requires the NEM-sensitive fusion protein. *Nature.* 339:397-8.

Beh, C.T., V. Brizzio, and M.D. Rose. 1997. KAR5 encodes a novel pheromone-inducible protein required for homotypic nuclear fusion. *J Cell Biol.* 139:1063-76.

Bender, A., and G.F. Sprague, Jr. 1989. Pheromones and pheromone receptors are the primary determinants of mating specificity in the yeast *Saccharomyces cerevisiae*. *Genetics.* 121:463-76.

Bennett, M.K., N. Calakos, and R.H. Scheller. 1992. Syntaxin: a synaptic protein implicated in docking of synaptic vesicles at presynaptic active zones. *Science.* 257:255-9.

Bentz, J. 2000a. Membrane fusion mediated by coiled coils: a hypothesis. *Biophys J.* 78:886-900.

Bentz, J. 2000b. Minimal aggregate size and minimal fusion unit for the first fusion pore of influenza hemagglutinin-mediated membrane fusion. *Biophys J.* 78:227-45.

Bhalla, A., M.C. Chicka, W.C. Tucker, and E.R. Chapman. 2006. Ca(2+)- synaptotagmin directly regulates t-SNARE function during reconstituted membrane fusion. *Nat Struct Mol Biol.* 13:323-330.

Blobel, C.P., T.G. Wolfsberg, C.W. Turck, D.G. Myles, P. Primakoff, and J.M. White. 1992. A potential fusion peptide and an integrin ligand domain in a protein active in sperm-egg fusion. *Nature.* 356:248-52.

Blumenthal, R., and S.J. Morris. 1999. The influenza haemagglutinin-induced fusion cascade: effects of target membrane permeability changes. *Mol Membr Biol.* 16:43-7.

Bostian, K.A., Q. Elliott, H. Bussey, V. Burn, A. Smith, and D.J. Tipper. 1984. Sequence of the preprotoxin dsRNA gene of type I killer yeast: multiple processing events produce a two-component toxin. *Cell.* 36:741-51.

Brizzio, V., A.E. Gammie, and M.D. Rose. 1998. Rvs161p interacts with Fus2p to promote cell fusion in *Saccharomyces cerevisiae*. *J Cell Biol.* 141:567-84.

Brizzio, V., W. Khalfan, D. Huddler, C.T. Beh, S.S. Andersen, M. Latterich, and M.D. Rose. 1999. Genetic interactions between KAR7/SEC71, KAR8/JEM1, KAR5, and KAR2 during nuclear fusion in *Saccharomyces cerevisiae*. *Mol Biol Cell.* 10:609-26.

Cao, J., I.W. Park, A. Cooper, and J. Sodroski. 1996. Molecular determinants of acute single-cell lysis by human immunodeficiency virus type 1. *J Virol.* 70:1340-54.

Cappellaro, C., V. Mersa, and W. Tanner. 1998. New potential cell wall glucanases of *Saccharomyces cerevisiae* and their involvement in mating. *J Bacteriol.* 180:5030-7.

- Cervený, K.L., Y. Tamura, Z. Zhang, R.E. Jensen, and H. Sesaki. 2007. Regulation of mitochondrial fusion and division. *Trends Cell Biol.* 17:563-9.
- Chen, E.H., and E.N. Olson. 2005. Unveiling the mechanisms of cell-cell fusion. *Science.* 308:369-373.
- Chen, E.H., E. Grote, W. Mohler, and A. Vignery. 2007. Cell-cell fusion. *FEBS Lett.* 581:2181-93.
- Chen, X., D. Arac, T.M. Wang, C.J. Gilpin, J. Zimmerberg, and J. Rizo. 2006. SNARE-mediated lipid mixing depends on the physical state of the vesicles. *Biophys J.* 90:2062-74.
- Chernomordik, L.V., V.A. Frolov, E. Leikina, P. Bronk, and J. Zimmerberg. 1998. The pathway of membrane fusion catalyzed by influenza hemagglutinin: restriction of lipids, hemifusion, and lipidic fusion pore formation. *J Cell Biol.* 140:1369-82.
- Cho, C., D.O. Bunch, J.E. Faure, E.H. Goulding, E.M. Eddy, P. Primakoff, and D.G. Myles. 1998. Fertilization defects in sperm from mice lacking fertilin beta. *Science.* 281:1857-9.
- Cho, C., H. Ge, D. Branciforte, P. Primakoff, and D.G. Myles. 2000. Analysis of mouse fertilin in wild-type and fertilin beta(-/-) sperm: evidence for C-terminal modification, alpha/beta dimerization, and lack of essential role of fertilin alpha in sperm-egg fusion. *Dev Biol.* 222:289-95.

Cho, S.J., M. Kelly, K.T. Rognlien, J.A. Cho, J.K. Horber, and B.P. Jena. 2002. SNAREs in opposing bilayers interact in a circular array to form conducting pores. *Biophys J.* 83:2522-7.

Coorssen, J.R., P.S. Blank, F. Albertorio, L. Bezrukov, I. Kolosova, X. Chen, P.S. Backlund, Jr., and J. Zimmerberg. 2003. Regulated secretion: SNARE density, vesicle fusion and calcium dependence. *J Cell Sci.* 116:2087-97.

Creutz, C.E., S.L. Snyder, and T.A. Schulz. 2004. Characterization of the yeast tricalbins: membrane-bound multi-C2-domain proteins that form complexes involved in membrane trafficking. *Cell Mol Life Sci.* 61:1208-1220.

Cuasnicu, P.S., D.A. Ellerman, D.J. Cohen, D. Busso, M.M. Morgenfeld, and V.G. Da Ros. 2001. Molecular mechanisms involved in mammalian gamete fusion. *Arch Med Res.* 32:614-8.

Danino, D., and J.E. Hinshaw. 2001. Dynamin family of mechanoenzymes. *Curr Opin Cell Biol.* 13:454-60.

Davletov, B.A., and T.C. Sudhof. 1993. A single C2 domain from synaptotagmin I is sufficient for high affinity Ca²⁺/phospholipid binding. *J Biol Chem.* 268:26386-90.

del Campo, J.J., E. Opoku-Serebuoh, A.B. Isaacson, V.L. Scranton, M. Tucker, M. Han, and W.A. Mohler. 2005. Fusogenic activity of EFF-1 is regulated via dynamic localization in fusing somatic cells of *C. elegans*. *Curr Biol.* 15:413-23.

Doberstein, S.K., R.D. Fetter, A.Y. Mehta, and C.S. Goodman. 1997. Genetic analysis of myoblast fusion: blown fuse is required for progression beyond the prefusion complex. *J Cell Biol.* 136:1249-61.

Doherty, K.R., A. Cave, D.B. Davis, A.J. Delmonte, A. Posey, J.U. Earley, M. Hadhazy, and E.M. McNally. 2005. Normal myoblast fusion requires myoferlin. *Development.* 132:5565-5575.

Duzgunes, N., J. Wilschut, R. Fraley, and D. Papahadjopoulos. 1981. Studies on the mechanism of membrane fusion. Role of head-group composition in calcium- and magnesium-induced fusion of mixed phospholipid vesicles. *Biochim Biophys Acta.* 642:182-195.

Dworak, H.A., and H. Sink. 2002. Myoblast fusion in *Drosophila*. *Bioessays.* 24:591-601.

Elia, L., and L. Marsh. 1996. Role of the ABC transporter Ste6 in cell fusion during yeast conjugation. *J Cell Biol.* 135:741-51.

Elia, L., and L. Marsh. 1998. A role for a protease in morphogenic responses during yeast cell fusion. *J Cell Biol.* 142:1473-85.

Elion, E.A., J. Trueheart, and G.R. Fink. 1995. Fus2 localizes near the site of cell fusion and is required for both cell fusion and nuclear alignment during zygote formation. *J Cell Biol.* 130:1283-96.

Ellens, H., J. Bentz, and F.C. Szoka. 1985. H⁺- and Ca²⁺-induced fusion and destabilization of liposomes. *Biochemistry.* 24:3099-3106.

Erdman, S., L. Lin, M. Malczynski, and M. Snyder. 1998. Pheromone-regulated genes required for yeast mating differentiation. *J Cell Biol.* 140:461-483.

Fernandez, I., D. Arac, J. Ubach, S.H. Gerber, O. Shin, Y. Gao, R.G. Anderson, T.C. Sudhof, and J. Rizo. 2001. Three-dimensional structure of the synaptotagmin 1 C2B-domain: synaptotagmin 1 as a phospholipid binding machine. *Neuron.* 32:1057-69.

Fuller, R.S., A. Brake, and J. Thorner. 1989. Yeast prohormone processing enzyme (KEX2 gene product) is a Ca²⁺-dependent serine protease. *Proc Natl Acad Sci U S A.* 86:1434-8.

Gammie, A.E., V. Brizzio, and M.D. Rose. 1998. Distinct morphological phenotypes of cell fusion mutants. *Mol Biol Cell.* 9:1395-410.

Geppert, M., Y. Goda, R.E. Hammer, C. Li, T.W. Rosahl, C.F. Stevens, and T.C. Sudhof. 1994. Synaptotagmin I: a major Ca²⁺ sensor for transmitter release at a central synapse. *Cell.* 79:717-27.

Grote, E., M. Baba, Y. Ohsumi, and P.J. Novick. 2000. Geranylgeranylated SNAREs are dominant inhibitors of membrane fusion. *J Cell Biol.* 151:453-66.

Han, X., C.T. Wang, J. Bai, E.R. Chapman, and M.B. Jackson. 2004. Transmembrane segments of syntaxin line the fusion pore of Ca²⁺-triggered exocytosis. *Science.* 304:289-92.

Han, X., H. Sterling, Y. Chen, C. Saginario, E.J. Brown, W.A. Frazier, F.P. Lindberg, and A. Vignery. 2000. CD47, a ligand for the macrophage fusion receptor, participates in macrophage multinucleation. *J Biol Chem.* 275:37984-92.

Harbury, P.A. 1998. Springs and zippers: coiled coils in SNARE-mediated membrane fusion. *Structure.* 6:1487-91.

Heiman, M.G., and P. Walter. 2000. Prm1p, a pheromone-regulated multispinning membrane protein, facilitates plasma membrane fusion during yeast mating. *J Cell Biol.* 151:719-30.

Hemler, M.E. 2001. Specific tetraspanin functions. *J Cell Biol.* 155:1103-1107.

Hemler, M.E. 2005. Tetraspanin functions and associated microdomains. *Nat Rev Mol Cell Biol.* 6:801-11.

Hernandez, L.D., L.R. Hoffman, T.G. Wolfsberg, and J.M. White. 1996. Virus-cell and cell-cell fusion. *Annu Rev Cell Dev Biol.* 12:627-61.

Herskowitz, I. 1995. MAP kinase pathways in yeast: for mating and more. *Cell.* 80:187-97.

Hu, C., M. Ahmed, T.J. Melia, T.H. Sollner, T. Mayer, and J.E. Rothman. 2003. Fusion of cells by flipped SNAREs. *Science.* 300:1745-9.

Hua, Y., and R.H. Scheller. 2001. Three SNARE complexes cooperate to mediate membrane fusion. *Proc Natl Acad Sci U S A.* 98:8065-70.

- Hughson, F.M. 1995. Structural characterization of viral fusion proteins. *Curr Biol.* 5:265-74.
- Iida, H., Y. Yagawa, and Y. Anraku. 1990. Essential role for induced Ca²⁺ influx followed by [Ca²⁺]_i rise in maintaining viability of yeast cells late in the mating pheromone response pathway. A study of [Ca²⁺]_i in single *Saccharomyces cerevisiae* cells with imaging of fura-2. *J Biol Chem.* 265:13391-9.
- Jackson, C.L., and L.H. Hartwell. 1990. Courtship in *S. cerevisiae*: both cell types choose mating partners by responding to the strongest pheromone signal. *Cell.* 63:1039-51.
- Jahn, R., T. Lang, and T.C. Sudhof. 2003. Membrane fusion. *Cell.* 112:519-533.
- Jaiswal, J.K., S. Chakrabarti, N.W. Andrews, and S.M. Simon. 2004. Synaptotagmin VII restricts fusion pore expansion during lysosomal exocytosis. *PLoS Biol.* 2:E233.
- Jin, H., C. Carlile, S. Nolan, and E. Grote. 2004. Prm1 prevents contact-dependent lysis of yeast mating pairs. *Eukaryot Cell.* 3:1664-73.
- Julius, D., L. Blair, A. Brake, G. Sprague, and J. Thorner. 1983. Yeast alpha factor is processed from a larger precursor polypeptide: the essential role of a membrane-bound dipeptidyl aminopeptidase. *Cell.* 32:839-52.
- Jung, U.S., and D.E. Levin. 1999. Genome-wide analysis of gene expression regulated by the yeast cell wall integrity signalling pathway. *Mol Microbiol.* 34:1049-57.

Kaji, K., S. Oda, T. Shikano, T. Ohnuki, Y. Uematsu, J. Sakagami, N. Tada, S. Miyazaki, and A. Kudo. 2000. The gamete fusion process is defective in eggs of Cd9-deficient mice. *Nat Genet.* 24:279-82.

Katsov, K., M. Muller, and M. Schick. 2006. Field theoretic study of bilayer membrane fusion: II. Mechanism of a stalk-hole complex. *Biophys J.* 90:915-26.

Kemble, G.W., T. Danieli, and J.M. White. 1994. Lipid-anchored influenza hemagglutinin promotes hemifusion, not complete fusion. *Cell.* 76:383-91.

Kielian, M., and F.A. Rey. 2006. Virus membrane-fusion proteins: more than one way to make a hairpin. *Nat Rev Microbiol.* 4:67-76.

Kim, J., and D.J. Klionsky. 2000. Autophagy, cytoplasm-to-vacuole targeting pathway, and pexophagy in yeast and mammalian cells. *Annu Rev Biochem.* 69:303-42.

Koh, T.W., and H.J. Bellen. 2003. Synaptotagmin I, a Ca²⁺ sensor for neurotransmitter release. *Trends Neurosci.* 26:413-422.

Komano, H., and R.S. Fuller. 1995. Shared functions in vivo of a glycosyl-phosphatidylinositol-linked aspartyl protease, Mkc7, and the proprotein processing protease Kex2 in yeast. *Proc Natl Acad Sci U S A.* 92:10752-6.

Kozlov, M.M., and L.V. Chernomordik. 1998. A mechanism of protein-mediated fusion: coupling between refolding of the influenza hemagglutinin and lipid rearrangements. *Biophys J.* 75:1384-96.

Kurihara, L.J., C.T. Beh, M. Latterich, R. Schekman, and M.D. Rose. 1994. Nuclear congression and membrane fusion: two distinct events in the yeast karyogamy pathway. *J Cell Biol.* 126:911-23.

Kurjan, J., and I. Herskowitz. 1982. Structure of a yeast pheromone gene (MF alpha): a putative alpha-factor precursor contains four tandem copies of mature alpha-factor. *Cell.* 30:933-43.

Lawless, M.K., S. Barney, K.I. Guthrie, T.B. Bucy, S.R. Petteway, Jr., and G. Merutka. 1996. HIV-1 membrane fusion mechanism: structural studies of the interactions between biologically-active peptides from gp41. *Biochemistry.* 35:13697-708.

Le Naour, F., E. Rubinstein, C. Jasmin, M. Prenant, and C. Boucheix. 2000. Severely reduced female fertility in CD9-deficient mice. *Science.* 287:319-21.

Leibowitz, M.J., and R.B. Wickner. 1976. A chromosomal gene required for killer plasmid expression, mating, and spore maturation in *Saccharomyces cerevisiae*. *Proc Natl Acad Sci U S A.* 73:2061-5.

Li, F., F. Pincet, E. Perez, W.S. Eng, T.J. Melia, J.E. Rothman, and D. Tareste. 2007. Energetics and dynamics of SNAREpin folding across lipid bilayers. *Nat Struct Mol Biol.* 14:890-6.

Link, E., L. Edelmann, J.H. Chou, T. Binz, S. Yamasaki, U. Eisel, M. Baumert, T.C. Sudhof, H. Niemann, and R. Jahn. 1992. Tetanus toxin action: inhibition of neurotransmitter release linked to synaptobrevin proteolysis. *Biochem Biophys Res Commun.* 189:1017-23.

Littleton, J.T., J. Bai, B. Vyas, R. Desai, A.E. Baltus, M.B. Garment, S.D. Carlson, B. Ganetzky, and E.R. Chapman. 2001. synaptotagmin mutants reveal essential functions for the C2B domain in Ca²⁺-triggered fusion and recycling of synaptic vesicles in vivo. *J Neurosci.* 21:1421-33.

Longtine, M.S., A. McKenzie, 3rd, D.J. Demarini, N.G. Shah, A. Wach, A. Brachat, P. Philippsen, and J.R. Pringle. 1998. Additional modules for versatile and economical PCR-based gene deletion and modification in *Saccharomyces cerevisiae*. *Yeast.* 14:953-61.

Madani, N., A.M. Hubicki, A.L. Perdigo, M. Springer, and J. Sodroski. 2007. Inhibition of human immunodeficiency virus envelope glycoprotein-mediated single cell lysis by low-molecular-weight antagonists of viral entry. *J Virol.* 81:532-8.

Malhotra, V., L. Orci, B.S. Glick, M.R. Block, and J.E. Rothman. 1988. Role of an N-ethylmaleimide-sensitive transport component in promoting fusion of transport vesicles with cisternae of the Golgi stack. *Cell.* 54:221-7.

McCaffrey, G., F.J. Clay, K. Kelsay, and G.F. Sprague, Jr. 1987. Identification and regulation of a gene required for cell fusion during mating of the yeast *Saccharomyces cerevisiae*. *Mol Cell Biol.* 7:2680-90.

McDonald, K. 1999. High-pressure freezing for preservation of high resolution fine structure and antigenicity for immunolabeling. *Methods Mol Biol.* 117:77-97.

McDonald, K., and T. Müller-Reichert. 2002. Cryomethods for thin section electron microscopy. *Methods Enzymol.* 351:96-123.

McNew, J.A., F. Parlati, R. Fukuda, R.J. Johnston, K. Paz, F. Paumet, T.H. Sollner, and J.E. Rothman. 2000a. Compartmental specificity of cellular membrane fusion encoded in SNARE proteins. *Nature*. 407:153-9.

McNew, J.A., T. Weber, D.M. Engelman, T.H. Sollner, and J.E. Rothman. 1999. The length of the flexible SNAREpin juxtamembrane region is a critical determinant of SNARE-dependent fusion. *Mol Cell*. 4:415-21.

McNew, J.A., T. Weber, F. Parlati, R.J. Johnston, T.J. Melia, T.H. Sollner, and J.E. Rothman. 2000b. Close is not enough: SNARE-dependent membrane fusion requires an active mechanism that transduces force to membrane anchors. *J Cell Biol*. 150:105-17.

Meeusen, S., R. DeVay, J. Block, A. Cassidy-Stone, S. Wayson, J.M. McCaffery, and J. Nunnari. 2006. Mitochondrial inner-membrane fusion and crista maintenance requires the dynamin-related GTPase Mgm1. *Cell*. 127:383-95.

Melia, T.J., T. Weber, J.A. McNew, L.E. Fisher, R.J. Johnston, F. Parlati, L.K. Mahal, T.H. Sollner, and J.E. Rothman. 2002. Regulation of membrane fusion by the membrane-proximal coil of the t-SNARE during zippering of SNAREpins. *J Cell Biol*. 158:929-40.

Merz, A.J., and W.T. Wickner. 2004. Trans-SNARE interactions elicit Ca²⁺ efflux from the yeast vacuole lumen. *J Cell Biol*. 164:195-206.

Mi, S., X. Lee, X. Li, G.M. Veldman, H. Finnerty, L. Racie, E. LaVallie, X.Y. Tang, P. Edouard, S. Howes, J.C. Keith, Jr., and J.M. McCoy. 2000. Syncytin is a captive retroviral envelope protein involved in human placental morphogenesis. *Nature*. 403:785-9.

Min, G., H. Wang, T.T. Sun, and X.P. Kong. 2006. Structural basis for tetraspanin functions as revealed by the cryo-EM structure of uroplakin complexes at 6-A resolution. *J Cell Biol.* 173:975-83.

Miyado, K., G. Yamada, S. Yamada, H. Hasuwa, Y. Nakamura, F. Ryu, K. Suzuki, K. Kosai, K. Inoue, A. Ogura, M. Okabe, and E. Mekada. 2000. Requirement of CD9 on the egg plasma membrane for fertilization. *Science.* 287:321-4.

Mohler, W.A., G. Shemer, J.J. del Campo, C. Valansi, E. Opoku-Serebuoh, V. Scranton, N. Assaf, J.G. White, and B. Podbilewicz. 2002. The type I membrane protein EFF-1 is essential for developmental cell fusion. *Dev Cell.* 2:355-62.

Molk, J.N., E.D. Salmon, and K. Bloom. 2006. Nuclear congression is driven by cytoplasmic microtubule plus end interactions in *S. cerevisiae*. *J Cell Biol.* 172:27-39.

Mrsa, V., T. Seidl, M. Gentsch, and W. Tanner. 1997. Specific labelling of cell wall proteins by biotinylation. Identification of four covalently linked O-mannosylated proteins of *Saccharomyces cerevisiae*. *Yeast.* 13:1145-54.

Muller, E.M., E.G. Locke, and K.W. Cunningham. 2001. Differential regulation of two Ca²⁺ influx systems by pheromone signaling in *Saccharomyces cerevisiae*. *Genetics.* 159:1527-38.

Muller, E.M., N.A. Mackin, S.E. Erdman, and K.W. Cunningham. 2003. Fig1p facilitates Ca²⁺ influx and cell fusion during mating of *Saccharomyces cerevisiae*. *J Biol Chem.* 278:38461-9.

- Muller, M., K. Katsov, and M. Schick. 2003. A new mechanism of model membrane fusion determined from Monte Carlo simulation. *Biophys J.* 85:1611-23.
- Naider, F., and J.M. Becker. 2004. The alpha-factor mating pheromone of *Saccharomyces cerevisiae*: a model for studying the interaction of peptide hormones and G protein-coupled receptors. *Peptides.* 25:1441-63.
- Nelson, B., A.B. Parsons, M. Evangelista, K. Schaefer, K. Kennedy, S. Ritchie, T.L. Petryshen, and C. Boone. 2004. Fus1p interacts with components of the Hog1p mitogen-activated protein kinase and Cdc42p morphogenesis signaling pathways to control cell fusion during yeast mating. *Genetics.* 166:67-77.
- Nern, A., and R.A. Arkowitz. 1999. A Cdc24p-Far1p-Gbetagamma protein complex required for yeast orientation during mating. *J Cell Biol.* 144:1187-202.
- Ng, D.T., and P. Walter. 1996. ER membrane protein complex required for nuclear fusion. *J Cell Biol.* 132:499-509.
- Nickel, W., T. Weber, J.A. McNew, F. Parlati, T.H. Sollner, and J.E. Rothman. 1999. Content mixing and membrane integrity during membrane fusion driven by pairing of isolated v-SNAREs and t-SNAREs. *Proc Natl Acad Sci U S A.* 96:12571-6.
- Nolan, S., A.E. Cowan, D.E. Koppel, H. Jin, and E. Grote. 2006. FUS1 regulates the opening and expansion of fusion pores between mating yeast. *Mol Biol Cell.* 17:2439-50.
- Nonaka, H., K. Tanaka, H. Hirano, T. Fujiwara, H. Kohno, M. Umikawa, A. Mino, and Y. Takai. 1995. A downstream target of RHO1 small GTP-binding protein is PKC1, a

homolog of protein kinase C, which leads to activation of the MAP kinase cascade in *Saccharomyces cerevisiae*. *Embo J.* 14:5931-8.

Novick, P., and R. Schekman. 1979. Secretion and cell-surface growth are blocked in a temperature-sensitive mutant of *Saccharomyces cerevisiae*. *Proc Natl Acad Sci U S A.* 76:1858-62.

Novick, P., C. Field, and R. Schekman. 1980. Identification of 23 complementation groups required for post-translational events in the yeast secretory pathway. *Cell.* 21:205-15.

Ohsumi, Y., and Y. Anraku. 1985. Specific induction of Ca²⁺ transport activity in MATa cells of *Saccharomyces cerevisiae* by a mating pheromone, alpha factor. *J Biol Chem.* 260:10482-6.

O'Rourke, S.M., and I. Herskowitz. 2002. A third osmosensing branch in *Saccharomyces cerevisiae* requires the Msb2 protein and functions in parallel with the Sho1 branch. *Mol Cell Biol.* 22:4739-49.

Osumi, M., C. Shimoda, and N. Yanagishima. 1974. Mating reaction in *Saccharomyces cerevisiae*. V. Changes in the fine structure during the mating reaction. *Arch Mikrobiol.* 97:27-38.

Oyler, G.A., G.A. Higgins, R.A. Hart, E. Battenberg, M. Billingsley, F.E. Bloom, and M.C. Wilson. 1989. The identification of a novel synaptosomal-associated protein, SNAP-25, differentially expressed by neuronal subpopulations. *J Cell Biol.* 109:3039-52.

Papa, F.R., C. Zhang, K. Shokat, and P. Walter. 2003. Bypassing a kinase activity with an ATP-competitive drug. *Science*. 302:1533-7.

Papahadjopoulos, D., S. Nir, and N. Duzgunes. 1990. Molecular mechanisms of calcium-induced membrane fusion. *J Bioenerg Biomembr*. 22:157-79.

Parlati, F., J.A. McNew, R. Fukuda, R. Miller, T.H. Sollner, and J.E. Rothman. 2000. Topological restriction of SNARE-dependent membrane fusion. *Nature*. 407:194-8.

Peisajovich, S.G., S.A. Gallo, R. Blumenthal, and Y. Shai. 2003. C-terminal octylation rescues an inactive T20 mutant: implications for the mechanism of HIV/SIMIAN immunodeficiency virus-induced membrane fusion. *J Biol Chem*. 278:21012-7.

Peters, C., M.J. Bayer, S. Buhler, J.S. Andersen, M. Mann, and A. Mayer. 2001. Trans-complex formation by proteolipid channels in the terminal phase of membrane fusion. *Nature*. 409:581-8.

Philips, J., and I. Herskowitz. 1997. Osmotic balance regulates cell fusion during mating in *Saccharomyces cerevisiae*. *J Cell Biol*. 138:961-74.

Philips, J., and I. Herskowitz. 1998. Identification of Kel1p, a kelch domain-containing protein involved in cell fusion and morphology in *Saccharomyces cerevisiae*. *J Cell Biol*. 143:375-89.

Podbilewicz, B., E. Leikina, A. Sapir, C. Valansi, M. Suissa, G. Shemer, and L.V. Chernomordik. 2006. The *C. elegans* developmental fusogen EFF-1 mediates homotypic fusion in heterologous cells and in vivo. *Dev Cell*. 11:471-81.

- Proszynski, T.J., R. Klemm, M. Bagnat, K. Gaus, and K. Simons. 2006. Plasma membrane polarization during mating in yeast cells. *J Cell Biol.* 173:861-6.
- Qiao, H., R.T. Armstrong, G.B. Melikyan, F.S. Cohen, and J.M. White. 1999. A specific point mutant at position 1 of the influenza hemagglutinin fusion peptide displays a hemifusion phenotype. *Mol Biol Cell.* 10:2759-69.
- Ramalho-Santos, J., and M.C. de Lima. 1998. The influenza virus hemagglutinin: a model protein in the study of membrane fusion. *Biochim Biophys Acta.* 1376:147-54.
- Reddy, A., E.V. Caler, and N.W. Andrews. 2001. Plasma membrane repair is mediated by Ca(2+)-regulated exocytosis of lysosomes. *Cell.* 106:157-169.
- Rice, L.M., P. Brennwald, and A.T. Brunger. 1997. Formation of a yeast SNARE complex is accompanied by significant structural changes. *FEBS Lett.* 415:49-55.
- Roberts, C.J., B. Nelson, M.J. Marton, R. Stoughton, M.R. Meyer, H.A. Bennett, Y.D. He, H. Dai, W.L. Walker, T.R. Hughes, M. Tyers, C. Boone, and S.H. Friend. 2000. Signaling and circuitry of multiple MAPK pathways revealed by a matrix of global gene expression profiles. *Science.* 287:873-80.
- Rockwell, N.C., D.J. Krysan, T. Komiyama, and R.S. Fuller. 2002. Precursor processing by kex2/furin proteases. *Chem Rev.* 102:4525-48.
- Russo, P., N. Kalkkinen, H. Sareneva, J. Paakkola, and M. Makarow. 1992. A heat shock gene from *Saccharomyces cerevisiae* encoding a secretory glycoprotein. *Proc Natl Acad Sci U S A.* 89:8857.

Salsman, J., D. Top, J. Boutilier, and R. Duncan. 2005. Extensive syncytium formation mediated by the reovirus FAST proteins triggers apoptosis-induced membrane instability. *J Virol.* 79:8090-100.

Santos, B., and M. Snyder. 2003. Specific protein targeting during cell differentiation: polarized localization of Fus1p during mating depends on Chs5p in *Saccharomyces cerevisiae*. *Eukaryot Cell.* 2:821-5.

Sapir, A., J. Choi, E. Leikina, O. Avinoam, C. Valansi, L.V. Chernomordik, A.P. Newman, and B. Podbilewicz. 2007. AFF-1, a FOS-1-regulated fusogen, mediates fusion of the anchor cell in *C. elegans*. *Dev Cell.* 12:683-98.

Schulz, T.A., and C.E. Creutz. 2004. The tricalbin C2 domains: lipid-binding properties of a novel, synaptotagmin-like yeast protein family. *Biochemistry.* 43:3987-3995.

Shangguan, T., D. Alford, and J. Bentz. 1996. Influenza-virus-liposome lipid mixing is leaky and largely insensitive to the material properties of the target membrane. *Biochemistry.* 35:4956-65.

Shemer, G., M. Suissa, I. Kolotuev, K.C. Nguyen, D.H. Hall, and B. Podbilewicz. 2004. EFF-1 is sufficient to initiate and execute tissue-specific cell fusion in *C. elegans*. *Curr Biol.* 14:1587-91.

Sikorski, R.S., and P. Hieter. 1989. A system of shuttle vectors and yeast host strains designed for efficient manipulation of DNA in *Saccharomyces cerevisiae*. *Genetics.* 122:19-27.

Singh, A., E.Y. Chen, J.M. Lugovoy, C.N. Chang, R.A. Hitzeman, and P.H. Seeburg. 1983. *Saccharomyces cerevisiae* contains two discrete genes coding for the alpha-factor pheromone. *Nucleic Acids Res.* 11:4049-63.

Skehel, J.J., and D.C. Wiley. 2000. Receptor binding and membrane fusion in virus entry: the influenza hemagglutinin. *Annu Rev Biochem.* 69:531-69.

Sollner, T., S.W. Whiteheart, M. Brunner, H. Erdjument-Bromage, S. Geromanos, P. Tempst, and J.E. Rothman. 1993. SNAP receptors implicated in vesicle targeting and fusion. *Nature.* 362:318-24.

Sollner, T.H. 2004. Intracellular and viral membrane fusion: a uniting mechanism. *Curr Opin Cell Biol.* 16:429-435.

Starai, V.J., Y. Jun, and W. Wickner. 2007. Excess vacuolar SNAREs drive lysis and Rab bypass fusion. *Proc Natl Acad Sci U S A.* 104:13551-8.

Steinhardt, R.A., G. Bi, and G. Alderton. 1994. Cell membrane resealing by a vesicular mechanism similar to neurotransmitter release. *Science.* 263:390-393.

Sutton, R.B., D. Fasshauer, R. Jahn, and A.T. Brunger. 1998. Crystal structure of a SNARE complex involved in synaptic exocytosis at 2.4 Å resolution. *Nature.* 395:347-53.

Szule, J.A., S.E. Jarvis, J.E. Hibbert, J.D. Spafford, J.E. Braun, G.W. Zamponi, G.M. Wessel, and J.R. Coorssen. 2003. Calcium-triggered membrane fusion proceeds independently of specific presynaptic proteins. *J Biol Chem.* 278:24251-4.

Talbot, P., B.D. Shur, and D.G. Myles. 2003. Cell adhesion and fertilization: steps in oocyte transport, sperm-zona pellucida interactions, and sperm-egg fusion. *Biol Reprod.* 68:1-9.

Tang, J., A. Maximov, O.H. Shin, H. Dai, J. Rizo, and T.C. Sudhof. 2006. A complexin/synaptotagmin 1 switch controls fast synaptic vesicle exocytosis. *Cell.* 126:1175-87.

Taylor, M.V. 2002. Muscle differentiation: how two cells become one. *Curr Biol.* 12:R224-228.

Tomishige, N., Y. Noda, H. Adachi, H. Shimoi, A. Takatsuki, and K. Yoda. 2003. Mutations that are synthetically lethal with a *gas1D* allele cause defects in the cell wall of *Saccharomyces cerevisiae*. *Mol Genet Genomics.* 269:562-73.

Top, D., R. de Antueno, J. Salsman, J. Corcoran, J. Mader, D. Hoskin, A. Touhami, M.H. Jericho, and R. Duncan. 2005. Liposome reconstitution of a minimal protein-mediated membrane fusion machine. *Embo J.* 24:2980-8.

Trimble, W.S., D.M. Cowan, and R.H. Scheller. 1988. VAMP-1: a synaptic vesicle-associated integral membrane protein. *Proc Natl Acad Sci U S A.* 85:4538-42.

Trueheart, J., J.D. Boeke, and G.R. Fink. 1987. Two genes required for cell fusion during yeast conjugation: evidence for a pheromone-induced surface protein. *Mol Cell Biol.* 7:2316-28.

Van Itallie, C.M., and J.M. Anderson. 2004. The molecular physiology of tight junction pores. *Physiology (Bethesda)*. 19:331-338.

Wang, L., E.S. Seeley, W. Wickner, and A.J. Merz. 2002. Vacuole fusion at a ring of vertex docking sites leaves membrane fragments within the organelle. *Cell*. 108:357-69.

Weber, T., B.V. Zemelman, J.A. McNew, B. Westermann, M. Gmachl, F. Parlati, T.H. Sollner, and J.E. Rothman. 1998. SNAREpins: minimal machinery for membrane fusion. *Cell*. 92:759-72.

Weidman, P.J., P. Melancon, M.R. Block, and J.E. Rothman. 1989. Binding of an N-ethylmaleimide-sensitive fusion protein to Golgi membranes requires both a soluble protein(s) and an integral membrane receptor. *J Cell Biol*. 108:1589-96.

White, J.M., and M.D. Rose. 2001. Yeast mating: getting close to membrane merger. *Curr Biol*. 11:R16-20.

Wilson, I.A., J.J. Skehel, and D.C. Wiley. 1981. Structure of the haemagglutinin membrane glycoprotein of influenza virus at 3 Å resolution. *Nature*. 289:366-73.

Yawo, H., and M. Kuno. 1985. Calcium dependence of membrane sealing at the cut end of the cockroach giant axon. *J Neurosci*. 5:1626-1632.

Young, J.D., G.P. Young, Z.A. Cohn, and J. Lenard. 1983. Interaction of enveloped viruses with planar bilayer membranes: observations on Sendai, influenza, vesicular stomatitis, and Semliki Forest viruses. *Virology*. 128:186-94.

Yu, L., K.J. Blumer, N. Davidson, H.A. Lester, and J. Thorner. 1989. Functional expression of the yeast alpha-factor receptor in *Xenopus* oocytes. *J Biol Chem.* 264:20847-50.

Zhang, N.N., D.D. Dudgeon, S. Paliwal, A. Levchenko, E. Grote, and K.W. Cunningham. 2006. Multiple signaling pathways regulate yeast cell death during the response to mating pheromones. *Mol Biol Cell.* 17:3409-22.

Zhu, Y.S., X.Y. Zhang, C.P. Cartwright, and D.J. Tipper. 1992. Kex2-dependent processing of yeast K1 killer preprotoxin includes cleavage at ProArg-44. *Mol Microbiol.* 6:511-20.

It is the policy of the University to encourage the distribution of all theses and dissertations. Copies of all UCSF theses and dissertations will be routed to the library via the Graduate Division. The library will make all theses and dissertations accessible to the public and will preserve these to the best of their abilities, in perpetuity.

I hereby grant permission to the Graduate Division of the University of California, San Francisco to release copies of my thesis or dissertation to the Campus Library to provide access and preservation, in whole or in part, in perpetuity.



Author Signature

1/3/2008
Date